LA-UR-17-22647
Approved for public release; distribution is unlimited.

Title: Comparative Assessment of Copper-Coated Kapton: Analysis of Microclad from Several Manufacturing Lots

Author(s): Martz, Joseph Christopher; Spearing, Dane Robert; Labouriau, Andrea; Judge, Elizabeth; Kelly, Daniel; Dirmyer, Matthew R.; Milenski, Helen Marie; Patterson, Brian M.; Sandoval, Cynthia Wathen; Usov, Igor Olegovich; Beaux, Miles Frank II; Henderson, Kevin C.; Torres, Joseph Angelo; Edwards, Stephanie Lynn; Vodnik, Douglas R.; Keller, Jennie; Mccabe, Rodney James; Livescu, Veronica; Cowan, Joseph Sarno; Aragonez, Robert J.; Tokash, Justin Charles; et al.

Intended for: Report

Issued: 2017-04-03

Comparative Assessment of Copper-Coated Kapton: Analysis of Microclad from Several Manufacturing Lots

Edited by:

Joseph C. Martz and Dane R. Spearing

Contributions from:

Andrea Labouriau, Elizabeth Judge, Daniel Kelly, Matthew Dirmyer, Helen Milenski, Brian Patterson, Cynthia Sandoval, Igor Usov, Miles Beaux, Kevin Henderson, Joseph Torres, Stephanie Edwards, Doug Vodnik, Jennie Keller, Rod McCabe, Veronica Livescu, Joe Cowan, Robert Aragonez, Justin Tokash, Samantha Lawrence, Neliza León Brito, Dane Spearing, and Joseph Martz

Revision 3.0

March 31, 2017

CONFIGURATION CONTROL LOG

Revision No.	*Document Date*	*Reason for Revision*
1	March 22, 2017	Initial Draft
2	March 29, 2017	Author Input
3	March 31, 2017	Final

Comparative Assessment of Copper-Coated Kapton: Analysis of Microclad from Several Manufacturing Lots

March 31, 2017

Background

Microclad is a composite material consisting of a thin copper coating applied on a single side over a Kapton substrate. Kapton is the commercial designator for polyimide supplied by DuPont. Microclad is a key material in detonator manufacture and function. Detonators which utilize Microclad function when a large current applied through a thin bridge etched into the copper produces a plasma, accelerating a Kapton flyer into an explosive (PETN) pellet. The geometry and properties of the Microclad are a critical element of this process.

Historically, Microclad has been produced by a number of manufacturers. When DuPont ceased Microclad production in the early 1980s, the Fortin company bought the rights to produce this material, and supplied Microclad to the weapons complex for detonator production. A large quantity of Fortin-supplied Microclad was procured in 1985, and this material provided feedstock until the early 2000s. Fortin ceased Microclad production in this timeframe when the Datex company assumed production.

Another large lot of material was provided by Datex in 2003, and this material has been used in detonator production to this time frame. In 2013 Datex announced they would no longer supply Microclad. A final order was placed and a second Datex production lot was received in 2013. This 2013 material was inspected and a fraction was found to not meet specification for copper thickness as determined by 4-point probe measurements. As a result, the 2013 Datex material has not been used in any production to date.

By 2016, Microclad supplies were nearly depleted. Either a new source of Microclad is required, or qualification of the 2013 Datex material is needed. The Datex production equipment and process technology was procured by yet another independent supplier in early 2016. An order was placed for additional material, and this was received in mid-2016. A need to determine the suitability of these new Microclad lots has motivated this assessment project.

As part of the Product Realization Team (PRT) for detonator manufacture, a subgroup was tasked with determining the "similitude" of these various lots of Microclad. The charter was to measure and inspect these various lots to determine if any differences existed, and if so, what those differences might mean for detonator manufacture and function.

This report documents the results of this extensive assessment. It consists of individual chapters providing data, comparison, and assessment of Microclad from various sources. We detail the approach and techniques used in this assessment, describe the sample methodology, present the key findings and differences, and provide recommendations for the PRT. This work was conducted on an aggressive schedule to meet a challenging deadline for the PRT, in order to support a determination of a suitable Microclad source such that production schedules would not be impacted.

While findings here have been cross checked and reviewed by both internal team members and external members of the PRT, further analysis of data may result in future modifications to our findings. As such, recommendations presented in this report should be considered preliminary. Updates will be issued when warranted and documented in the change log at the beginning of this report.

Methodology and Approach

The determination of assessment techniques was guided by 2 key principles: measurement of key properties that would elucidate similitude, and availability of instruments and techniques that could be efficiently and rapidly employed.

To support the construction of an assessment plan, a brainstorm session was held to identify both the key material properties and the available techniques for measurement of those properties. Emphasis was placed on material properties relevant to Microclad manufacture or performance. Much of this work was guided by the formal specification for Microclad, spec 9Y294599. This specification is critical for acceptance of Microclad, but incomplete in its description of material properties for adequate determination of similitude. Figure 1 provides a summary of the key specifications from 9Y294599.

Kapton

Polyimide - DuPont Type H (EUC 713)

Thickness: 0.002 ± 0.0002 in

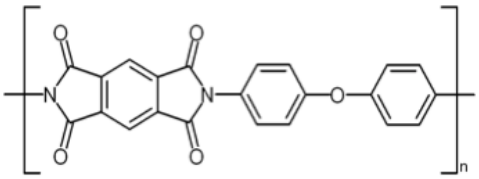

Copper

> 99.8% purity

Thickness: 146 – 180 µin (3.71 – 4.57µm)

< 18 µin (0.46 µm) difference between max. and min. thickness on any given roll

Plating Adhesion

Test according to IPC-TM-650 2.4.10 (cellophane tape test)

Other

No visibly detectable discoloration or contamination

Less than 1 pinhole/foot when inspected using backlit lighting

Cu shall not crack when the foil is bent around a 6 mm radius cylinder (with Kapton located against cylinder)

Surface shall be scratch-free when visually inspecting at 14-16x magnification

Figure 1. Summary of specifications for Microclad from Specification 9Y294599.

To help organize our assessment, key properties were categorized into 3 main areas: Kapton properties, copper properties, and integrated system properties and characteristics. For each of these, the group listed a suite of possible material properties for measurement. These form the y-axis of the matrix shown in Table 1. For each of these, a determination of the value of that data to assessing similitude in the intended application was made. This determination was given on a 3-step scale: high priority measurements critical to the assessment; medium priority measurements useful to the assessment, and low priority measurements that would assist the assessment.

Next, possible measurement techniques were listed with the condition that they be available for immediate deployment to meet our aggressive schedule, and that group members had access to the equipment and authorization and approvals to conduct the proposed measurements. This list of measurement techniques is given as the x-axis in Table 1. Finally, the list of desired properties was cross-referenced to the list of available techniques to identify those measurements of specific properties to be made by each individual method. The previous prioritization was applied to each of these assessments, and a list of ranked measurements was constructed. This formed the basis of our evaluation plan. Note that several techniques and properties were excluded from the final list based on priority, resource, and time constraints.

Once this list was constructed, individual researchers began evaluation of samples distributed to the team, see the following section on sample methodology for details. Team members met weekly to discuss preliminary results, share findings, develop plans for future measurements, and cross-check results and findings among samples. [For example, copper "scabs" from adhesion pull-testing proved very useful to the interface chemistry team to determine the precise point of failure within the composite.]

All measurements were completed on the predetermined schedule, and overall findings were briefed to the PRT at a workshop on Feb. 14, 2017. Subsequent chapters of this report provide these detailed results as well as summaries of each evaluation method. Lastly, a summary of differences is given along with our basic findings on similitude. These are given immediate following the section on sample methodology and prior to the detailed evaluation results.

	Radiography (B. Patterson, MST-7)	FTIR (C-CDE)	ICP/MS (D. Kelly, C-CDE)	NMR (A. Labouriau)	GPC	SEM/μ-probe/met. (McCabe & Livescu, MST-8)	XRF (D. Kelly, C-CDE)	TEM	TGA (C-CDE)	DSC (C-CDE)	AFM (J. Tokash, SIGMA)	Spectral Reflectometry (M. Beaux, MST-7)	Optical Microscopy	Profilometry (M. Beaux, MST-7)	Load Testing (C. Sandoval, MST-7)	4-Point Probe (MST-7)	Eddy Current	ECR	XPS (D. Kelly, C-CDE)	SIMS (C-NR)	Adhesion Testing (D. Vodnik, MST-7)	Bend Test
Kapton																						
thickness																						
density																						
composition																						
polymer structure																						
thermal																						
modulus																						
refractive index																						
dielectric constant																						
surface roughness																						
tensile strength																						
Copper																						
thickness																						
resistivity																						
density																						
composition																						
microstructure/grain																						
orientation/morphology																						
surface roughness																						
Integrated Microclad																						
interface																						
bond strength/adhesion																						
chemistry																						
bridge geometry																						
high priority - will do																						
medium priority - may do																						
low priority - could do																						

Table 1. Microclad Assessment Matrix

Sampling Strategy

A description of the Microclad sample lots provided by Q-6 for evaluation is given below. The subject matter experts for each of the analytical techniques used chose samples from these lots as they deemed appropriate in order to get a representative distribution of samples needed for evaluation of similitude.

Fortin

Two sets of Microclad samples from Fortin were provided: one set was coated with 160 µin of Cu (manufactured 5/24/85), and the other with 175 µin of Cu (manufactured 7/24/85). Both sets consisted of multiple (8-10) 4 in. long x 1 in. wide strips of Microclad from undetermined locations within the roll, and were delivered as two lots in zip-lock bags (see Figure 2). Samples from these sets are referred to as: Fortin, F85, Fortin-160, Fortin-175, "Mound", or "Donn".

Datex 2003

Manufactued by Datex in 2003, a total of 18 samples were provided for evaluation. These consisted of two 12 in. long x 1 in. wide strips from the first two feet of 9 different rolls. Those samples labeled "A" came from the first foot in the roll, while those labeled "B" came from the second foot. Samples from this set are referred to as Datex 2003, or D03. Each strip was individually packaged in a mylar sleeve.

Datex 2013

Provided to LANL in 2013 by Datex (actual manufacture date unknown), a total of 72 samples were provided for evaluation. As with the Datex 2003, these consisted of two 12 in. long x 1 in. wide strips from the first two feet of 36 different rolls, each individually packaged in a mylar sleeve. Those samples labeled "A" came from the first foot in the roll, while those labeled "B" came from the second foot. Samples from this set are referred to as Datex 2013, or D13.

Datex 2016

Provided to LANL in 2016 by Datex (actual manufacture date also unknown), a total of 40 samples from 9 different rolls were provided. As with the other Datex samples, these consisted of 12 in. long x 1 in. wide strips, each individually packaged in a mylar sleeve. A variable number of samples from each roll were provided, labeled with a letter corresponding to the subsequent one foot sections from each roll (i.e. – "A" came from the first foot, "B" from the second foot, etc.) Samples from this set are referred to as Datex 2016, or D16.

An example of the size and packaging of the Datex samples is shown in Figure 3, and a listing of all Microclad samples provided is given in Table 2.

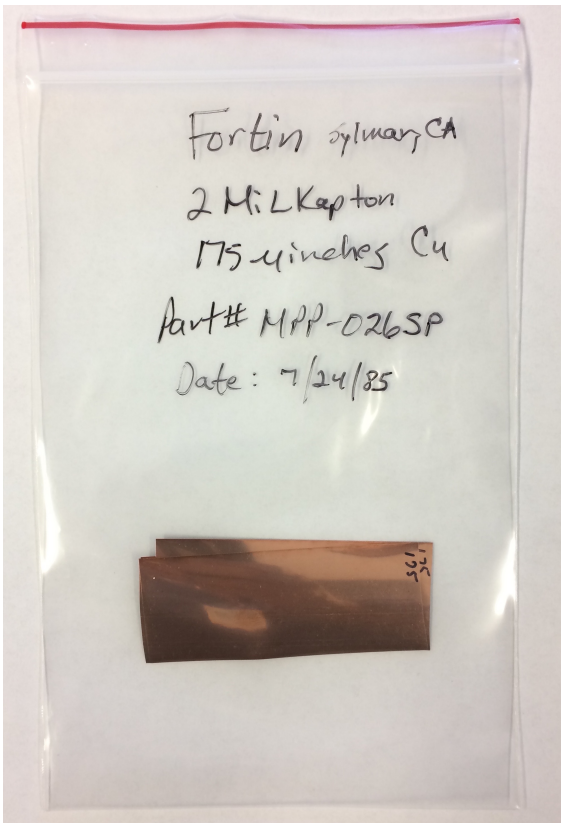

Figure 2. Example of Fortin Sample.

Figure 3. Example of Datex Samples. Samples shown are from the Datex 2016 lot, and are roughly 12 in. long by 1 in. wide, and packaged in mylar sleeves. All Datex samples were similarly packaged and labeled.

Fortin Part#MPP-026SP
160 µin Copper
175 µin Copper

Datex 2003 WO25637	
D03 Roll #6 A	D03 Roll #6 B
D03 Roll #7 A	D03 Roll #7 B
D03 Roll #8 A	D03 Roll #8 B
D03 Roll #9 A	D03 Roll #9 B
D03 Roll #16 A	D03 Roll #16 B
D03 Roll #19 A	D03 Roll #19 B
D03 Roll #24 A	D03 Roll #24 B
D03 Roll #26 A	D03 Roll #26 B
D03 Roll #28 A	D03 Roll #28 B

Datex 2013 WO25637	
D13 Roll #50 A	D13 Roll #50 B
D13 Roll #51 A	D13 Roll #51 B
D13 Roll #52 A	D13 Roll #52 B
D13 Roll #53 A	D13 Roll #53 B
D13 Roll #54 A	D13 Roll #54 B
D13 Roll #55 A	D13 Roll #55 B
D13 Roll #56 A	D13 Roll #56 B
D13 Roll #57 A	D13 Roll #57 B
D13 Roll #58 A	D13 Roll #58 B
D13 Roll #59 A	D13 Roll #59 B
D13 Roll #60 A	D13 Roll #60 B
D13 Roll #61 A	D13 Roll #61 B
D13 Roll #62 A	D13 Roll #62 B
D13 Roll #63 A	D13 Roll #63 B
D13 Roll #64 A	D13 Roll #64 B
D13 Roll #65 A	D13 Roll #65 B
D13 Roll #66 A	D13 Roll #66 B
D13 Roll #67 A	D13 Roll #67 B
D13 Roll #68 A	D13 Roll #68 B
D13 Roll #69 A	D13 Roll #69 B
D13 Roll #70 A	D13 Roll #70 B
D13 Roll #71 A	D13 Roll #71 B
D13 Roll #72 A	D13 Roll #72 B
D13 Roll #73 A	D13 Roll #73 B
D13 Roll #74 A	D13 Roll #74 B
D13 Roll #75 A	D13 Roll #75 B
D13 Roll #76 A	D13 Roll #76 B
D13 Roll #77 A	D13 Roll #77 B
D13 Roll #78 A	D13 Roll #78 B
D13 Roll #79 A	D13 Roll #79 B
D13 Roll #80 A	D13 Roll #80 B
D13 Roll #81 A	D13 Roll #81 B
D13 Roll #82 A	D13 Roll #82 B
D13 Roll #83 A	D13 Roll #83 B
D13 Roll #84 A	D13 Roll #84 B
D13 Roll #85 A	D13 Roll #85 B

Datex 2016 PO388937
Roll # 1-A
Roll # 1-D
Roll # 1-E
Roll # 1-F
Roll # 1-G
Roll # 1-H
Roll # 2-E
Roll # 2-F
Roll # 3-D
Roll # 4-C
Roll # 4-D
Roll # 4-F
Roll # 4-G
Roll # 5-C
Roll # 5-D
Roll # 5-E
Roll # 5-F
Roll # 5-H
Roll # 5-O
Roll # 6-B
Roll # 6-?
Roll # 6-?
Roll # 7-B
Roll # 7-C
Roll # 7-D
Roll # 7-E
Roll # 7-F
Roll # 9-B
Roll # 9-D
Roll # 9-E
Roll # 9-F
Roll # 9-G
Roll # 9-H
Roll # 10-C
Roll # 10-D
Roll # 10-E
Roll # 10-F
Roll # 10-G
Roll # 10-H
Roll # 10-I

Table 2. A listing of all Microclad samples provided for evaluation.

Summary of Findings

All work as specified in the original evaluation plan has been completed. A summary of the findings, including key noted differences, is outlined below:

Kapton Chemistry

Kapton chemistry appears quite similar between sample lots. FTIR, NMR, and solvent swelling experiments all show a similar response. No significant quantities of extracts were detected by ^{1}H NMR. DSC shows a more prevalent exotherm at ~130°C for D16 samples, which is hypothesized to be due to slightly elevated levels of poly(amic acid) intermediate that has yet to be fully thermally converted to polyimide. Weight loss observed in TGA at the same temperature corroborates this, and could be explained by the release of water as a byproduct.

Kapton Thermomechanical Properties

All samples displayed shrinkage when exposed to heat. The D03, D13, and D16 samples were the most similar, as they all shrank 1-5% upon heating to 160°C. Whereas the Fortin samples shrank 10-20% upon heating to 160°C. Overall, the Datex samples all behave similarly both inter- and intra-lot with MTMA.

The tensile strength of all Datex samples was within a standard deviation (which appears to be predominantly controlled by the tensile strength of the Kapton), while the original Fortin 160 has a statistically stronger average tensile strength.

Copper Chemistry and Morphology

The ICP-MS results show that the copper is very pure in all samples (≥99.9986%), greatly exceeding the purity specification of 99.8%, and the intra- and inter-sample variations in chemistry are comparable within error. The total amount of copper (wt % and coverage in mg/cm^2) was roughly 10% lower for the D16 lot compared to the D03, D13 and Fortin lots.

Copper morphology varies widely among all samples, both inter- and intra-lot, with the D16 samples showing a slightly larger surface roughness as measured by both SEM and AFM. Copper thickness is consistent among the Datex samples, and varies slightly from the Fortin samples. The most dissimilar aspect of the different batches pertains to the Cu microstructure, with the Datex material having a significantly smaller grain structure than Fortin, and a difference in the densities of grain boundary types.

Surface Layer

Based on SEM analysis, there is a great deal of variability in the Cu surface layers between lots. Both the Fortin and D16 material show a visible surface (contamination?) layer. There is some evidence of a similar, though smaller, layer on the D03 material, and almost none on D13 samples evaluated.

X-ray photoelectron spectroscopy (XPS) measurements show the elemental composition of both the Kapton and copper surfaces and near-surface regions of Datex microclad laminates to be very similar across the three Datex lots analyzed. This suggests that the variability in the surface layer as observed by SEM is strictly morphological in nature, and not due to a difference in surface chemistry.

Cu-Kapton Interface

Significant variation in the measured adhesion values was observed, both inter- and intra-lot. However, statistically no clear difference in adhesive performance between the Microclad samples was observed.

ICP-MS chemical analysis revealed the presence of both Sn and Pd, which are used as catalysts in the electrodeless copper plating process. The Sn:Pd ratio was observed to be ~3:1 for the D03 and D13 lots, and was found to be ~2:1 for the D16 lot, perhaps due to a change in manufacturing techniques between the D13 and D16 lots.

Discussion and Recommendations

In general, the analyses conducted suggest that all Datex samples (D03, D13, and D16) look very similar. Our evaluations of Kapton in these samples show remarkable similarity among all the materials studied, including both chemistry and thermomechanical properties. The only difference found in the Kapton evaluation was a slight exotherm in the D16 samples, postulated to arise from a very small amount of unreacted monomer. This is likely due to the young age of the Kapton in D16 compared to other samples. In sum, nothing in our Kapton evaluation suggested concerns for use in the intended application.

With respect to the metallization layer, the two most significant differences are the difference in copper morphology, specifically grain size and structure, and the ~10% reduction in copper mass seen in the D16 samples compared to D03 and D13. Copper thickness does not vary significantly among these lots. Hence, it appears that copper density is lower in some portion of the D16 samples. The defected surface layer seen in SEM cross section of D16 (and other samples such as Fortin and some D03) may explain this reduction in density.

Will this slightly lower copper density at the surface impact performance or function? In the opinion of the subject matter experts on our analysis team, probably not. None-the-less, a thorough qualification program of D16 will measure threshold voltages and flier velocities of composite assemblies, and this will allow rigorous qualification of D16 material. In our opinion, there is low risk from this slight difference, and D16 material is suitable for further qualification and testing.

The other key difference is that of copper morphology. Again, a rigorous test and evaluation program should answer any questions regarding the impact of these differences on performance. In the estimation of the SMEs on the analysis team, we don't expect any substantial change in performance due to this difference in copper morphology. We note that D03 samples show similar morphology to D16, and the D03 material has been accepted and qualified for over 15 years. It is only in comparison to Fortin material that such a substantial change in morphology is observed.

Perhaps the biggest impact of copper morphology on function is the corrosion and aging behavior of the material. Grain size in particular can impact the susceptibility to corrosion and the ultimate corrosion rate. Fine-grained materials generally are more likely to form passivating films (due to more uniform corrosion) compared to large-grained metals. It will still be prudent to subject D16 materials to a series of accelerating aging tests to gain confidence in the long-term behavior of this material. As such, our team has recommended that the PRT consider a phase II of this study with a focus on corrosion behavior and aging.

The PRT asked a specific question about differences in roughness found by our various techniques. We performed 3 measurements of roughness in this evaluation, all at different length scales. These techniques were optimized for nano-, meso-, and bulk roughness measurements. Each found differences in roughness at each of these length scales. This is common in roughness measurements, and suggests the complex nature of these surface geometries that contain features at many length scales.

In summary, our comprehensive evaluation of Microclad from various manufacturing lots shows that the materials are quite similar. In the opinion of the SMEs on the evaluation team, the differences found are sufficiently small that they present acceptable risk in the continued qualification of this material. *Specifically, we conclude that the D16 material is of sufficient similitude to D03 and D13 to warrant continued evaluation and use.*

Microclad Characterization by FTIR

Dan Kelly and Helen Milenski
Chemistry Division - Chemical Diagnostics and Engineering Group

Summary

Infrared (IR) spectroscopy measurements show the molecular structure of polyimide from a variety of microclad lots (Fortin, Datex 03, Datex 13, and Datex 16) to be similar. Qualitatively, spectra compare well across all material lots and closely resemble published spectra of "kapton". The spectra show very little or no indication of unreacted monomer peaks. Quantitatively, as determined by a match factor analysis, individual specimens are uniform and data compare well across all material lots. ***Datex 16 shows the highest intralot variability. Datex 13 and Datex 16 lots show the greatest lot-to-lot difference. Nothing in the IR data or its analysis suggests any microclad lot should be considered unacceptable in comparison to any other lot.***

Experiments, Results, and Discussion

We performed Fourier Transform Infrared Spectroscopy (FTIR) on the polyimide (kapton) of microclad lots (Fortin, Datex 03, Datex 13, and Datex 16; we also had several small legacy microclad samples available in Chemistry Division, identified as "Asher" and "Mound" samples). FTIR is a vibrational spectroscopy well suited to probing polymer structure; as IR energy is absorbed by a molecule it excites vibrational motion (e.g. C-C, C-N, C-H stretches and bends). No two compounds produce identical FTIR spectra, and the technique allows quantitative information between samples since peak intensities scale with the amount of material present. The analysis is quick and non-destructive. We performed IR measurements using a Nicolet 6700 instrument in attenuated total reflection (ATR) mode. In FTIR-ATR the IR excitation spills from the crystal and penetrates ~ 1 micron into a kapton sample contacting the crystal. The use of a germanium crystal provided high quality data in the IR fingerprint region (700-2000 cm^{-1}). Ten FTIR-ATR spectra were collected from each individual microclad specimen (two Fortin, five Datex 03, eight Datex 13, and six Datex 16). IR spectra were compared quantitatively using a match factor method, which is a derivatized correlation calculation that removes baseline effects, enhances peak positions and small wavenumber shifts, and compares peak intensities. Match factor results comparing two spectra generate a numerical result between 0 and 100. A match factor of 100 indicates identical spectra. In general, identical compounds will generate match factors above 95, while homologous compounds will generate match factors above 90.

Figure 1 shows an FTIR-ATR spectrum from Datex 03-A6. Two IR peaks in Figure 1 are diagnostic of polyimide: the C=O carboxylic acid ~ 1715 cm^{-1}, and the C-N aromatic ~ 1375 cm^{-1}. Additionally, we observe no strong peaks indicating unreacted monomers (primary amines at ~ 3400 cm^{-1}, or cyclic anhydrides ~ 1825 cm^{-1}). Based on this we believe the kapton to be at least nearly fully cured. Figure 2 shows representative FTIR-ATR spectra from all lots of material (Fortin, Datex, Asher, Mound) in the 'fingerprint' region 700-200 cm^{-1}. Visual observation of the entirety of the microclad IR data confirms what is seen in Figure 2; qualitatively all spectra are very similar.

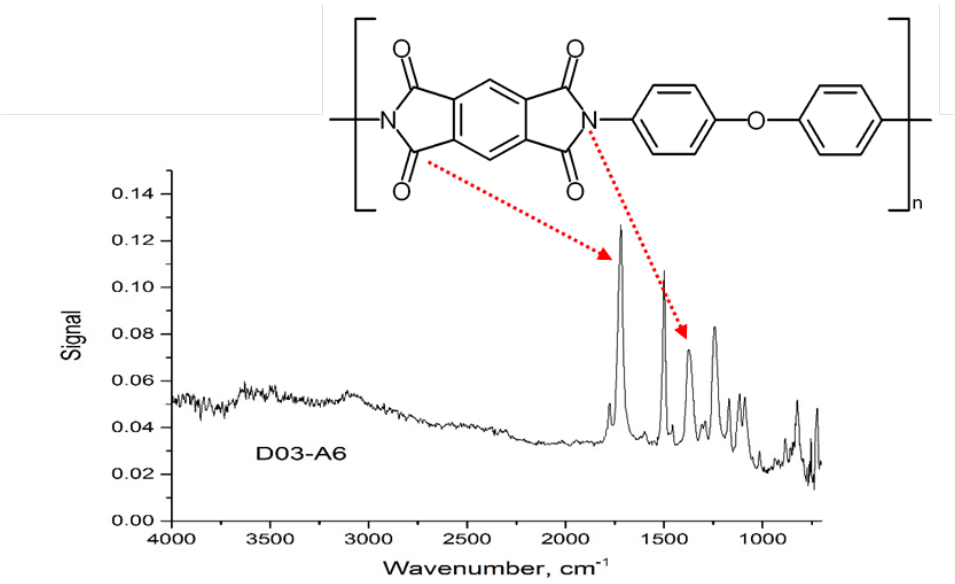

Figure 1*: FTIR-ATR spectrum from Datex 03-A6 sample.*

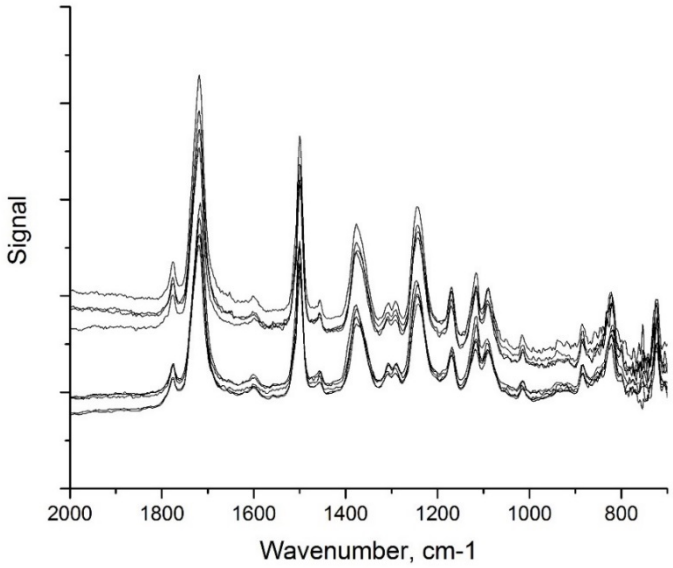

Figure 2*: Representative FTIR-ATR spectra from Fortin, Datex 03, Datex 13, Datex 16 microclad lots. Also included are historical microclad samples available to Chemistry Division, known as "Asher" and "Mound".*

Quantitatively, we evaluated microclad IR spectra using a match factor comparison, a technique we employed previously for chemical certification of polymeric materials for Weapons Production activities. An IR match factor of greater than 90 between a new sample and a known spectrum was one requirement to confirm similarity of two samples. Given ten individual IR

spectra, 45 unique match factors can be generated for each microclad sample. Figure 3 shows the average match factor for each microclad sample is approximately 95, and is greater than 90 for all samples. For eighteen of the twenty-one samples, all 45 individual match factors were greater than 90. This is evidence that each microclad specimen is uniform.

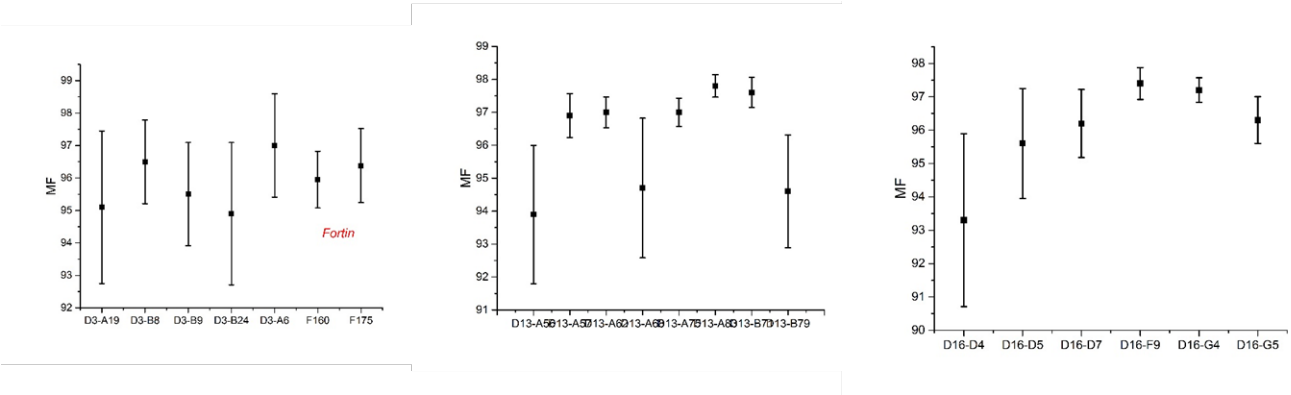

Figure 3*: Average match factors (MF) for IR spectra for each microclad sample. Datex 03 and Fortin samples on left. Datex 13 samples in center. Datex 16 samples on right.*

Comparison of microclad samples within a lot (*e.g.*, comparison of all Datex 03 samples amongst themselves), and between lots (*e.g.*, comparison of Datex 03 samples to Datex 13 samples) was also done using a match factor comparison. The methodology was to select, for each of the 21 samples, the IR spectrum with the highest average match factor, and then to compare each spectrum with all 209 individual spectra for all other samples. Table 1 shows a tabular results for the Datex 03 lot using this methodology. Tables 1 and 2 show the results of intralot and lot-to-lot match factor comparisons for microclad samples and lots. Note that the numbers in Tables 1 and 2 are not match factors; rather they are the percentage of measurements that generated match factors greater than 90. Table 1 shows comparison of individual Datex 03 samples to Datex 03, Datex 13, and Datex 16 lots. Intralot Datex 03 comparisons are in the first column of Table 1, while comparison of Datex 03 samples to Datex 13 and Datex 16 lots are found in the second and third columns. The great majority of match factors are greater than 90. In general individual Datex 03 samples compare well to all other samples; Datex 03 samples are similar to other Datex 03 samples, as well as to Datex 13 and Datex 16 samples. Sample A19 shows the poorest comparison to other Datex 03 samples, as well as to the other Datex lots. The remaining Datex 03 samples compare well to all samples.

Analysis identical to Table 1 was also carried out for Datex 13 and Datex 16 samples (tables not shown). Table 2 shows the summary of IR match factor comparisons of Datex lots, and a comparison to the two Fortin samples. Again, the great majority of comparisons generate match factors greater than 90, and from this we infer that all samples are very similar. Intralot comparisons in Table 2 are noted by asterisks; Datex 16 shows the greatest intralot variability. The remaining percentages in Table 2 are lot-to-lot comparisons. Datex 16 shows the poorest lot-to-lot comparison of the three Datex lots. Fortin 160 compares well to Datex 03 and Datex 13, but less so to Datex 16. Fortin 175 compares poorer to all Datex lots. [Note though that only a single sample of Fortin 160 and Fortin 175 were measured.] For each of the 19 individual Datex samples, we can define an 'ideal' sample as one with 90% of its match factor measurements at > 90 in comparison to at least two of three Datex lots. From this standpoint Datex 03 has the most number of ideal samples, and Datex 16 has the least number of ideal samples.

Summary

The IR data and analysis for Datex microclad lots suggests:

- Datex 03 samples show similarity to other Datex 03 samples, and to the Datex 13 and Datex 16 lots.
- Datex 13 samples show similarity to other Datex 13 samples, and to the Datex 03 lot. They are less similar to the Datex 16 lot.
- Datex 16 samples show the greatest intralot variability. They are similar to Datex 03 lot, but less similar to Datex 13 and Fortin materials.
- Individual samples are uniform, and generally compare well to other samples.
- ***Nothing in the IR data or its analysis suggests any microclad lot should be considered unacceptable in comparison to any other lot.***

Datex 03 Samples	**Compare to Datex 03 lot** (49 measurements)	**Compare to Datex 13 lot** (80 measurements)	**Compare to Datex 16 lot** (60 measurements)
	% of measurements with MF > 90		
D03-A6	100	99	98
D03-A19	82	86	80
D03-B8	96	90	88
D03-B9	96	94	98
D03-B24	92	94	95
Average	**93**	**93**	**92**

Table 1*: Match factor comparison of individual Datex 03 samples to all other Datex samples. Intralot comparisons between Datex 03 samples are in the first column. Lot-to-lot comparisons between individual Datex 03 samples and Datex 13 and Datex 16 lots are in columns two and three. Note the entries in the table are not match factors, they are percentages of measurements that generate match factors of greater than 90.*

LOT	***Compare to Datex 03***	***Compare to Datex 13***	***Compare to Datex 16***	**# "Ideal" samples**
	Average % of measurements with MF > 90			
Datex 03	**93***	93	92	4 of 5
Datex 13	93	**91***	85	4 of 8
Datex 16	91	86	**82***	2 of 6
Fortin 160	92	90	77	1 of 1
Fortin 175	68	74	50	0 of 1

***Table 2**: Summary of IR match factor comparison of Datex lots. Intralot comparisons are noted by asterisks; all other percentages are lot-to-lot comparisons. Note the entries in the table are not match factors, they are percentages of measurements that generate match factors of greater than 90.*

Microclad Characterization by XPS

Dan Kelly and Helen MilenskiChemistry Division - Chemical Diagnostics and Engineering Group

Summary

X-ray photoelectron spectroscopy (XPS) measurements show the elemental composition of both the kapton and copper surfaces and near-surface regions of Datex microclad laminates to be very similar across the three Datex lots analyzed. There is a persistent small amount of chlorine in the copper, possibly due to the use of metal chloride catalysts for electroless copper deposition. The oxide layer on the copper is similarly thin on all Datex lots. There is a thin surface layer where tin and copper are observed on the kapton side of all Datex lots; these elements are not observed on the kapton of non-Datex microclad. Calcium is observed on the kapton from all Datex lots, and may be associated with polymerization catalysts or processing methods. For all Datex lots, at the interface between kapton and copper, an approximately 80 nm layer containing Sn and Pd is observed. These elements are associated with catalysts for electroless copper deposition. ***Nothing in the XPS data or its analysis suggests any Datex microclad lot should be considered unacceptable in comparison to any other Datex lot.***

Experiments, Results, and Discussion

X-ray photoelectron spectroscopy (XPS) is a surface-sensitive analytical technique used to determine the elemental composition and valence state at the top ~ 5 nm of solid materials. XPS analysis combined with ion sputtering to ablate material from a substrate surface is routinely used to probe the chemical composition of metal surfaces as a function of depth into the substrate (depth profiling). For microclad characterization, XPS was used to determine the surface and subsurface composition of both copper and kapton, and to characterize the transition region between kapton and copper on the laminate. XPS data were collected using a Physical Electronics VersaProbe II system with a base pressure below 1 x 10^{-7} Pa. A variable-size, monochromated Al kα x-ray source (1487 eV) was used throughout, and photoelectrons were energy sorted using a hemispherical analyzer. Samples were at room temperature. XP spectra are shown in terms of binding energy (BE) and instrument calibration was performed in accordance with ASTM procedure. Elemental composition was determined using survey scans at a pass energy of 117 eV. A pass energy of 29 eV was used for high-resolution scans to determine chemical valence state and quantify material composition. Depth profiling was carried out using 2 kV argon ions. Charge neutralization for insulating samples is accomplished by focusing low energy ions and electrons at the spot of x-ray impingement.

Figure 1 (left) shows XPS survey scans of the copper side of a Datex 03 sample (as-received and after ~ 50 nm of material is removed). The as-received material shows the presence of Cu, along with C, N, and O arising from ambient exposure and handling. Ablating ~ 50 nm of material exposes the underlying copper surface, and the red spectrum of Figure 1 compares well to a reference spectrum of "pure" copper. Figure 2 shows the atomic concentration of copper and oxygen during depth profiling of Datex 03, Datex 13, and Datex 16 samples. Oxygen is quickly depleted as the surface is penetrated,

and the sample lots behave similarly. Table 1 shows the average atomic concentration of C, N, O, Cu, and Cl on the copper from Datex lots, before and after ion sputtering. The copper in all Datex lots appears similar by XPS measurements. The only impurity "in" the copper, detected by XPS, is chlorine which is present in low levels. The microclad process involves the use of metal chloride catalysts and chlorine is a ubiquitous impurity in many metals.

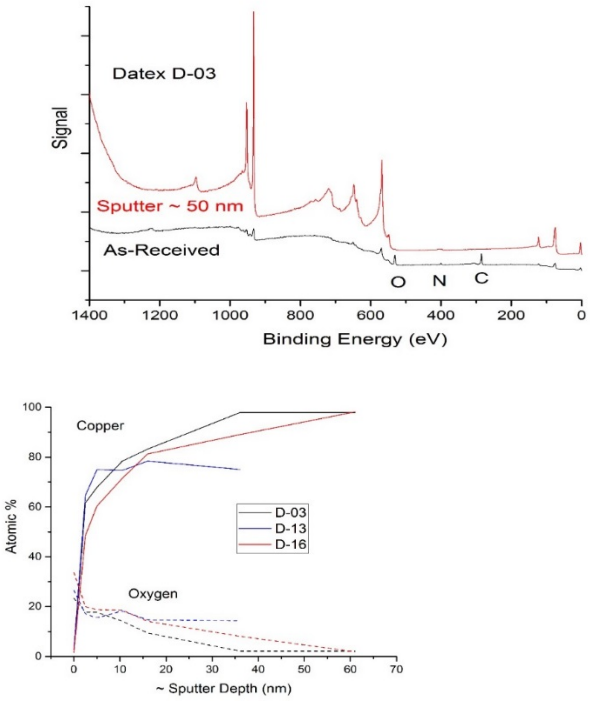

Figure 1: *(left) XPS survey scans of copper side of Datex D03 sample, as-received and after ~ 50 nm of material is removed; (right) depth profile of copper and oxygen of copper side of laminate of Datex samples.*

As-Received	C	N	O	Cl	Cu	~ Sputter Depth (nm)
D03	64	5	24	1	6	
D13	66	5	24	1	3	
D16	59	7	27	1	6	
After ion sputtering						
D03	5	2	2	0	91	60
D13	13	4	15	1	66	40
D16	7	2	4	1	87	60

Table 1: *Lot averages of elemental composition (atomic percent) of copper side of Datex lots, as-received and ion sputtered surfaces.*

Figure 3 (left) shows XPS survey scans of the kapton side of a Datex 16 sample (as-received and after ~ 100 nm of material is removed). All Datex lots showed substantial tin signals, and small copper signals, on the as-received kapton side of the laminate. This is in contrast to Fortin microclad, and two legacy samples known as "Mound" and "Asher", on which no tin or copper was found on the kapton surface. On the right side of Figure 3 is shown the copper and tin atomic concentration of Datex kapton during depth profiling, indicating the copper and tin on the kapton surface is confined to the top ~ 20 nm. Table 2 shows the average atomic concentration of C, N, O, Cu, Sn, Cl, and Ca on the kapton from Datex lots, before and after ion sputtering. The calcium observed is ubiquitous on XPS of polymer samples, and may be associated with polymerization catalysts and/or processing methods (mold releases and lubricants in polymer manufacturing often contain calcium). Overall, the kapton side of all Datex lots appear similar by XPS.

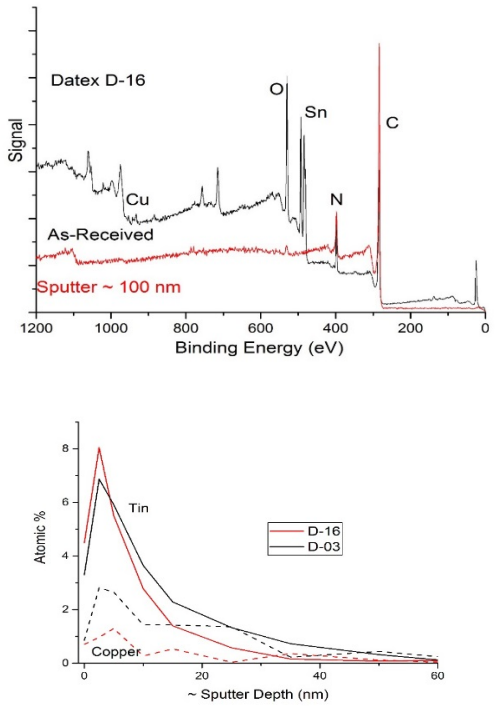

Figure 3: *(left) XPS survey scans of kapton side of Datex D16 sample, as-received and after ~ 100 nm of ion sputtering; (right)* ***d****epth profile of copper and tin on kapton side of laminate of Datex D03 and D16 samples.*

As-Received	C	N	O	Cu	Sn	Cl	Ca	~ Sputter Depth (nm)
D03	67	10	19	0.5	3	0.6	0.6	
D13	64	10	22	0.3	3	0.4	0.4	
D16	65	10	22	0.6	3	0.0		
After ion sputtering								
D03	86	12	2	0.1	0.1	0.1	0.1	100
D13	82	9	5	0.7	3	0.0	0.3	10
D16	90	9	1.4	0.0	0.0	0.0		100

Table 2: *Lot averages of elemental composition (atomic percent) of kapton side of Datex lots, as-received and ion sputtered surfaces.*

We used XPS to analyze Datex microclad samples that had been pulled apart (separating the kapton from the copper) after adhesion strength tests were performed. XPS results of the kapton/copper interface from adhesion strength test samples were similar for all Datex microclad lots. From a single adhesion strength test we get two samples for XPS, the "copper side" and the "kapton side". These samples would be pure kapton and pure copper if separation occurred "perfectly" at their interface. XPS analysis of the kapton side of separated samples indicated expected results; the presence of elements indicative of kapton only (C, N, O), with no detection of copper. XPS analysis of the copper side of separated samples indicated the surfaces to be kapton, not copper, meaning that the separation did not occur perfectly at the interface and some kapton is riding atop the copper side sample. Figure 4 shows XPS survey scan results of a representative copper-side sample. Initially the pulled surface shows only C, O, N, indicative of kapton. However, ion sputtering to remove ~ 10 nm of material reveals a very strong copper signal, suggesting the separation of kapton and copper occurs very near their interface. Continued sputtering to remove ~ 30 nm of material shows almost complete removal of kapton, as indicated by very small carbon and nitrogen peaks. Also at this depth, XPS detects tin and palladium, elements associated with catalysts for electroless copper deposition atop kapton. Figure 5 shows the normalized XPS signals for C, O, Sn, Pd, and Cu during depth profiling of a copper-side sample. The initially (at the surface) high carbon and oxygen signals associated with kapton quickly decrease as the surface in ablated. This is associated with an immediate rise in copper signals. As the surface is ablated 20 to 30 nm, tin and palladium are observed and oxygen increases, suggesting the presence of a layer metal oxides. The tin and palladium layer is approximately 80 nm thick. The amounts of tin and palladium at their highest concentrations are modest; four atomic percent Sn and one to two atomic percent Pd. Copper concentration increases continuously with depth profiling, and within ~ 180 nm of the surface the copper is very pure.

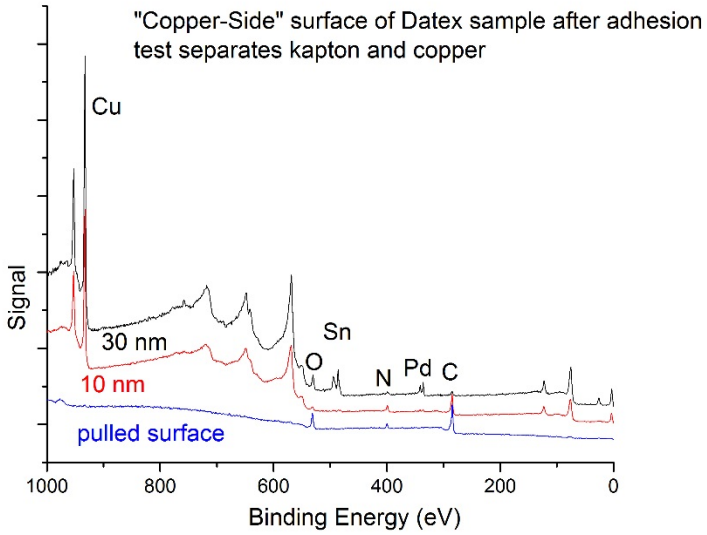

***Figure 4**: XPS survey scans of copper-side Datex microclad sample after adhesion testing has separated the kapton and copper. The sample conditions are as-received (the pulled surface), and after ~ 10 and 30 nm of ion sputtering.*

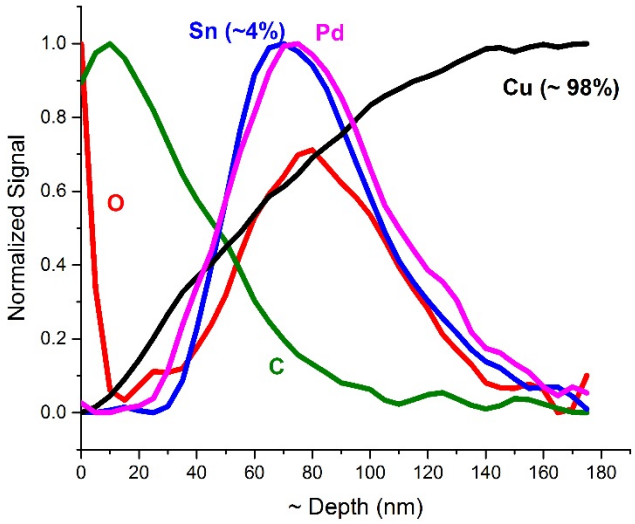

Figure 5: *XPS depth profile of the "copper side" of a Datex microclad sample that has been pulled apart (separating kapton from copper) during adhesion strength testing.*

Chemical Characterization of Microclad: Copper Purity via ICP-MS

Elizabeth Judge

Chemistry Division

The copper component of the microclad system was chemically characterized for purity via inductively coupled plasma mass spectrometry (ICP-MS). The copper purity was determined by measuring the impurities. The main impurities detected were tin and palladium which are the catalysts for the electroless plating process. Therefore, they were not considered in the purity calculation. Several minor differences were determined including copper weight percent of the microclad and impurity level. The purity results for all lots analyzed varied from 99.9986-99.9992%. Therefore, there is a high degree of similitude in the purity of the copper across the lots.

Introduction

ICP-MS is a robust analytical technique for measuring metals and some non-metals. ICP-MS is most widely known for its high throughput, very low detection limits (<ppb), and isotopic capabilities. The sample is introduced into the ICP as an aerosol, either generated by a nebulizer (solutions and dissolved solids) or through laser ablation (solids). The argon plasma ionizes the sample, the ions are separated based on mass, and then detected.

Experimental

The microclad samples were obtained from the Microclad Characterization Team. The samples that were analyzed are shown in Table 1. A 1 x 1 cm square sample from each Datex Lot (D03, D13, and D16) and Fortin Lot were cut in ~ 1 x 1 cm squares for inter-lot comparison. One sample from each lot was analyzed for intra-lot comparison and is highlighted in italics in Table 1 and denoted by a, b, and c. The mass, length and width were recorded for each 1 x 1 cm square. Next, each sample was etched in ~25% HNO_3 for 5 minutes. The Kapton was removed from the acid and dried. The final weight of the Kapton was recorded and the difference between the microclad and the etched Kapton was the amount of copper etch. The mass of copper was used to determine the purity, based on the impurities detected.

Datex 2003 Lot	Datex 2013 Lot	Datex 2016 Lot	Fortin Lot
D03-8B-A	*D13-68A-A*	*D16-10-I-A*	FORTIN 160
D03-8B-B	*D13-68A-B*	*D16-10-I-B*	FORTIN 175
D03-8B-C	*D13-68A-C*	*D16-10-I-C*	
D03-9B	D13-75A	D16-4-G	
D03-24B	D13-83A	D16-5-G	
D03-19A	D13-56A	D16-7-D	
D03-6A	D13-57A	D16-5-D	
	D13-79B	D16-4-D	
	D13-62A	D16-9-F	
	D13-71B		
N=7	N=10	N=9	N=2

Table 1. List of samples analyzed using ICP-MS. Italicized lot IDs represent the intra-lot samples. The number of samples per lot is recorded in the last row as N equals (N=).

A Thermo Scientific iCAP Q ICP-MS was used to analyze the copper solutions for impurities. A survey scan of the samples was performed to determine the impurities present. The survey scan showed many impurities including Al, Fe, Zn, Mo, Ag, Cd, Hg, Pb, Sn, and Pd. Therefore, standards were prepared in order to quantify the impurities. The standards were spiked with 10 ppb of the internal standard indium and 250 ppm of Cu to matrix match to the samples. The standards were finally diluted to 10 mL in 2% HNO_3. Calibration curves were obtained for all elements with correlation coefficients (R^2) greater than 0.99. Samples were diluted by a factor of 10 with 2% HNO_3 and spiked with 10 ppb of indium. The results presented here have been corrected for the dilution factors and mass of copper etched.

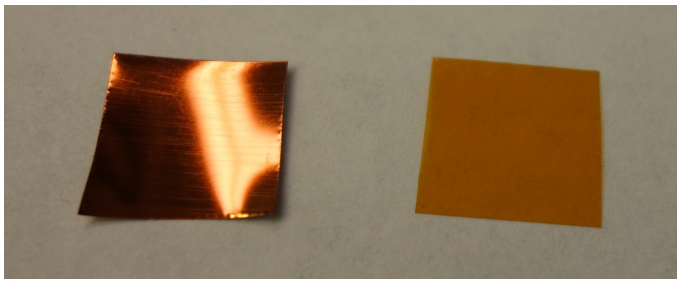

Figure 1. Photograph of the microclad before (left) and after (right) nitric acid etching.

Results and Discussion

Copper Mass and Coverage

The sample preparation yielded additional information about the mass of copper etched per lot, as shown in Table 2. The copper weight percent (mass:mass, wt%) of the microclad system is shown as an average of each lot in the second column of Table 2. The copper coverage, a measure of mass per area, is shown in the last column of Table 2. The D03, D13 and Fortin lots all have reported values within errors of each other. The outlier is lot D16 which has the lowest values for copper wt% and coverage.

	Cu Wt% of Microclad Average +/- Std. Dev.	**Cu Coverage (mg/cm^2) Average +/- Std. Dev.**
D03	35.56 +/- 0.98	3.71 +/- 0.15
D13	34.55 +/- 2.10	3.63 +/- 0.37
D16	32.91 +/- 0.83	3.26 +/- 0.12
Fortin	34.59 +/- 1.45	3.55 +/- 0.32

Table 2. Average mass of copper etched per lot reported as a weight percent (wt%) of the microclad and as a mass per area (mg/cm^2).

Interface Impurities

The two main impurities detected in the copper purity analysis were tin and palladium. Both tin and palladium are known to be catalysts ($SnCl_2$ and $PdCl_2$) for the electroless copper plating process. Therefore, these impurities are coming from the interface and not the copper metal. As such, Pd and Sn are reported as $\mu g/cm^2$ and not included in the purity calculation. Figure 2 shows the bar graphs for the Pd and Sn mass coverage area ($\mu g/cm^2$) where the lots are represented as follows: black - D03, red – D13, blue – D16, and green – Fortin. The average ratio of Sn:Pd for the electroless copper plating process varied between the lots. The D03 and D13 had an approximate ratio of 3:1 whereas the D16 and Fortin have closer to a 2:1 ratio.

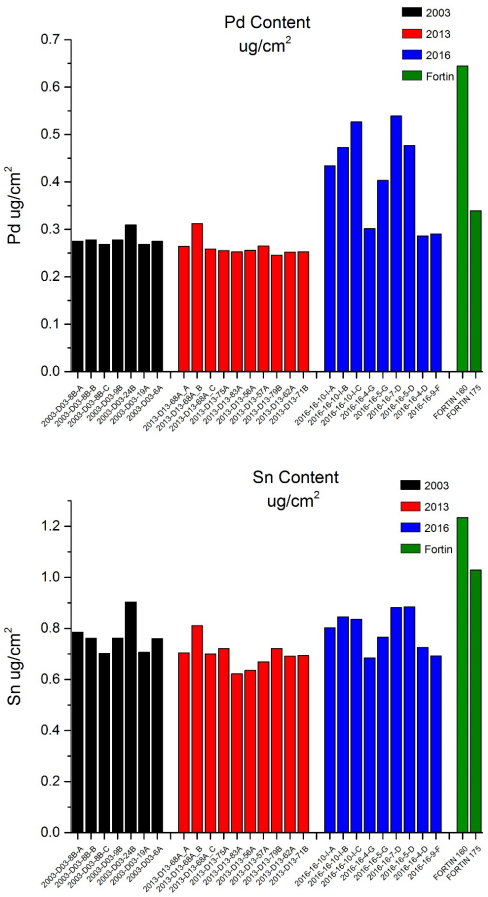

Figure 2. Palladium (left) and tin (right) mass per area (μg/cm^2) per lot. The bar graphs represent the different lots: black - D03, red – D13, blue – D16, and green – Fortin.

Impurities in Copper

The purity of the copper was determined based on the impurities detected. Equation 1 shows the calculation used to determine the purity. The requirement for the copper purity is >99.8% (Specification 9Y294599).

$$\text{Cu Purity} = 100\% - \%\ \text{impurities (Al, Pb, Ag, Fe)} \qquad (1)$$

The main impurities detected were aluminum (Al), lead (Pb), silver (Ag), and iron (Fe). Figure 4 shows the graphical representation of the impurities within each lot and between each lot. Aluminum varies between 4-9 ppm for most samples and lots. Silver shows more of a trend where the D03 and D13 lot have less than 1 ppm of Ag and the D16 lot has more than 2 ppm. This difference appears to be statistically represented however the difference between 1 and 2 ppm is very low and too much should not be gleaned from this difference. The lead contamination is much higher and more uniformly represented in the D16 and Fortin lot. Lastly, the iron impurity appears to be random. Based on these results, the copper purity was calculated

and is shown in Table 3. The differences observed in the impurity level are no longer obvious since the results are between 99.9986 and 99.9992 wt%. The final copper purity for all the lots are within the error (standard deviation). Figure 4 shows the graphical representation of the copper purity.

As a final measure, the tin and palladium were included in the purity calculation, Table 4. The results for all lots are still higher than 99.95 % copper where the Specification only requires > 99.8%.

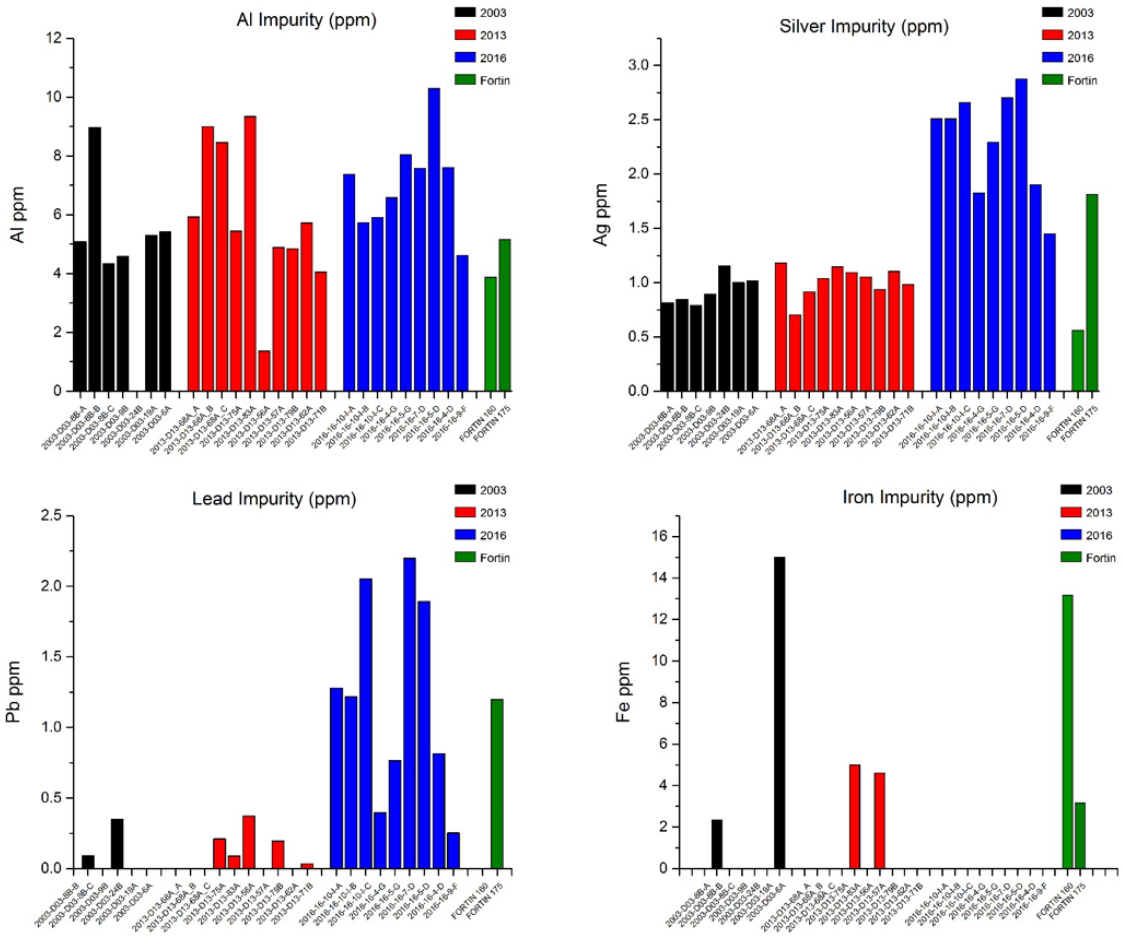

Figure 3. Four main impurities detected in the analysis of the copper coating: *top left* Aluminum (Al), *top right* Silver (Ag), *bottom left* Lead (Pb), and *bottom right* Iron (Fe).

	Average Cu Purity (wt%)	Std. Dev (wt%)
D03	99.9992	0.0007
D13	99.9992	0.0004
D16	99.9989	0.0002
Fortin	99.9986	0.0004

Table 3. Average copper purity for each lot based on the impurities detected.

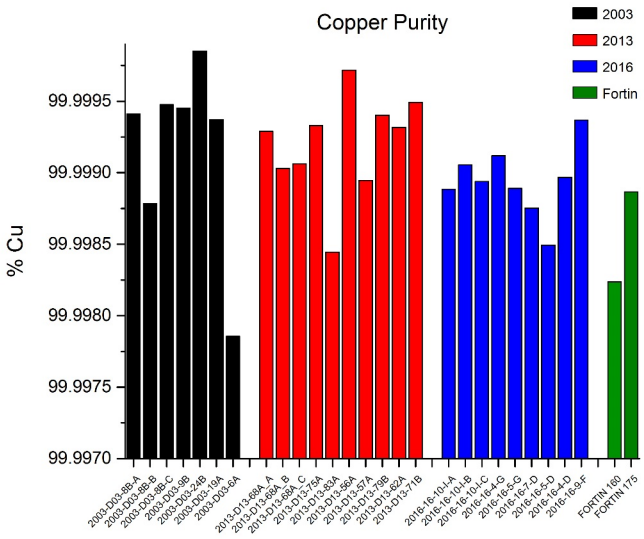

Figure 4. Bar graph of the copper purity as seen for each sample and grouped based on lot.

	Average Cu Purity* (wt%)	Std. Dev (wt%)
D03	99.9709	0.0017
D13	99.9726	0.0029
D16	99.9619	0.0056
Fortin	99.9522	0.0149

*Including Sn and Pd

Table 4. Average copper purity including the interface impurities, tin and palladium.

Conclusion

The ICP-MS results on the copper purity suggest the copper is very pure. The major impurities were the interface catalysts; tin and palladium. These were removed from the general calculation of copper purity. The impurities used to determine the copper purity were Al, Ag, Pb, and Fe. Some of these impurities varied from lot-to-lot, statistically speaking, but at such low levels that the final purity value for every lot was within error. The amount of copper (wt % and coverage in mg/cm^2) was lower for the D16 lot compared to the D03, D13 and Fortin lots. The interface catalysts, Sn and Pd, also showed a difference for the D16 lot. The ratio of Sn:Pd for the D03 and D13 lot was ~3:1 while it was ~2:1 for the D16 lot. Overall, the intra-sample (the replicates of a, b, and c for a single sample from each lot) were comparable to the entire lot. Finally, based on the purity calculations, the small fluctuations of impurities from the inter-lot comparison result in copper purities within standard deviations of each other. Therefore, there is a high degree of similitude in the purity of the copper across the lots.

Microclad Characterization by NMR and Solvent Swelling Experiments

Andrea Labouriau

Chemistry Division - Chemical Diagnostics and Engineering Group

Summary

Nuclear Magnetic Resonance (NMR) spectroscopy was used to evaluate extractable material from a variety of microclad lots (Datex 03, Datex 13, and Datex 16). No significant quantities of extracts were detected by ^{1}H NMR, probably an indication of very low concentration of unreacted species or other low molecular-weight compounds like additives. In addition, solvent swelling experiments were also performed to evaluate changes in the polymer microstructure. There was variability in the solvent uptake from lot to lot, but no trends were identified. ***Nothing in the NMR and solvent swelling data suggest any microclad lot should be considered unacceptable in comparison to any other lot.***

Experiments, Results, and Discussion

We performed solvent swelling and Nuclear Magnetic Resonance (NMR) experiments on the polyimide (Kapton) of microclad lots (Datex 03, Datex 13, and Datex 16) to identify any variations between lots. Solvent swelling experiments measure solvent uptake by the polymer and normally are dependent on the polymer cross-link density as established by the Flory-Higgins theory.[1,2] This experiment is one of the preferred methods to gauge variations in polymer network due to its easiness to perform. In the case of polyimides, it has been demonstrated that solvent swelling depends markedly on the preparation conditions of the polymer like deformation and molecular orientation.[3,4] Our swelling experiments were performed using approximately 0.11 g of Microclad immersed in 3 mL methyl sulfoxide (DMSO-d6). The solvent used was deuterated so it could be used in the ^{1}H NMR experiment as well. DMSO-d6 was purchased from Acros-Organics in 0.75 mL ampoules, 99.95% deuterated. Figure 1 shows that the microclad material curls after immersion in the solvent for 3 or more days. This effect demonstrates the wetting of the material by DMSO, whereas this curling effect was not observed when the material was immersed in water. It is worth pointing out that no delamination or separation was observed for any of the swollen samples, they remained whole after the solvent immersion.

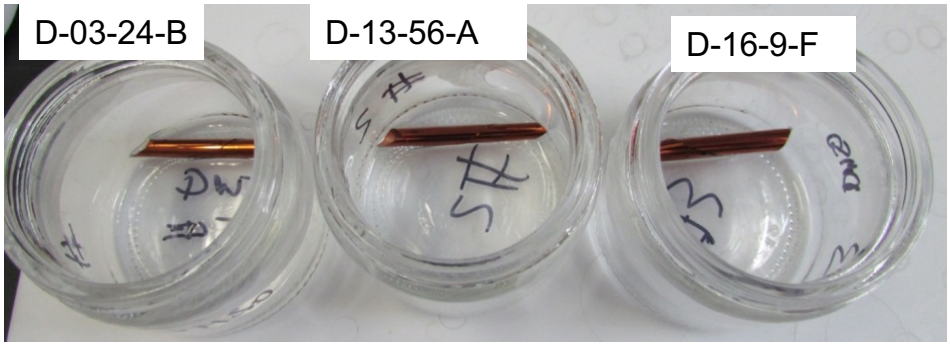

Figure 1. Samples swollen in DMSO.

Two specimens per lot were analyzed by this method. Swollen samples were periodically weighed until saturation was reached. Equilibrium weights were recorded at the end of the experiment. Results are listed in Table1. The average swelling for D-03 lot was 47%, 43% for the D-13 samples and 36% for D-16 samples. There were a few samples that had lower solvent uptake (and didn't curled completely) such as D-16-10-I and D-16-7-D. Thus, the spread was larger for D-16 samples than for the other lots.

Sample ID	%Swelling	Sample ID	%Swelling	Sample ID	%Swelling
D-03-9-B	41	D-13-56-A	36	D-16-4-D	59
D-03-19-A	50	D-13-62-A	53	D-16-5-G	50
D-03-24-B	43	D-13-68-A	38	D-16-9-F	40
D-03-6-A	45	D-13-71-B	49	D-16-4-G	59
D-03-8-B	58	D-13-75-A	47	D-16-5-D	50
		D-13-79-B	40	D-16-10-I	26
		D-13-83-A	49	D-16-7-D	31

Table 1. Swelling data obtained for various microclad samples.

NMR spectroscopy was used to probe changes in the material's chemistry. This technique is commonly used to obtain detailed information about the structure, dynamics, reaction state, and chemical environment of molecules. The basic condition for the NMR signal relies on the phenomenon of nuclear magnetic resonance, which is usually described by: $h\nu = \mu H_0 (1-\sigma)/I$, where ν is the radio frequency, H_0 is the applied magnetic field, σ is the shielding constant (resulting from diamagnetic susceptibility), μ is the magnetic moment of the nucleus, I is the spin quantum number ($\pm 1/2$ for ^1H) and h is the Planck's constant. NMR is particularly used in organic chemistry since it provides unique, well-resolved, and analytically useful chemical information. For instance, the number of signals found in the ^1H NMR spectrum corresponds to the number of non-equivalent proton groups in the molecule. Furthermore, identical functional groups with differing neighboring substituents may appear in the NMR spectrum as distinguishable signals as well. Extracted material was obtained from the microclad with the objective to isolate and detect low molecular weight fragments resulting from unreacted monomers, additives, synthesis by-products, etc. Extracts were analyzed by liquid-state ^1H NMR spectroscopy using a Bruker Avance spectrometer operating at 500.13 MHz for ^1H. The extracts were found to be composed mainly of a large peak corresponding to residual protons from the solvent and from residual water (Figure 2). Thus, even though DMSO is expected to be a good solvent for the starting compounds that make up the polymer in Microclad, no significant NMR signal was detected. In addition, we also used chloroform (another high polar solvent) to extract the samples and observe an NMR signal to no avail. Based on these results, we infer that the concentration of unreacted species or other low molecular-weight compounds is likely to be very low.

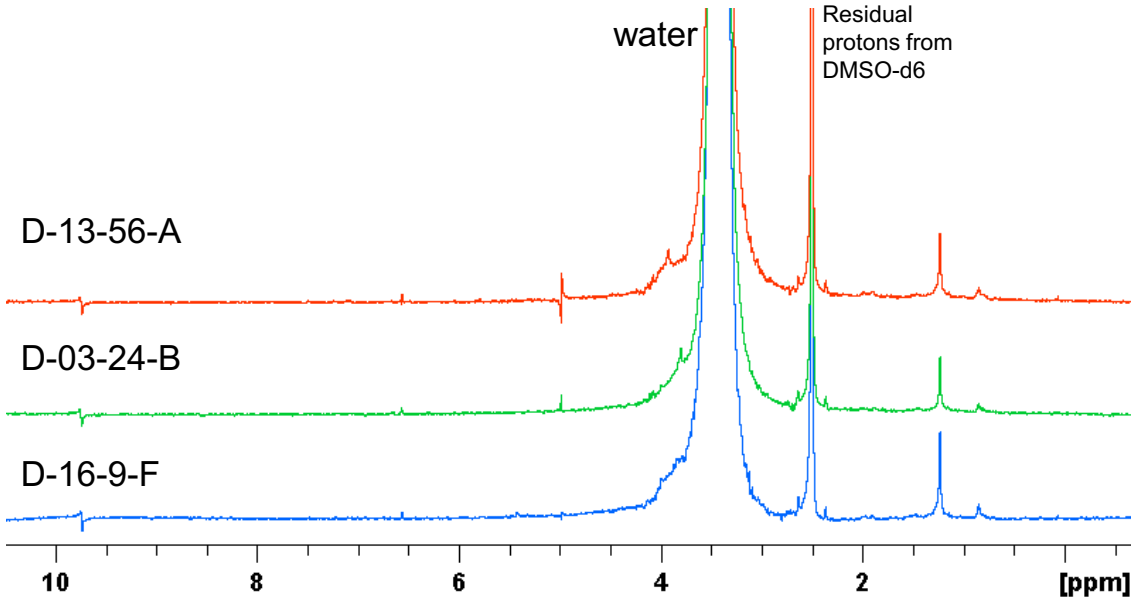

Figre 2. ^{1}H NMR spectr of extracts obtained from Microclad samples, the peak at about 1.25 ppm may be due to silicones like grease.

References.

(1) *Flory, P. J.; Rehner, J. Journal of Chemical Physics **1943**, 11, 512.*

(2) *Flory, P. J.; Rehner, J. Journal of Chemical Physics **1943**, 11, 521.*

(3) *Gattiglia, E.; Russell, T. P. J Polym Sci Pol Phys **1989**, 27, 2131.*

(4) *Russell, T. P.; Gattiglia, E.; Yang, A. C.; Brown, H. R.; Volksen, W.; Kramer, E. J. Abstr Pap Am Chem S **1987**, 194, 10.*

Scanning Electron Microscopy (SEM) and Electron Backscatter Diffraction (EBSD) of Cu/Kapton

Rodney J McCabe, Rafael Spillers, and Cody Miller

Materials Science and Technology Division

Experimental

Scanning electron microscopy (SEM) encompasses several analyses that involve scanning an electron beam across a sample in a grid pattern and analyzing the signals coming from the specimen. Techniques utilized in the microclad study include secondary electron imaging (SEI), backscatter electron imaging (BEI), x-ray energy dispersive spectroscopy (EDS), and electron backscatter diffraction (EBSD). SEI involves forming an image from the the low energy electrons emitted from the specimen surface as the incidence beam of electrons is scanned across the specimen in a grid, and usually provides topographical contrast of the specimen surface. BEI forms a similar image from the higher energy, back scattered electrons and normally provides z-number and/or density contrast. When incident electrons interact with bound electrons in the specimen, x-rays are emitted that are characteristic of the elements in the specimen. EDS techniques involve collecting these x-rays to create energy spectra that can be used to determine some aspects of sample chemistry. Finally, back scattered electrons will also form a Kikuchi pattern that can be collected to determine crystallographic orientation. This data is used to determine grain size, orientation, and morphology and orientation distributions (crystallographic texture).

Microclad samples were analyzed in the SEM in plan-view, looking down either on the Cu or Kapton surfaces, and in cross-section. Plan-view samples mounted for analysis of the Cu side were cut from the Microclad sheets and bonded to 10 mm diameter SEM stubs using super glue and electrically grounded by painting around the periphery with colloidal graphite. Plan-view samples mounted for analysis of the Kapton side were adhered to the SEM stubs using carbon tape, and were grounded by coating the Kapton surface with less than 1nm of sputtered gold. SEI and most EDS analysis was performed without any further preparation of the specimen surfaces. It was only possible to get good EBSD results from the as received surface of the Fortin 160 sample. For all other EBSD samples, the surfaces were first cleaned on a neoprene polishing cloth with acetone followed by isopropanol, and then electropolished in a stirred solution of 40% Phosphoric acid in water for 5 seconds at 20V. Cross-section samples were mounted on edge using vacuum impregnation with a slow curing epoxy (10:1 Epon 815 resin and diethylenetriamine) followed by pressure curing. Mounted samples were mechanically ground using SiC papers from 120 to 800 grit and then mechanically polished using 3µm diamond, 1µm diamond, and 0.05µm colloidal silica. SEM was performed in an FEI Inspect F and EBSD and EDS data was collected using TSL/EDAX systems. SEM of plan-view and in cross-section samples was performed on a single Fortin 160 sample, one Fortin 175 sample, three D03 samples, four D13 samples, and three D16 samples to examine inter-batch variability. The difficulty of obtaining good EBSD results limited EBSD to a single sample for every batch.

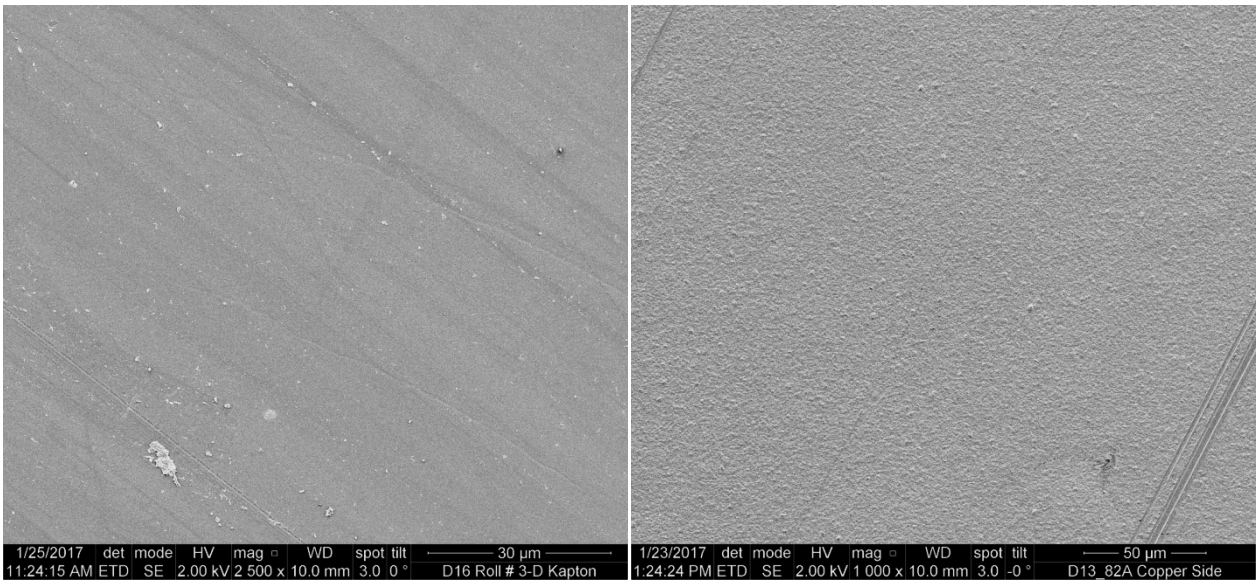

Figure 1. Relatively low magnification SEI images of a) the Kapton surface of the D16 3D sample and b) the Cu surface of the D13-B2A sample. All of the observed samples had some degree of scratching on both surfaces.

Results

SEI analysis of the Cu and Kapton surfaces in plan-view primarily provides qualitative information concerning surface defects and roughness. Figure 1 shows relatively low magnification SEI images of a D16 Kapton surface and a D13 Copper surface. Surfaces for all of the observed samples exhibited some scratches on both surfaces similar to as shown in Figure 1.

There is some variation in Kapton surfaces for the different lots. Qualitatively, Fortin 160, D03, and D16 appear very similar with a fine scale roughness on the surface, and an example from the D16 3D sample is shown if Figure 2a. Fortin 175 and D13 appear smoother with a fine scale cracking on the Kapton surface similar to as shown in Figure 2b. For inter-batch comparisons, the D03 and D16 samples are all similar and the D13 samples have some variance in the

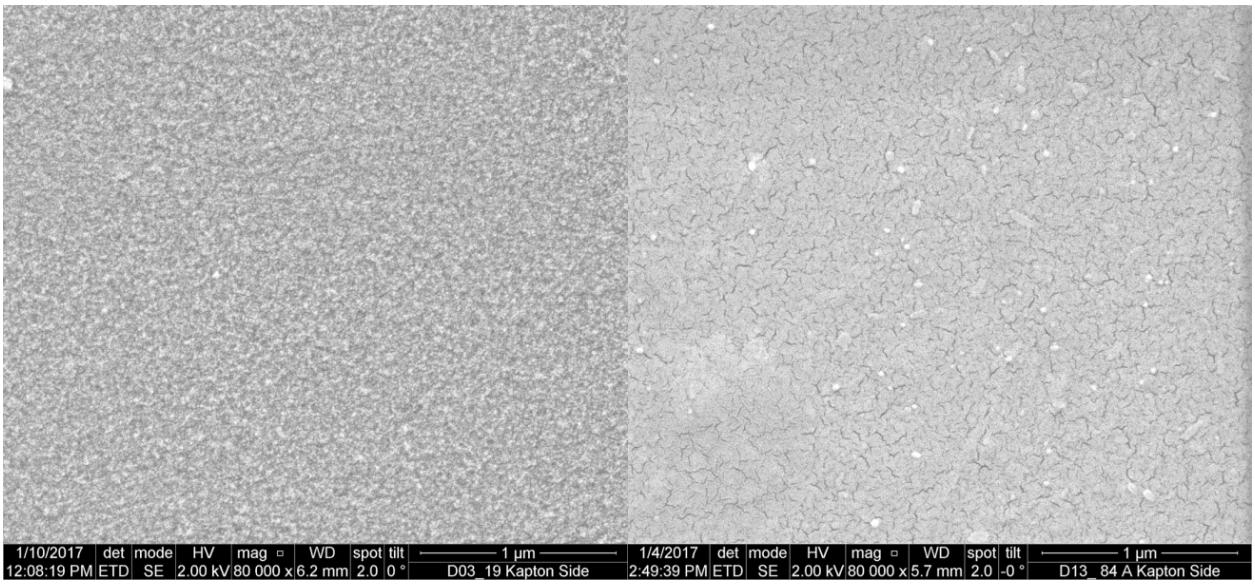

Figure 2. Kapton surfaces of a) D03 19 and b) D13 84A. Fortin 160, D03, and D16 exhibited similar surfaces with a fine scale roughness. Fortin 175 and D13 exhibited similar cracked surfaces.

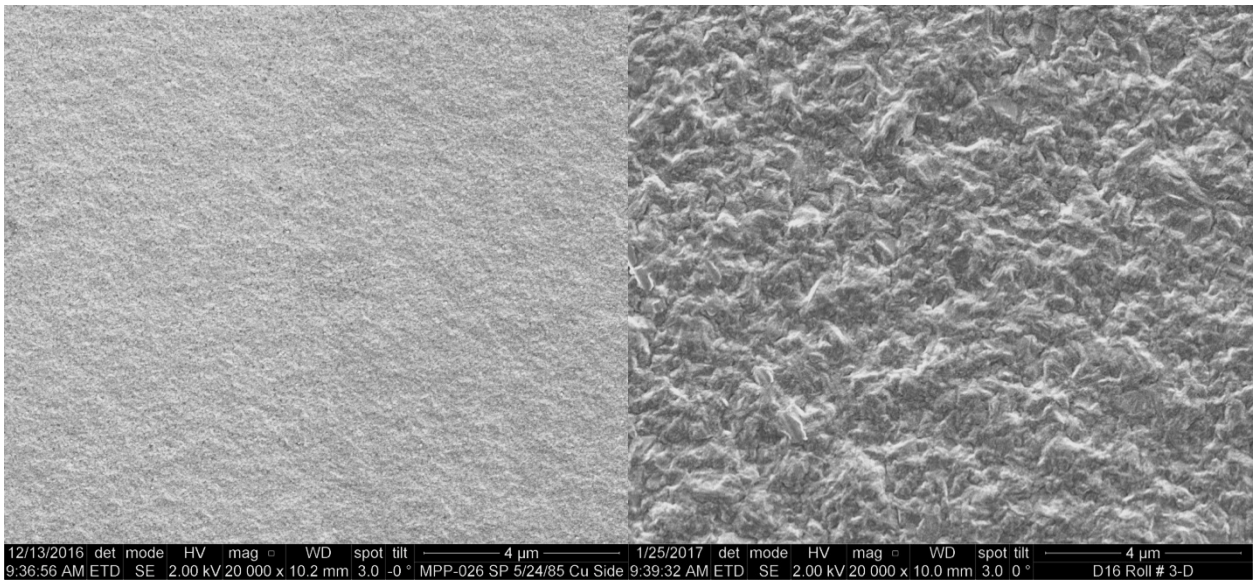

Figure 3. Copper surfaces for a) Fortin 16 and b) D16 3D. The Fortin 160 has the finest scale surface roughness and Fortin 175 has a similar though slightly rougher appearance. surFortin 160, D03, and D16 exhibited similar surfaces with a fine scale roughness. Fortin 175 and D13 exhibited similar cracked surfaces.

smoothness of the Kapton surfaces.

Similarly, there is batch to batch variation in the Cu surfaces with Fortin 160 having the finest scale roughness followed by Fortin 175. D03, D13, and D16 samples appear similar and all have considerably larger scale roughness than the Fortin samples. Examples for Fortin 160 and D16 are shown in Figure 3 a) and b), respectively. There is very little inter-batch variability for any of the batches.

Some SEI cross-section micrographs are shown in Figure 4 and **estimates** of Kapton and Cu thicknesses are given in Table I. It is difficult to accurately measure Cu thickness because there is significant variability in many of the specimens due to a lower density Cu layer on the top surface. All estimates in Table I are for the high density Cu layer. All of the samples have a relatively smooth interface between the Kapton and Cu, and in each Figure, the bottom of the Cu is the Cu/Kapton interface. There is significant variability in the Cu cross-sections batch to batch, sample to sample, and even within the same mounted sample as detailed in the Figure 4 caption.

Table I. Estimates of Kapton and high density Cu thicknesses for the different batches. Average Cu grain sizes measured from EBSD. Special (twin) boundaries are considered grain boundaries for this grain size calculation.

	Fortin 160	Fortin 175	D03	D13	D16
Kapton Thickness (µm)	47.5	48.5	48	47.5	48
Copper Thickness (µm)	4	4.3	4	4	4.2
Copper Average Grain Size(µm)	0.54	0.48	0.29	0.31	0.34

EDS analysis does not have the spatial or composition accuracy to examine the trace elements at the interface. All EDS analysis from the Kapton surfaces only show carbon and oxygen peaks, and EDS spectra from the Cu surfaces only exhibited copper with small carbon and oxygen peaks. Sample D16 7B had some organic contamination particles in the Cu that were brought out

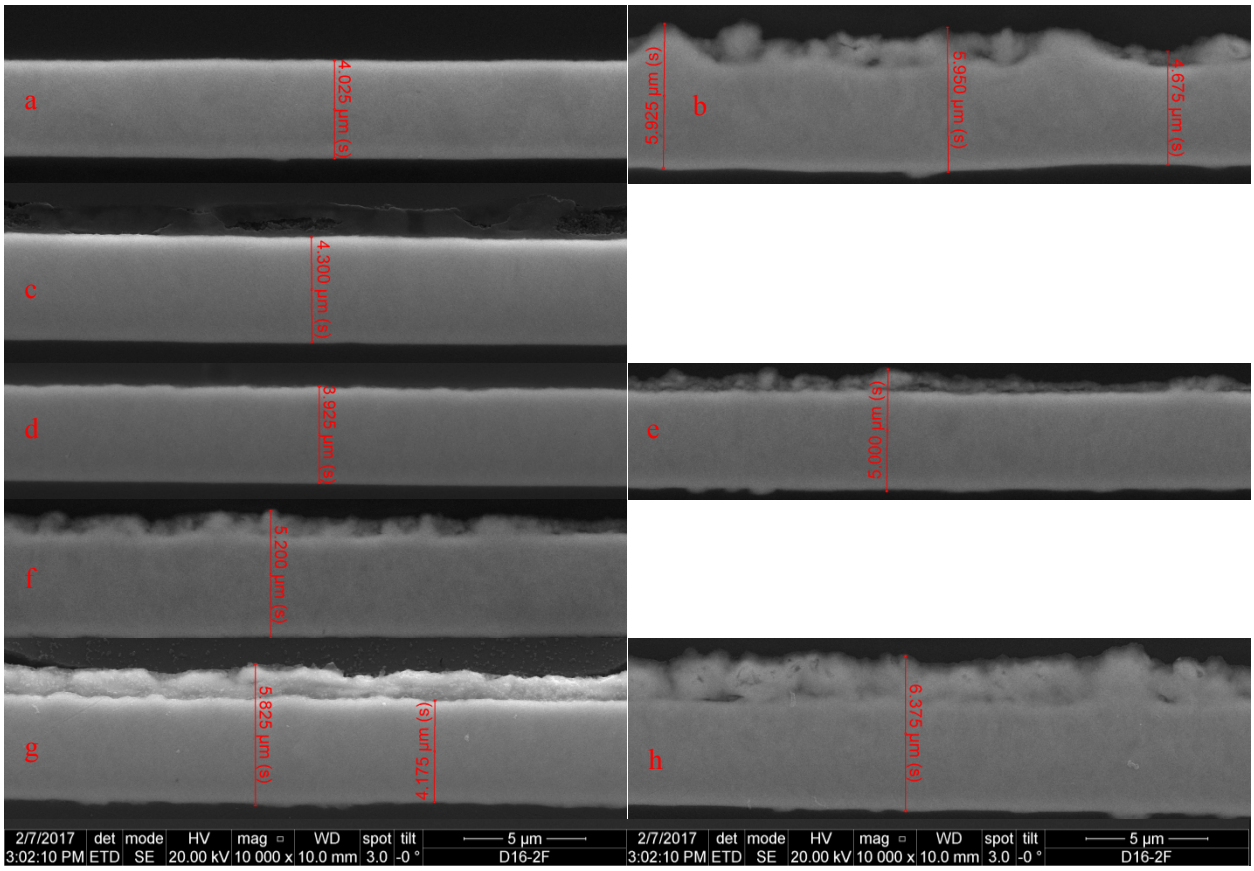

Figure 5. Cross sections of Cu with the bottom of the Cu being the Cu/Kapton interface. a) Fortin 160, b) Fortin 160 from a different area on the same mount exhibiting a lower density Cu region on the top surface, c) Fortin 175 exhibiting a contamination layer on the top of the Cu, d) an area of D03 19 with a relatively clean and smooth top surface, e) an area of the same D03 19 sample with a thin layer of lower density Cu on the top surface, f) D13 80A characteristic of most D13 samples examined, g) D16 2F, and h) D16 3D where both samples exhibit a relative thick layer of lower density Cu on the top surface. All samples have similar thickness of high density Cu, but some have significant differences in presence and thickness of low density Cu on the top surface.

during the electropolishing process. An SEM micrograph and EDS spectrum from one of the particles is shown in Figure 5.

EBSD orientation maps for Fortin 160 and D16 2F are shown in Figure 6. There are significant differences in the Cu microstructures between the Fortin samples and the Datex samples. The Cu grain size in the Fortin samples is around 67% bigger than for the Datex samples, and a majority of boundaries in the Fortin samples are special, low energy (twin/CSL) boundaries. Crystallographic textures for the Cu

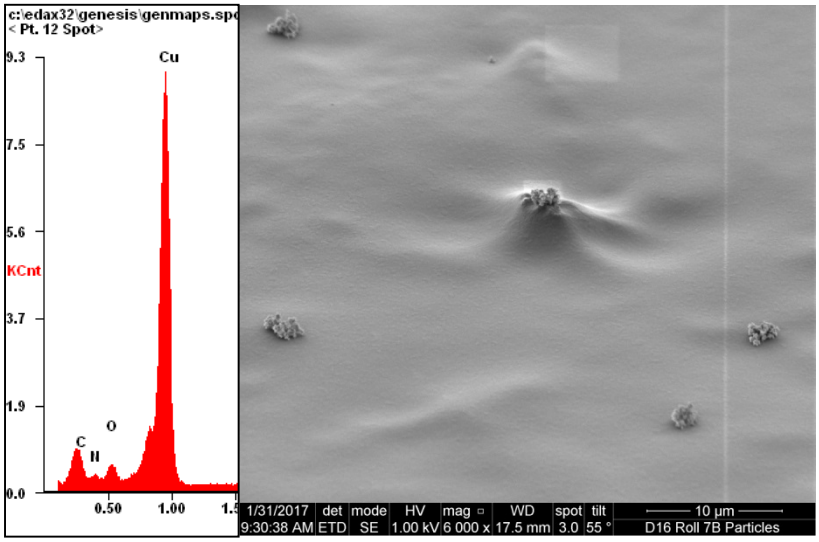

Figure 4. Organic particles that were embedded in the Cu for sample D16 7B brought out during electropolishing.

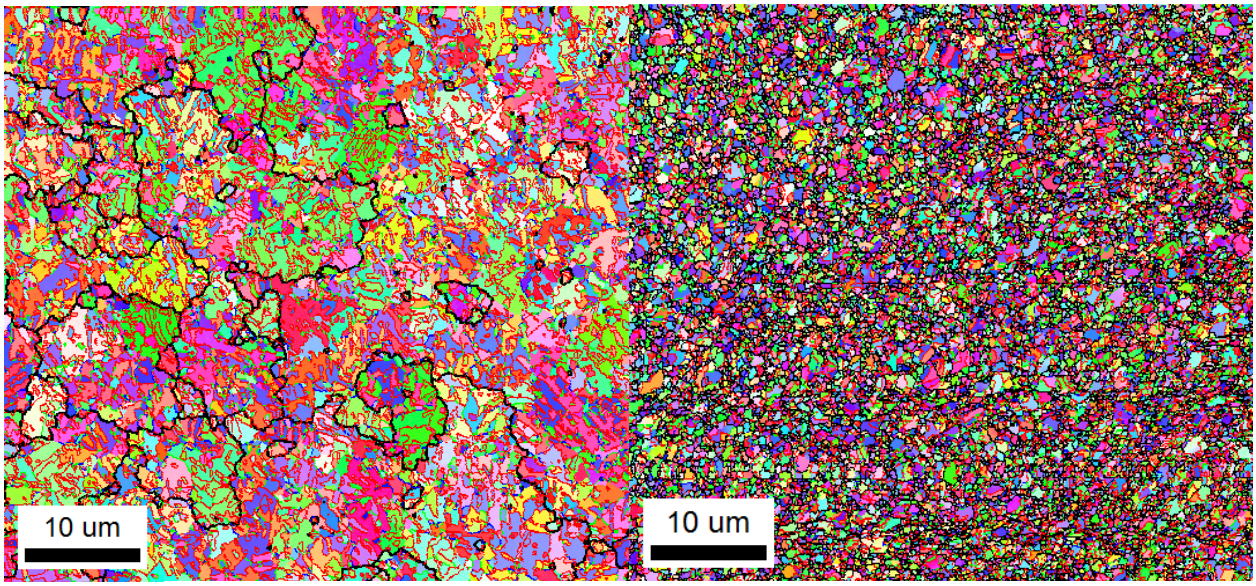

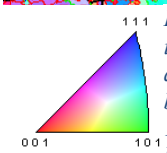

Figure 6. EBSD based inverse pole figure (IPF) orientation maps for a) Fortin 160 and b) D16-2F. The colors in the map indicate the copper grain crystal direction in the foil plane normal direction. The black boundaries are general high angle grain boundaries. The red, green, and blue boundaries are special low energy boundaries (also known as twin or coincident site lattice (CSL) boundaries) that are common in copper. Fortin 175 appears similar to the Fortin 160 with some clustered regions of grains with general high angle grain boundaries. D03 and D13 look similar to the D16 with slight differences in average grain size.

of the micro-clad specimens are weak for all batches. All of the samples have a small tendency to exhibit a (011) texture peak in the normal direction with magnitudes generally less than two.

Similitude

The most dissimilar aspect of the different batches pertains to the Cu microstructure. The thicknesses of the high density Cu regions of each sample are similar though the rough surface regions of the Cu in the different batches vary significantly. The grain sizes are somewhat different between the Fortin and Datex samples, and the densities of boundary types are significantly different.

Differences in boundary densities may be expected to have an effect on some properties of Cu. For instance, some defect densities in metals affect electrical resistivity and it might be expected that the Datex samples would have slightly higher resistivity. General high angle grain boundaries are also more likely to act as void nucleation sites during mechanical loading. Finally, and perhaps most importantly, high angle grain boundaries are expected to be more susceptible to corrosion and other environmental effects.

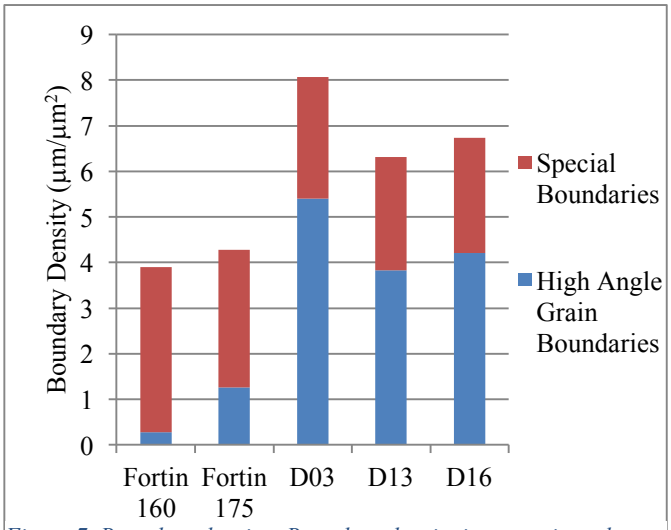

Figure 7. Boundary density. Boundary density is approximately inversely proportion to grain size. The Fortin samples have a low density of general grain boundaries and the Datex samples have a significantly higher density.

Appendix: SEM/EBSD

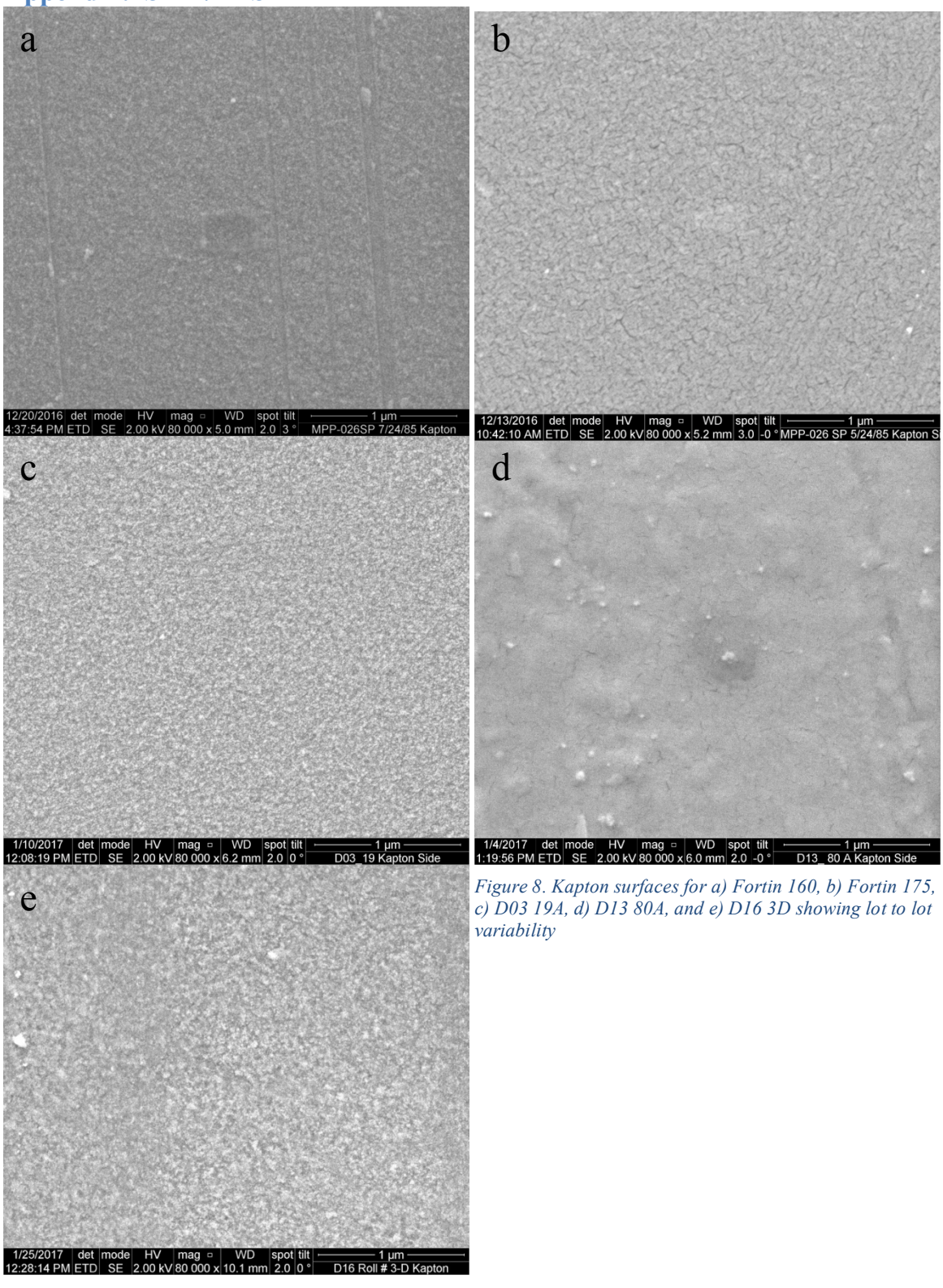

Figure 8. Kapton surfaces for a) Fortin 160, b) Fortin 175, c) D03 19A, d) D13 80A, and e) D16 3D showing lot to lot variability

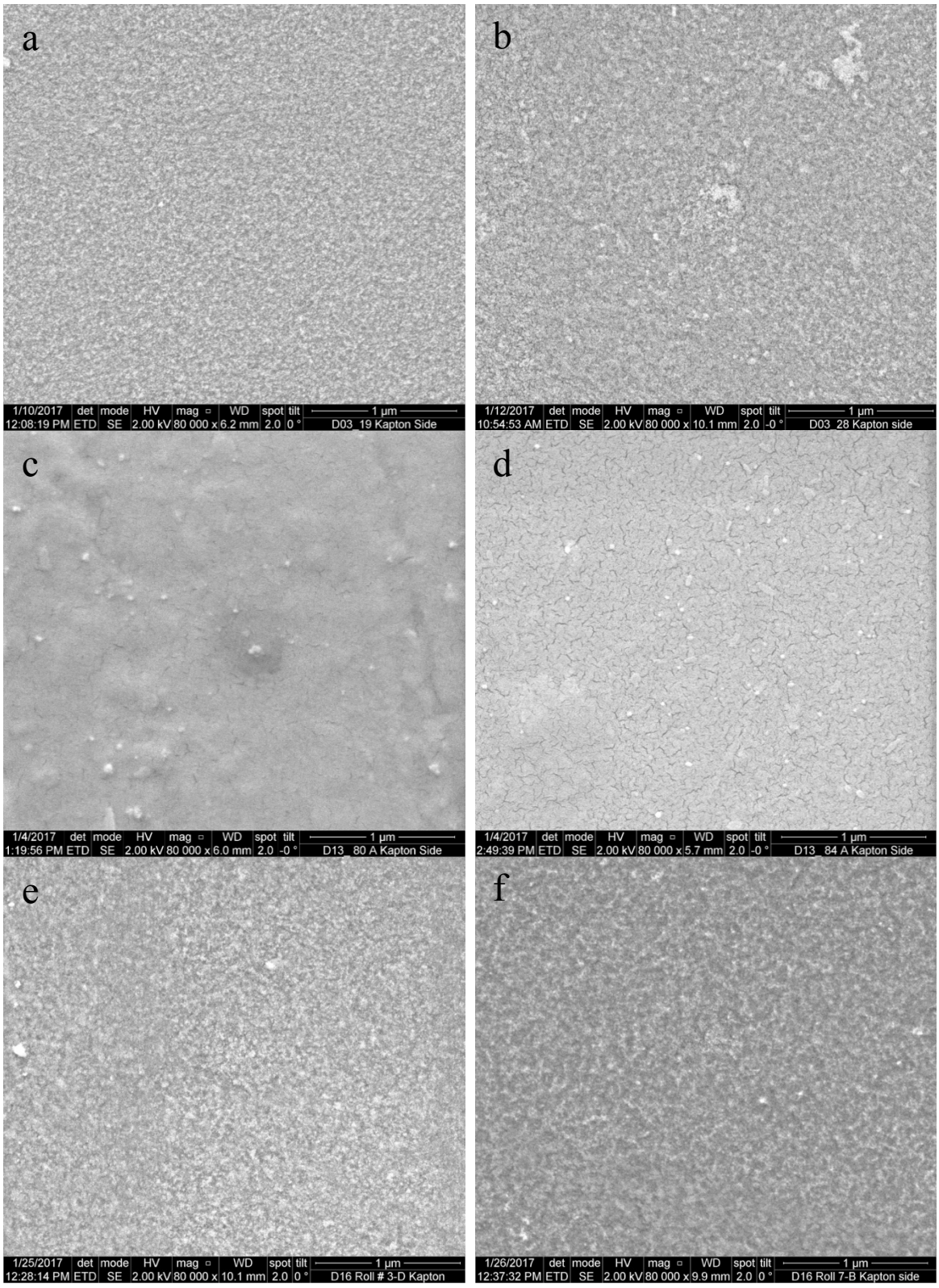

Figure 9. Kapton surfaces for a) D03 19A, b) D03 28A, c) D13 80A, d) D13 84A, e) D16 3D, and f) D16 7B showing inter-lot variability.

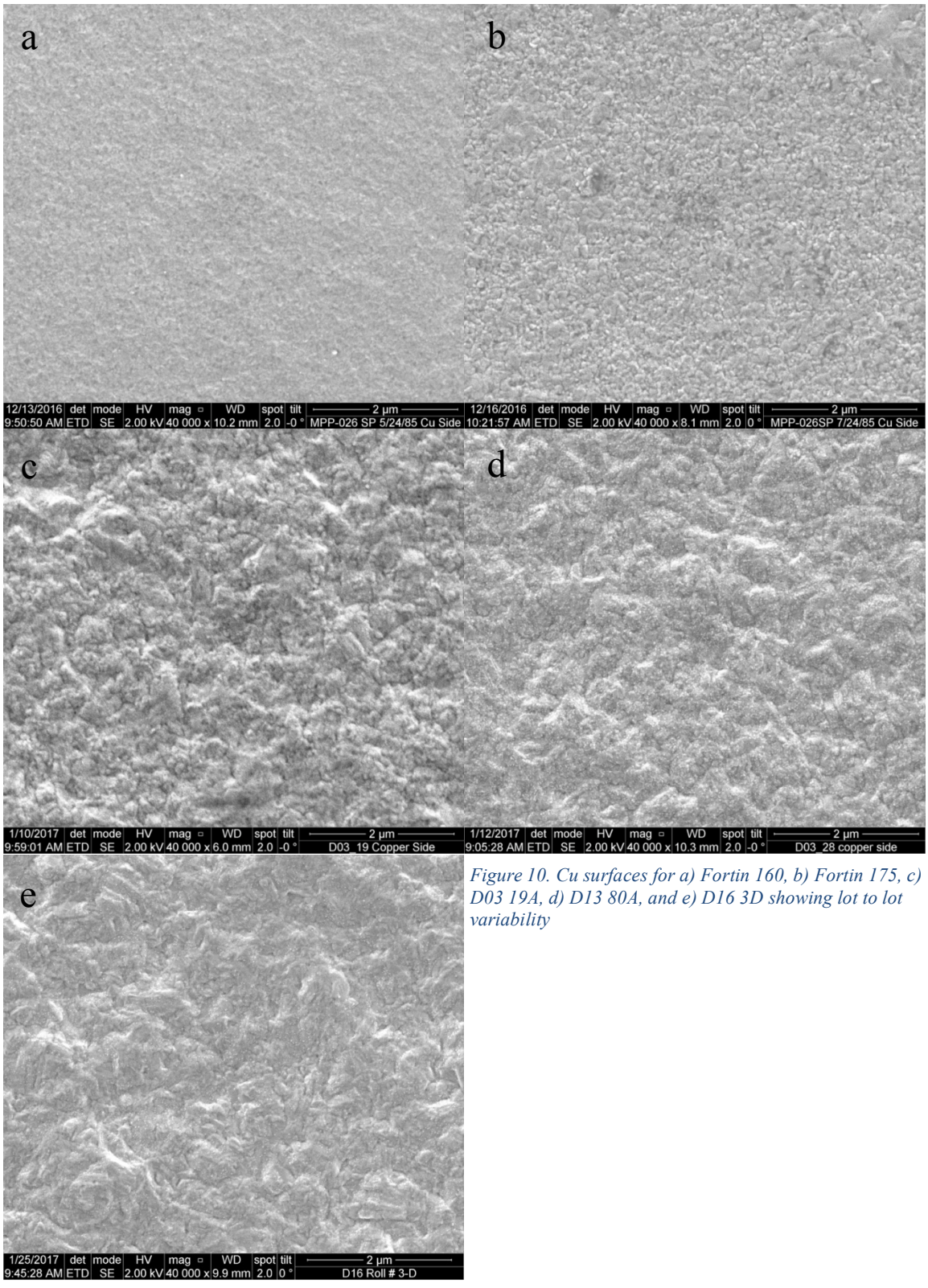

Figure 10. Cu surfaces for a) Fortin 160, b) Fortin 175, c) D03 19A, d) D13 80A, and e) D16 3D showing lot to lot variability

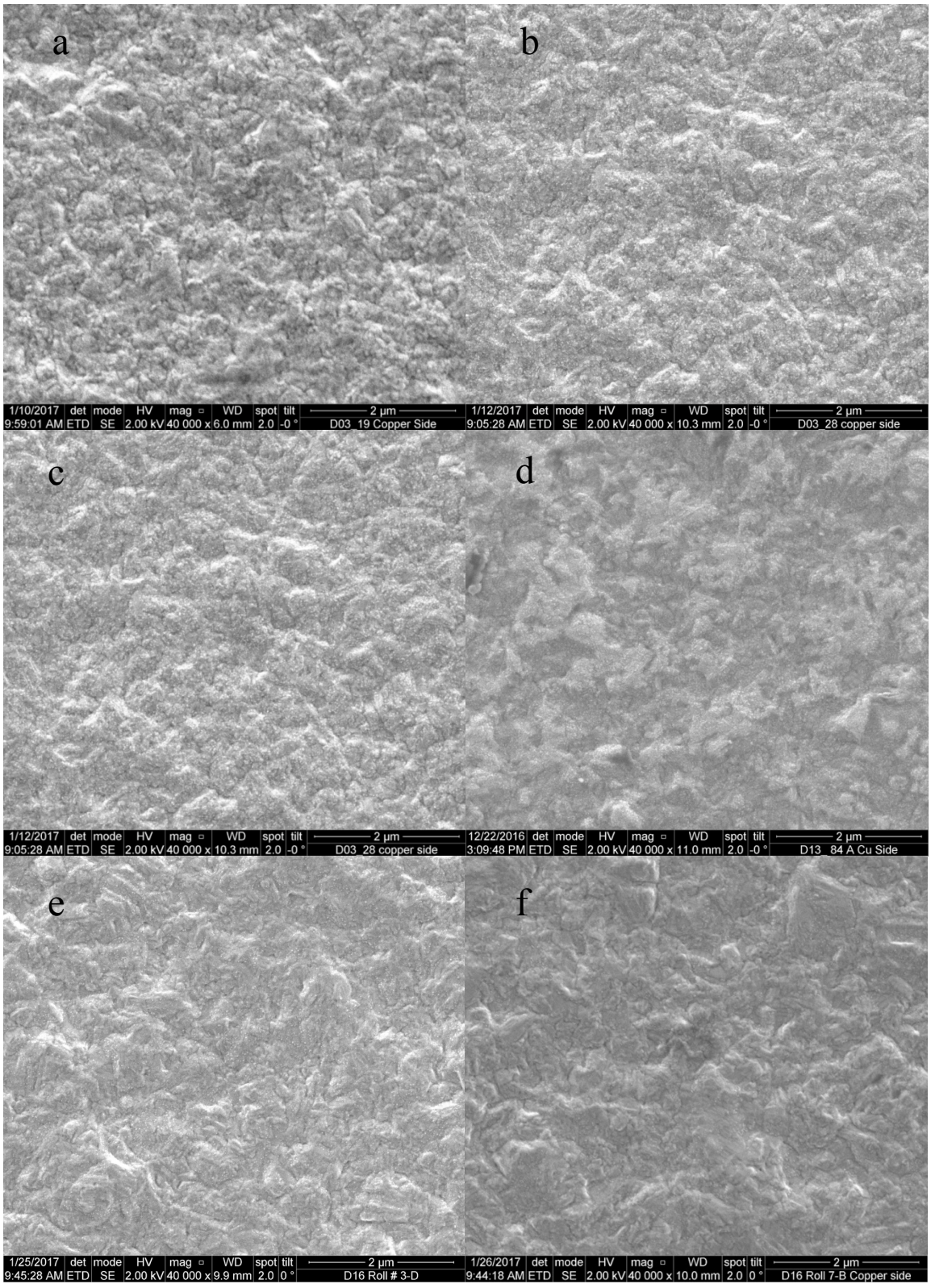

Figure 11. Cu surfaces for a) D03 19A, b) D03 28A, c) D13 80A, d) D13 84A, e) D16 3D, and f) D16 7B showing inter-lot variability.

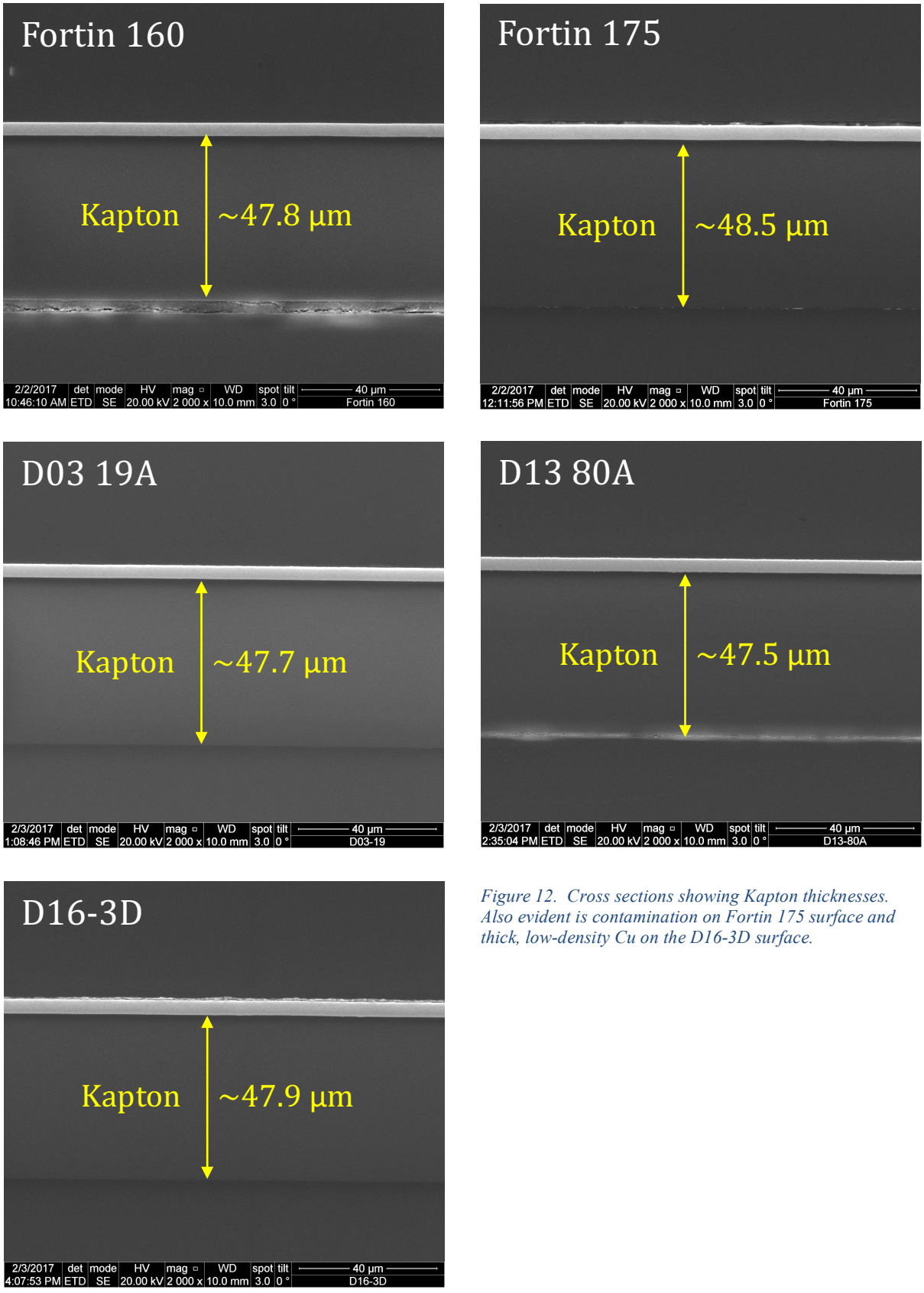

Figure 12. Cross sections showing Kapton thicknesses. Also evident is contamination on Fortin 175 surface and thick, low-density Cu on the D16-3D surface.

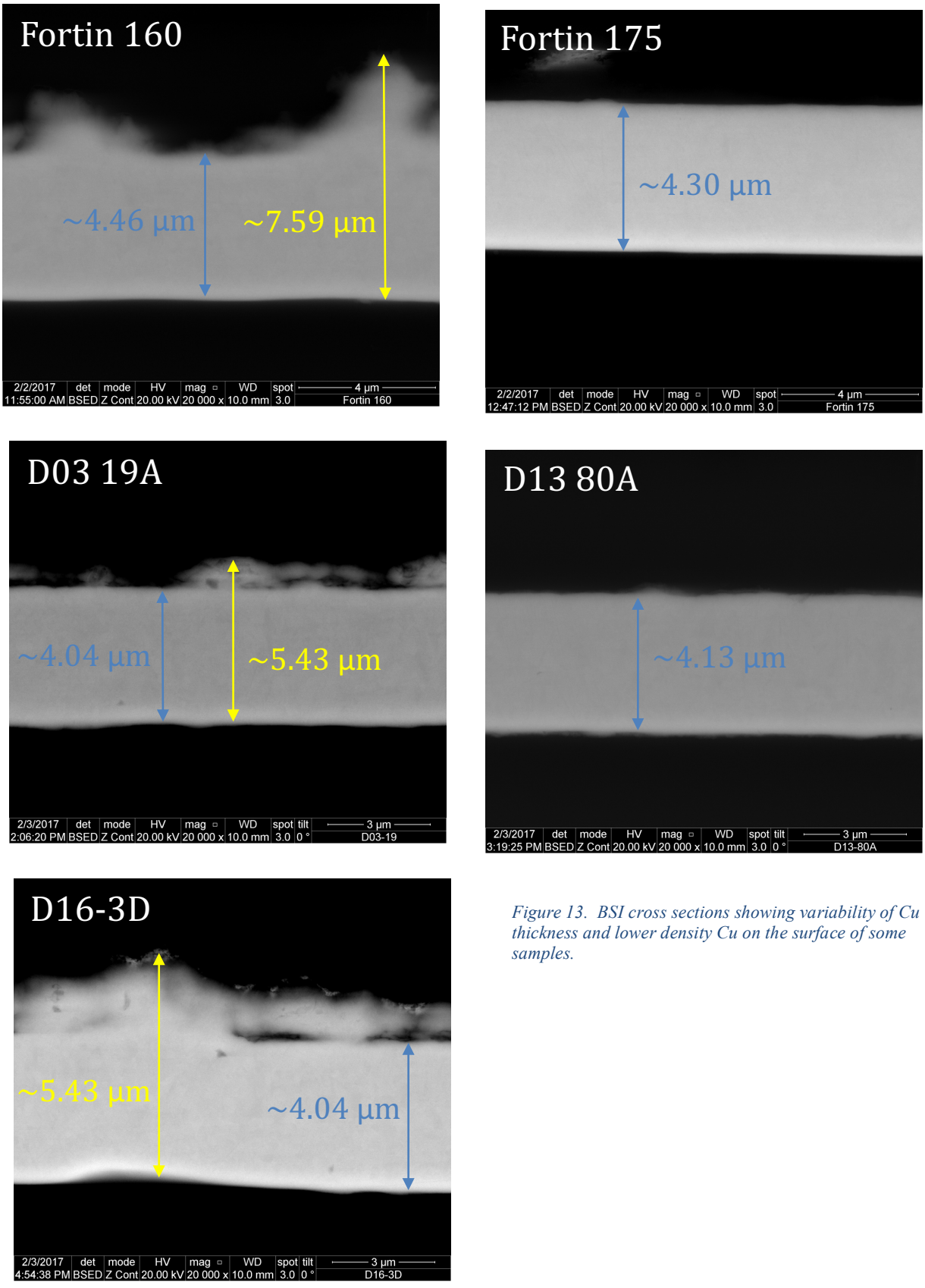

Figure 13. BSI cross sections showing variability of Cu thickness and lower density Cu on the surface of some samples.

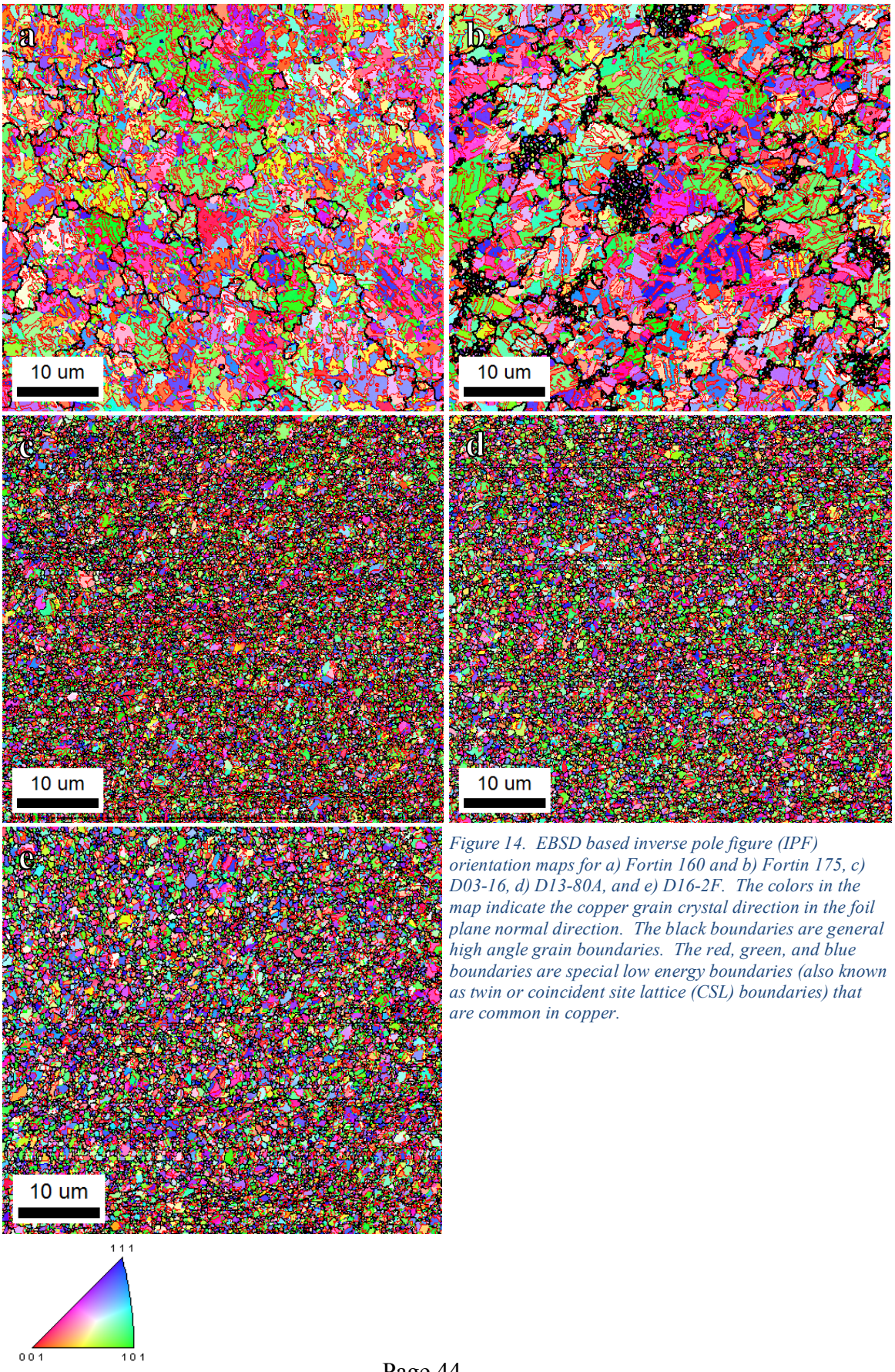

Figure 14. EBSD based inverse pole figure (IPF) orientation maps for a) Fortin 160 and b) Fortin 175, c) D03-16, d) D13-80A, and e) D16-2F. The colors in the map indicate the copper grain crystal direction in the foil plane normal direction. The black boundaries are general high angle grain boundaries. The red, green, and blue boundaries are special low energy boundaries (also known as twin or coincident site lattice (CSL) boundaries) that are common in copper.

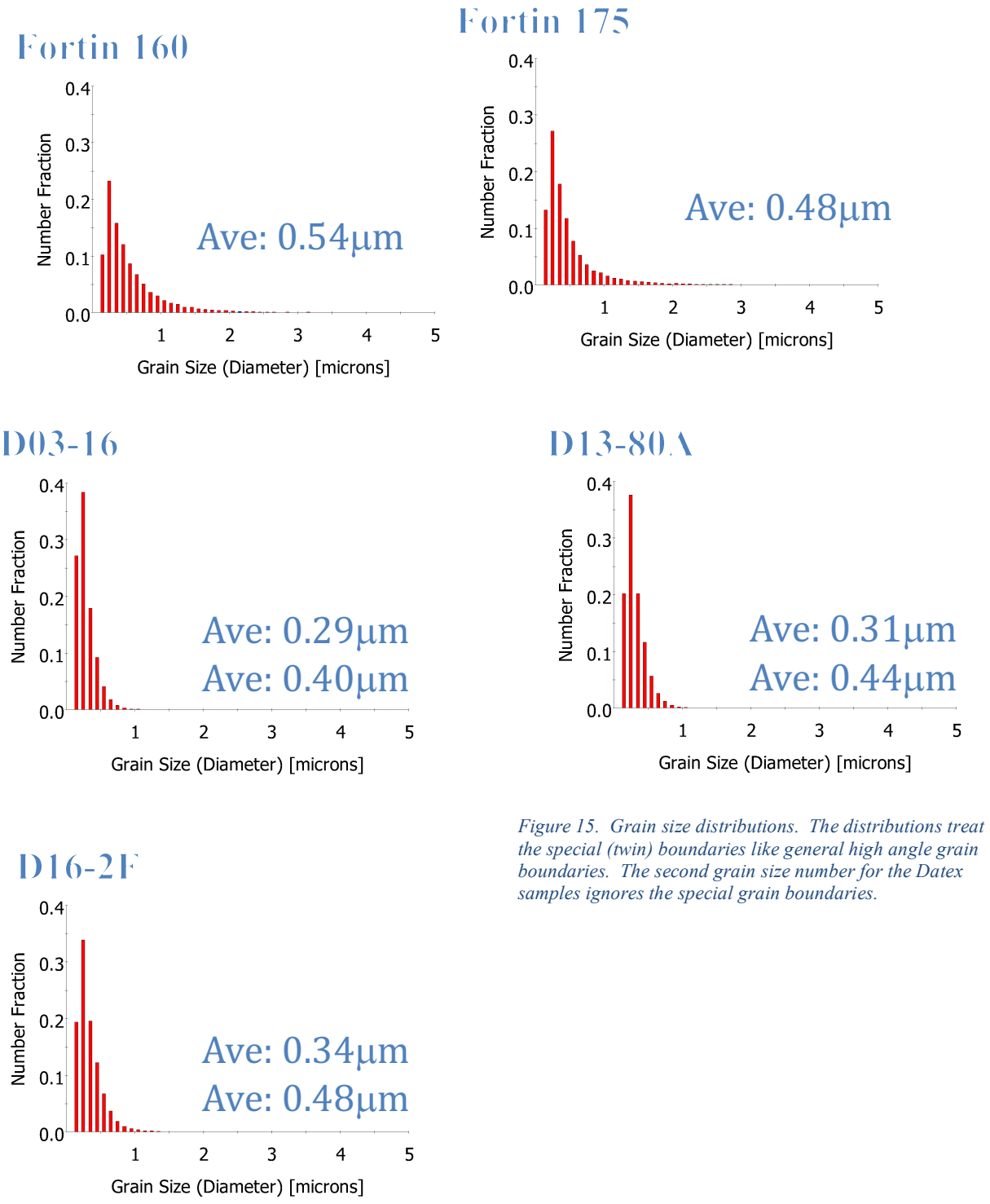

Figure 15. Grain size distributions. The distributions treat the special (twin) boundaries like general high angle grain boundaries. The second grain size number for the Datex samples ignores the special grain boundaries.

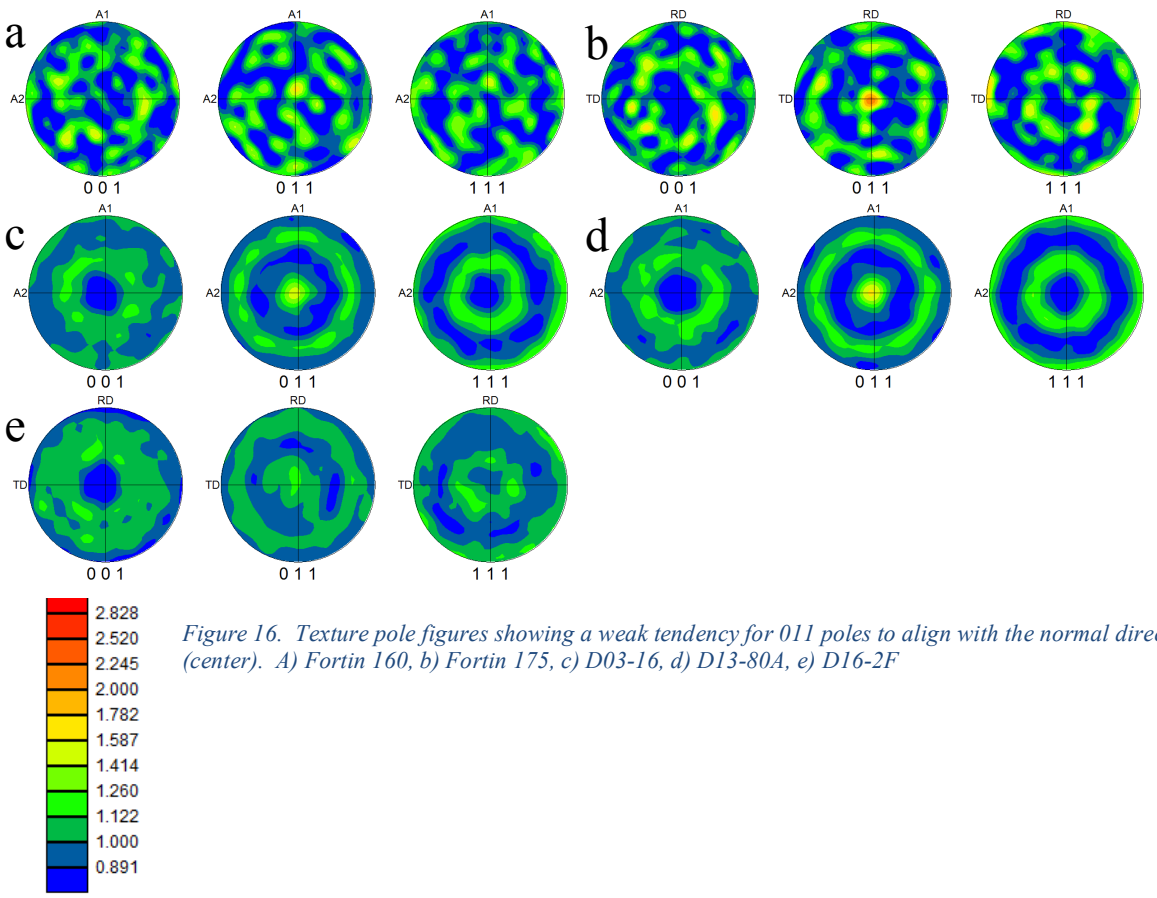

Figure 16. Texture pole figures showing a weak tendency for 011 poles to align with the normal direction (center). A) Fortin 160, b) Fortin 175, c) D03-16, d) D13-80A, e) D16-2F

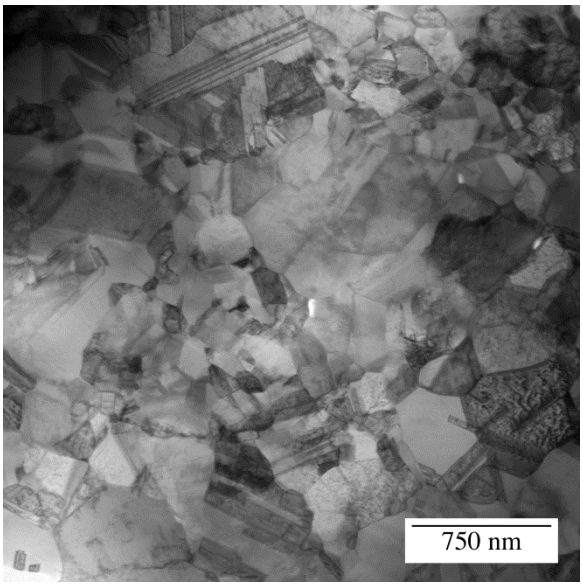

Figure 17 TEM Micrograph of D16 sample showing grain size and twins.

Roughness Measurements of Microclad Material from Profilometery

Miles F. Beaux II & Neliza León Brito, MST-7

Summary

Defects in the microclad materials lead to outlier data points with higher rms roughness values than the primary groupings for each sample. Both inter- and intra-lot variability in the Kapton rms roughness is similar across all samples. No apparent difference between the Kapton rms roughness of Datex 2016 samples and samples manufactured earlier was apparent. Cu rms roughness was consistent across all samples with primary group values ranging from 30 to 80 nm, except for the Datex 2016 samples that had consistently and significantly higher rms roughness values than earlier manufactured samples.

Introduction

Root-mean-square (rms) roughness measurements for microclad samples were collected using two different types of profilometers: an optical profilometer, and a contact stylus profilometer. Profilometry can be used for quantitative analysis of a broad range of surface parameters including roughness, waviness, spacing, and step height. Of these parameters, rms roughness was selected for determining similitude of microclad samples from different batches because it is readily available from a broad range of characterization techniques, providing a means for validating respective results. Differences in surface roughness can be indicative of variation in manufacturing processes, difference in microstructure, and differences in aging effects, all of which can potentially affect the performance of the microclad fliers.

Methods

Optical Profilometry

The optical profilometer utilized was a Zygo NewView 7300 (Figure 1), which functions as an optical microscope with light interferometers built into the microscope objectives, enabling scanning white light interferometry (SWLI). As the focal plane of the microscope is scanned across a sample surface, the interference patterns between light reflected from any sample surfaces within the focal plane of the microscope and an internal reference are used to construct a three dimensional image of the sample surface. While the lateral resolution of this technique is comparable to a standard optical microscope with similar optics, better height resolutions of 0.1 nm can be achieved.

Figure 2 shows a representative optical profilometer image, taken for a microclad bridge. All rms roughness measurements collected by the Zygo optical profilometer for this report were made using 530 μm by 710 μm image footprints. The microclad material has an inherent curvature, as can be seen in Figure 3A. Even though the material was not physically flattened during data acquisition, flattening of the images was performed on the data during post-processing by removal of a cylindrical baseline, as shown in Figure 3B, prior to collecting rms roughness values for each image. Although images were always taken at the apex of curvature, they were also collected at random locations across the length of each sample with no attempt to avoid defects. Ten images were obtained for each side (copper (Cu) side and Kapton side) of every microclad sample to enable a degree of statistical treatment.

Stylus Profilometry

The contact stylus profilometer utilized in this study was a Veeco Dektak 150, shown in Figure 4. This type of profilometer works by establishing, and maintaining a constant predetermined force between a stylus and the sample surface while the stylus is scanned along the sample surface. Unlike the optical profilometer that produces a three dimensional image of a sample surface, the contact stylus profilometer produces a height versus position plot representing a sample surface profile as shown in Figure 5. These profiles can be used to quantitatively analyze the same surface parameters as the optical profilometer.

In the case of the stylus profilometer measurements, attempts were made to avoid defects in order to obtain measurements more indicative of the inherent roughness of the material. Because defects can be strongly correlated with the rolling process direction, and the stylus profilometer measurements are one directional, measurements were taken for both directions, perpendicular and parallel to the roll direction. At least three perpendicular and three parallel measurements covering a 1 mm long distance were taken for each sample investigated with this method.

Results and Discussion

Optical Profilometry

Figure 6A shows a plot of the rms roughness values for the Cu side of various microclad samples. The larger outlier values for each sample are due primarily to defects within the area used to calculate rms roughness. If the outliers are ignored, tight groupings of rms roughness values are shown on the lower end of the range for each sample, typically less than 100 nm. Figure 6B shows the same data with a tighter range of rms roughness values, excluding the outliers. An exception to these general observations is the Fortin 175, which exhibited a greater distribution of higher values with no apparent grouping. Although the major groupings are fairly consistent across all the microclad samples, the lower ends of the rms roughness values for the Datex 2016 samples were slightly larger than samples manufactured earlier.

Respective representations of the rms roughness values for the Kapton side of the microclad samples are shown in Figure 7. Similar to the Cu side, the results show major groupings of rms values on the lower end of the range for each microclad sample with outliers at higher roughness due to defects present in the corresponding area. Exceptions for the Kapton side include the Fortin 175 and Datex Roll 50 samples which exhibited greater distributions of rms roughness with no apparent grouping. Overall, the major groupings across all samples are much more consistent on the Kapton side than for the Cu side with no apparent difference in roughness between the Datex 2016 and samples manufactured earlier. These results would suggest inter-lot variability is associated with the Cu layer, and not the Kapton material onto which the Cu was coated.

Stylus Profilometry

Figures 8 and 9 show the rms roughness values for the Cu and Kapton sides, respectively, of the microclad samples measured using the stylus profilometer. No predominance of higher rms roughness outliers is seen in these measurements, which is expected since efforts were made to avoid defects with this technique. Comparisons of the stylus profilometry scans taken perpendicular and parallel to the roll direction show greater variability on the Kapton side than the Cu side, with rms roughness values tending to be higher in the perpendicular direction than in the parallel direction of the Kapton side (see table 4). This is reasonable when we consider the gouge defects (i.e. scratches) running along the entire length of the roll. These defects were more readily avoided when scanning in the direction parallel to these defects than perpendicular; thus,

the greater roughnesses in the perpendicular roll direction. The absence of this trend on the Cu side suggests the Cu coating covers many of the gouge defects that appear more predominantly on the Kapton material.

The stylus profilometery rms roughness measurements are consistent with and confirm those of the optical profilometery results in that the lower end of the range of rms roughness values for the Cu side of the Datex 2016 microclad material is significantly greater than those for the earlier lots. Likewise, no significant inter-lot variability in the Kapton rms roughness was observed. While the Cu side rms roughness values are fairly consistent between the two techniques, the Kapton results approach an order of magnitude difference. Not only can this difference be explained in terms of the two techniques and methods applied, the stylus profilometery results can be reasonably reproduced from the data collected by the optical profilometer. This is illustrated in Figure 10 where an overall rms roughness of 39 nm is obtained for the whole area, but an rms roughness of only 5 nm is observed for the line path taken through the image avoiding surface defects.

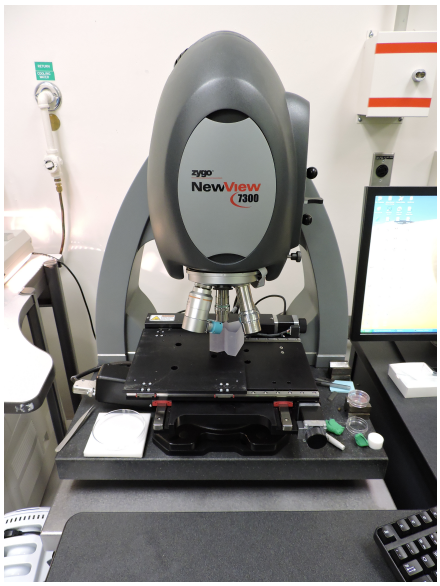

Figure 1. Picture of the Zygo NewView 7300 optical profilometer used in this study.

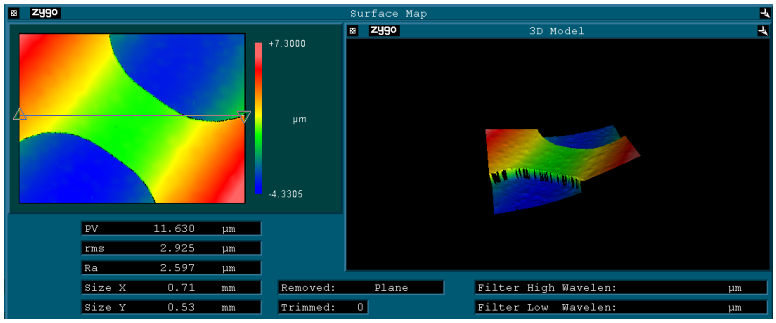

Figure 2. An image taken by the Zygo optical profilometer of a microclad bridge showing various surface characterization parameters of the image such as peak-to valley distance (PV), root-mean-square roughness (rms), average roughness (Ra), and the size of the imaged area (Size X and Size Y).

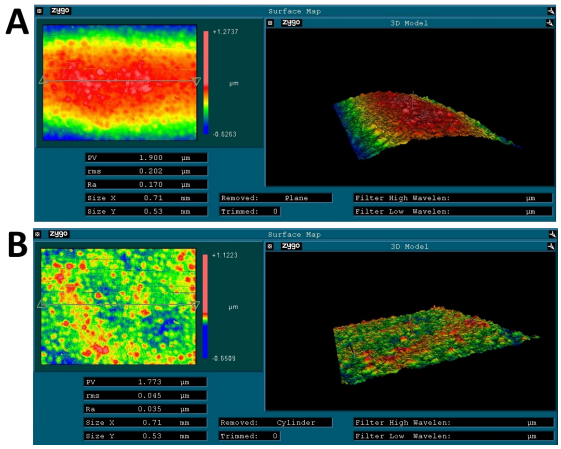

Figure 3. Two different renderings of the same data from the Cu side of a microclad sample before (A) and after (B) post-processing to remove a cylindrical baseline.

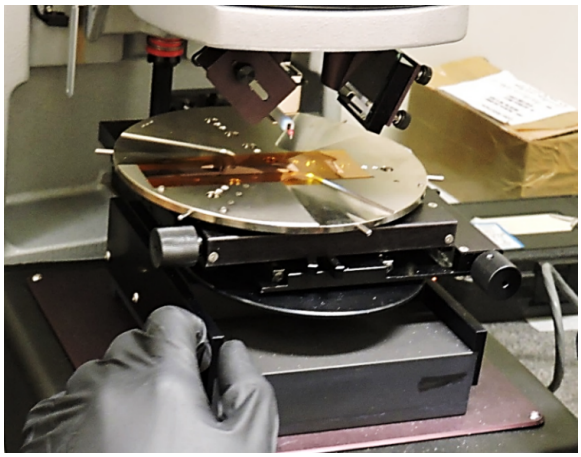

Figure 4. Picture of the Veeco Dektak 150 stylus profilometer used in this study.

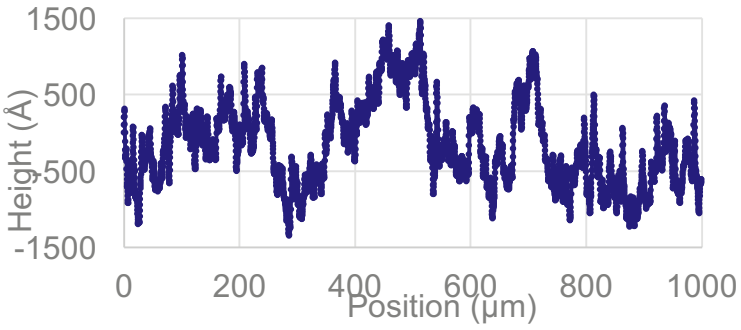

Figure 5. Example of a surface Z profile taken on the Cu side of a microclad sample.

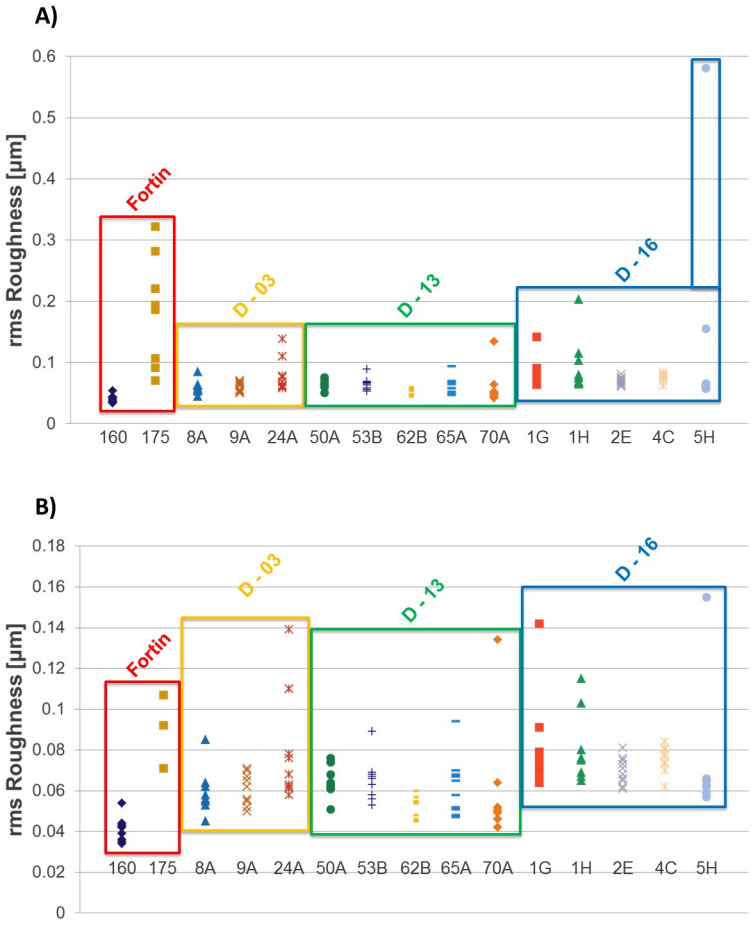

Figure 6. Plots of the rms roughness values taken from a 530 µm by 710 µm area of the Cu side of various microclad samples via optical profilometry. A) Shows the full range of values obtained, including outliers, while B) is focused on the major groupings closer to the bottom range of the measurements.

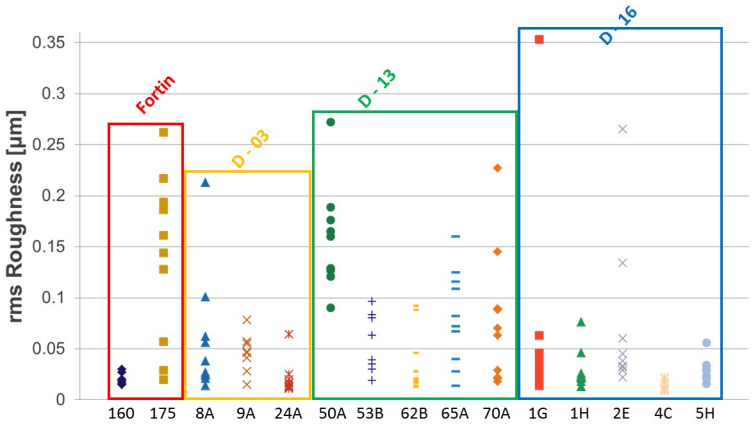

Figure 7. Plot of the rms roughness values collected from a 530 µm by 710 µm area of the Kapton side of various microclad samples via optical profilometery.

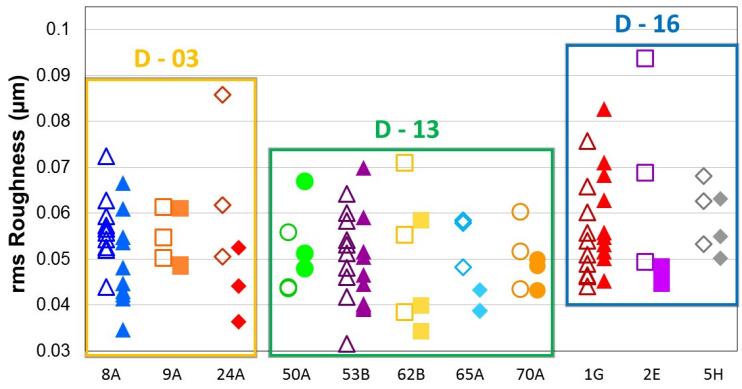

Figure 8. Plot of the rms roughness values taken for 1 mm lines on the Cu side of various microclad samples via stylus profilometry. Data taken parallel (perpendicular) to the roll direction are shown as open (closed) symbol in the plot.

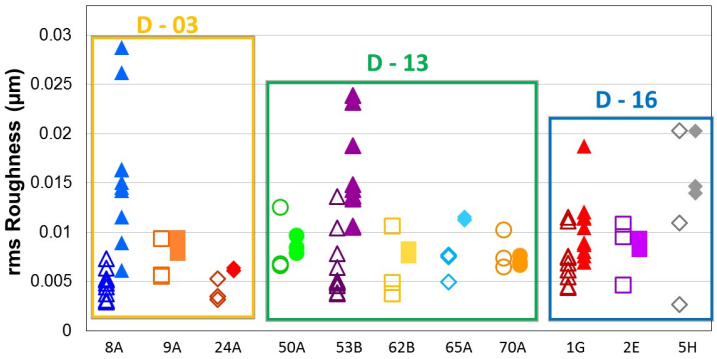

Figure 9. Plot of the rms roughness values taken for 1 mm lines on the Kapton side of various microclad samples via stylus profilometry. Data taken parallel (perpendicular) to the roll direction are shown as open (closed) symbol in the plot.

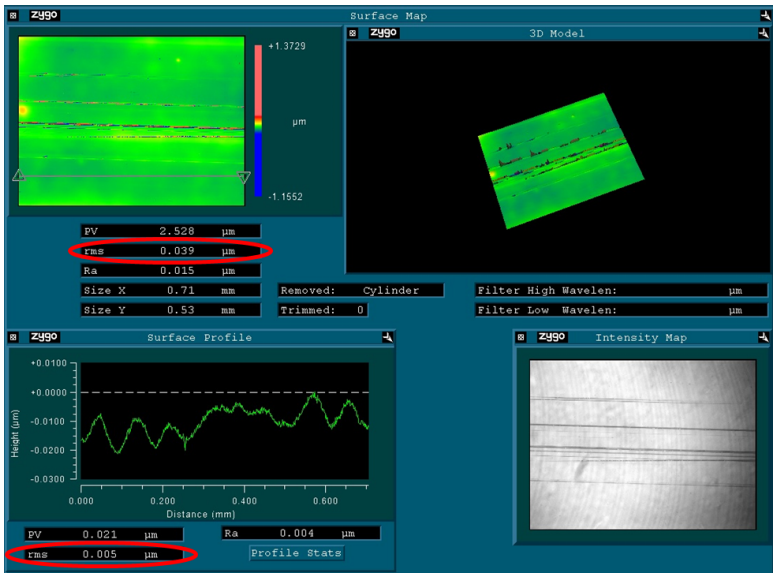

Figure 10. Optical profilometer image taken of the Kapton side of a microclad sample (D13 Roll 53 Section B) demonstrating reproduction of stylus profilometer results.

Appendix

Sample ID	Mean rms Roughness [nm]	Individual Roughness Measurements [nm]									
F-160	41.2 ± 5.8	39	35	43	54	42	43	42	44	34	36
F-175	174 ± 87.7	221	194	194	186	107	71	71	92	282	322
D03-R8A	59.6 ± 10.5	85	58	56	56	62	55	45	64	53	62
D03-R9A	60.3 ± 7.7	71	55	67	50	56	70	52	55	62	65
D03-R24A	82.5 ± 27.6	76	68	58	78	62	63	110	139	110	61
D13-R50A	64.2 ± 7.1	74	76	62	64	61	63	61	68	62	51
D13-R53B	65.2 ± 9.9	63	69	56	67	68	58	66	63	53	89
D13-R62B	52.8 ± 4.9	46	45	54	55	54	57	60	55	54	48
D13-R65A	62.0 ± 14.2	58	47	65	51	70	48	67	94	68	52
D13-R70A	57.6 ± 27.6	64	42	50	51	42	134	46	46	52	49
D16-R1G	82.0 ± 22.3	64	72	142	78	68	73	79	75	91	78
D16-R1H	92.8 ± 41.9	203	69	103	75	76	65	67	115	75	80
D16-R2E	69.8 ± 6.5	65	76	71	75	73	66	68	81	61	62
D16-R4C	76.0 ± 6.5	84	78	81	73	77	74	81	62	80	70
D16-R5H	122.6 ± 163.8	59	581	155	66	57	65	59	62	59	63

Table 1. Individual roughness measurements for the Cu side of microclad samples plotted in Figure 6, along with their calculated mean rms roughness and the measurement standard deviation.

Sample ID	Mean rms Roughness [nm]	Individual Roughness Measurements [nm]									
F-160	20.4 ± 4.7	20	16	20	20	18	27	15	18	20	30
F-175	139.8 ± 81.7	262	217	194	186	161	128	144	57	29	20
D03-R8A	58.1 ± 60.4	213	101	62	56	25	38	24	14	21	27
D03-R9A	46.8 ± 17.0	15	47	78	46	46	57	55	28	41	55
D03-R24A	20.5 ± 15.9	20	64	25	13	11	13	14	17	16	12
D13-R50A	155.7 ± 50.5	272	176	127	165	129	90	160	189	128	121
D13-R53B	57.1 ± 29.8	39	63	30	83	80	19	96	35	96	30
D13-R62B	36.6 ± 29.7	92	14	17	21	28	28	88	13	46	19
D13-R65A	81.3 ± 46.5	160	40	72	28	82	116	125	109	67	14
D13-R70A	77.2 ± 66.3	89	88	227	70	145	21	22	29	18	63
D16-R1G	64.7 ± 102.2	23	29	38	28	14	22	353	31	46	63
D16-R1H	28.2 ± 19.2	24	13	18	76	23	46	21	13	22	26
D16-R2E	68.7 ± 76.3	60	22	32	29	33	29	45	38	134	265
D16-R4C	13.8 ± 5.0	22	8	18	11	11	11	9	21	15	12
D16-R5H	29.5 ± 11.0	29	23	23	34	56	34	16	30	21	29

Table 2. Individual roughness measurements for the Kapton side of microclad samples plotted in Figure 7, along with their calculated mean rms roughness and the measurement standard deviation.

Sample ID	Mean rms roughness [nm]		
	Stylus Profilometer		Optical Profilometer
	Parallel	Perpendicular	
D03-R8A	56.7 ± 7.4	49.0 ± 9.8	59.6 ± 10.5
D03-R9A	55.3 ± 5.6	52.7 ± 7.2	60.3 ± 7.7
D03-R24A	66.6 ± 18.0	44.4 ± 8.1	82.5 ± 27.6
Average	**59.5 ± 10.3**	**48.7 ± 8.4**	**67.5 ± 14.6**
D13-R50A	47.7 ± 7.0	55.2 ± 10.2	64.2 ± 7.1
D13-R53B	50.9 ± 9.5	48.1 ± 10.1	65.2 ± 9.9
D13-R62B	54.7 ± 16.3	44.1 ± 12.6	52.8 ± 4.9
D13-R65A	54.9 ± 5.8	40.3 ± 2.6	62.0 ± 14.2
D13-R70A	51.7 ± 8.4	47.2 ± 3.5	57.6 ± 27.6
Average	**52.0 ± 9.4**	**47.0 ± 7.8**	**60.4 ± 12.7**
D16-R1G	54.8 ± 10.0	59.6 ± 11.5	82.0 ± 22.3
D16-R2E	70.5 ± 22.2	46.2 ± 1.9	69.8 ± 6.5
D16-R5H	61.4 ± 7.4	56.1 ± 6.6	122.6 ± 163.8
Average	**62.2 ± 13.2**	**54.0 ± 6.7**	**91.5 ± 64.2**

Table 3. Comparison of rms roughness measurements (including a standard deviation) for Cu taken in the parallel and perpendicular roll directions by the stylus profilometer to measurements taken by the optical profilometer.

Sample ID	Mean rms roughness [nm]		
	Stylus Profilometer		Optical Profilometer
	Parallel	Perpendicular	
D03-R8A	4.6 ± 1.4	15.8 ± 7.0	58.1 ± 60.4
D03-R9A	6.8 ± 2.2	8.4 ± 0.9	46.8 ± 17.0
D03-R24A	4.0 ± 1.1	6.2 ± 0.2	20.5 ± 15.9
Average	**5.1 ± 1.6**	**10.1 ± 2.7**	**41.8 ± 31.1**
D13-R50A	8.6 ± 3.4	8.6 ± 0.9	155.7 ± 50.5
D13-R53B	6.5 ± 3.2	15.7 ± 4.7	57.1 ± 29.8
D13-R62B	6.4 ± 3.7	7.9 ± 3.5	36.6 ± 29.7
D13-R65A	6.7 ± 1.5	11.4 ± 0.2	81.3 ± 46.5
D13-R70A	8.0 ± 2.0	7.1 ± 0.5	77.7 ± 66.3
Average	**7.2 ± 2.8**	**10.1 ± 2.0**	**81.7 ± 44.6**
D16-R1G	7.1 ± 2.5	10.5 ± 3.4	64.7 ± 102.2
D16-R2E	8.3 ± 3.3	8.9 ± 0.6	68.7 ± 76.3
D16-R5H	11.3 ± 8.8	16.3 ± 3.5	29.5 ± 11.0
Average	**8.9 ± 4.9**	**11.9 ± 2.5**	**54.3 ± 63.2**

Table 4. Comparison of rms roughness measurements (including a standard deviation) for Kapton taken in the parallel and perpendicular roll directions by the stylus profilometer to measurements taken by the optical profilometer.

Analysis of microclad materials using X-ray spectroscopy and radiography

Brian M. Patterson[1], Kevin Henderson[1], Joseph Cowan[2], Robert Aragonez[2], Nik Cordes[1]

MST-7[1], P-24[2], Los Alamos National Laboratory

Results

A variety of microclad Fortin and Datex samples were characterized using X-ray fluorescence and X-ray radiography to ascertain the similitude of the samples for elemental composition, copper layer thickness and copper layer uniformity. At the sensitivity and detection limit of the X-ray fluorescence instrument, it was determined that the materials are composed of copper. No other elements were detected at the ~1% composition detection limit. Nano-scale radiography of the materials in cross section determined that the Cu layer thickness varied between ~4.4 to 6.3 micrometers in thickness among the samples. On average, the sample thicknesses were not different among the sample types. Monochromatic radiography was used to measure the Cu layer uniformity within a sample and among samples. The density of the Cu was measured to vary between ~5.4 – 7.9 g/cm^3. The uniformity within each sample shows that the material is uniform in Cu thickness/density from one side of the ribbon to the other.

Instrumentation

Three types of X-ray instrumentation was used to analyze the samples. A custom X-ray fluorescence instrument was used to identify the elemental composition of the samples. This instrument can detect most elements on the periodic table down to approximately sodium at about a 1% composition detection limit. The instrument uses an XOS (X-ray Optical Systems) Mo anode X-ray tube with an SII detector. The 120 s spectrum was taken of each microclad sample while under vacuum. The spot of analysis is approximately 100 micrometers in diameter. A photograph of the instrument is shown in Figure 1a. To measure the thickness of the Cu layer, nano-scale X-ray radiographs were taken of the cross section of each sample. The samples were mounted upright in a pin vice and a 60 s exposure radiograph was taken. The field of view of the radiograph is 65 μm with a 150 nm measured resolution. The cross sectional radiographs were taken near the tip of the cut wedge to optimize X-ray transmission. A photograph of the instrument is shown in Figure 1b. Finally, monochromatic radiographs were taken of each sample. This custom instrument also uses an XOS Cu anode X-ray tube with a double-curved crystal to monochromatize the X-rays to 8.047 keV. The microclad strips were radiographed using the following conditions: gain = 2, 2 Mhz readout, 1.36 s exposure, 250 accumulations and 10 accumulations for dark current subtraction. A photograph of the instrument is shown in Figure 1c[1].

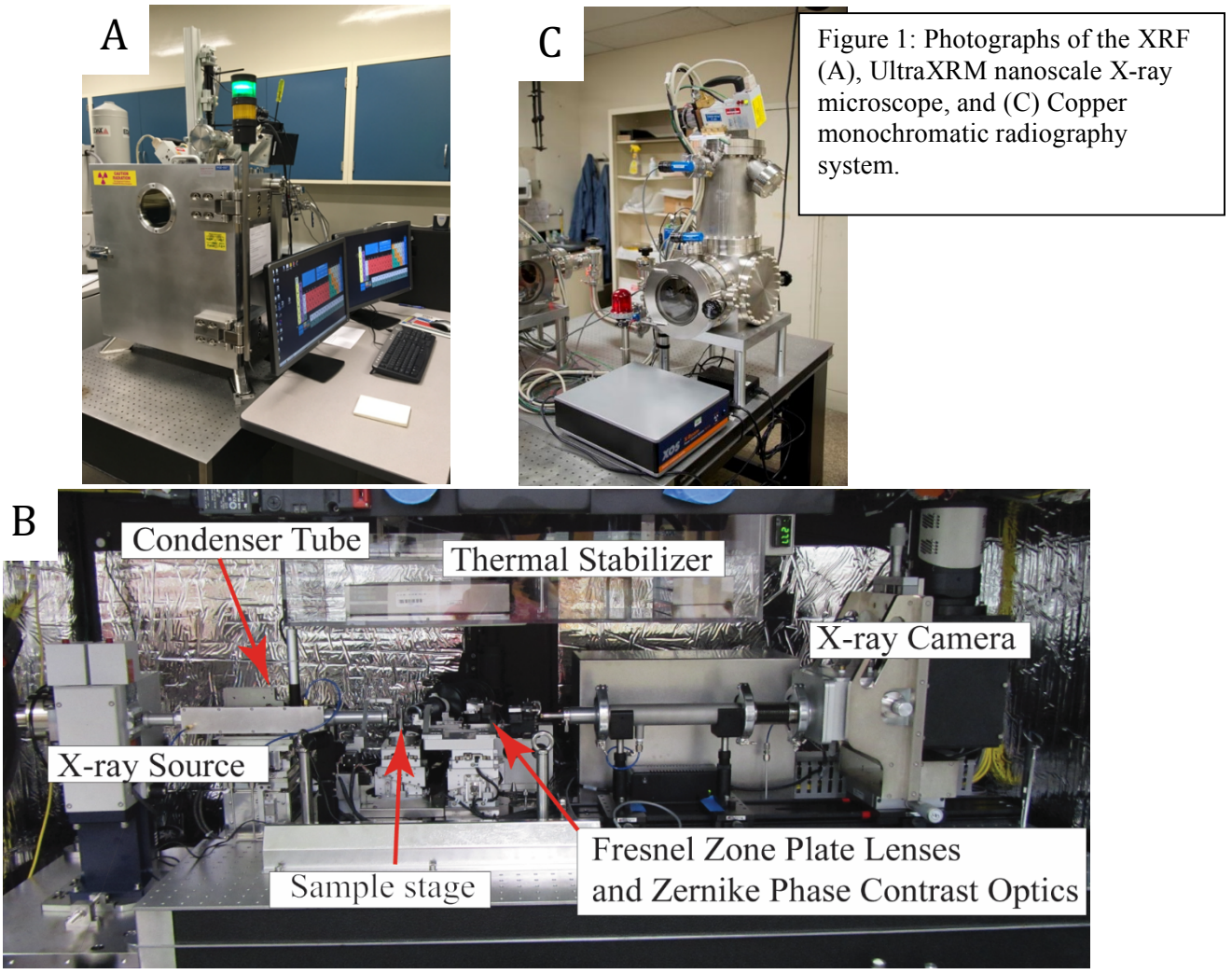

Figure 1: Photographs of the XRF (A), UltraXRM nanoscale X-ray microscope, and (C) Copper monochromatic radiography system.

Samples

Two Fortin samples were analyzed, Fortin 160 and Fortin 175. Three types of Datex samples were analyzed (D03, D13, and D16) and within the Datex, several rolls of materials were analyzed. The list of samples is provided below:

D03; Roll 8A, Roll 9A, Roll 16A, Roll 24A,

D13: Roll 50A, Roll 53B, Roll 62B, Roll 65A, Roll 70A,

D16: Roll 1G, Roll 1H, Roll 2E, Roll 4C, Roll 5H

Additionally, pure Kapton-H was analyzed to use as a background for the radiography measurements. Each of the analyzed specimens was cut from the sample strips using a fresh razor blade and a polymer cutting board. The strips are approximately 0.5 inches wide (length of the roll) and their length is the width of a roll. The length of the sample (width of the roll) was just slightly larger than the field of view of the monochromatic radiography system. For nano-radiography, a small 1-2 mm long wedge was cut from the samples and then radiographed on edge to see through the thickness of the sample.

Results

Figure 2 shows the XRF spectra collected of one sample of each of the four sample types (e.g., Fortin 160, D03 Roll 8A, D13 Roll 50A, and D16 Roll 4C). Figure 2(left) a shows the entire spectrum with the K_a and K_b peaks for the Cu layer labeled. Figure 2 (right) shows a magnified section of the spectrum. Two peaks are present at approximately 17 keV; these are scatter of the X-rays from the X-ray source. Also, there are several peaks at ~4-7 keV that are due to the scattered X-rays from the walls of the instrument chamber. No peaks were detected from the Al, Sn, or Pd as identified from higher spatial resolution elemental analysis, performed by Dan Kelly (C-CDE).

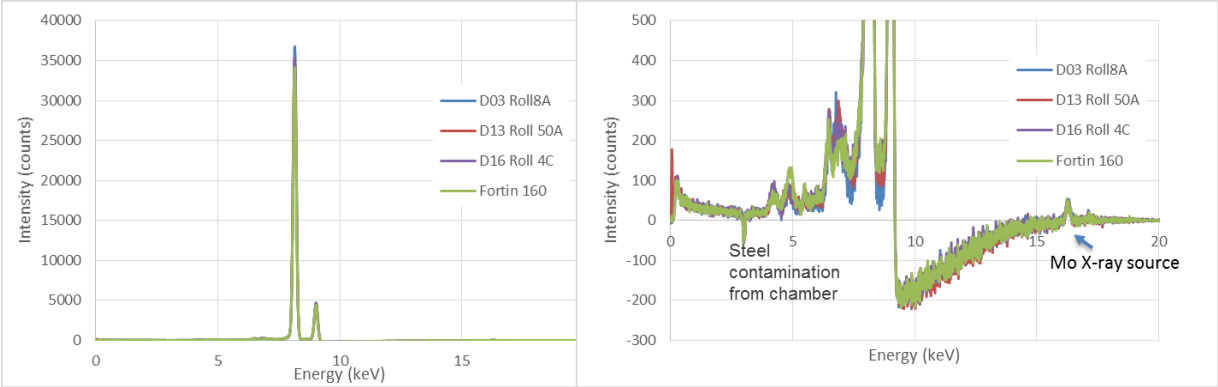

Figure 2: XRF spectra of four of the complete signal of the samples (l) and zoomed into the baseline (r). Spectral contamination from the steel chamber and the Mo X-ray source is noted, but no Al, Sn, or Pd is seen.

Representative radiographs of the microclad samples are shown in Figure 3. Line profiles were taken through each of the fourteen radiographed samples and the Cu layer thickness is plotted in Figure 4. The thickness varies between 4.4 and 6.3 µm. These thicknesses compare a little low to the specified thickness of 5.75-7.09 µm. These values compare to the quasi quantitative measures taken using electron microscopy of 4.04 - 7.6 µm.

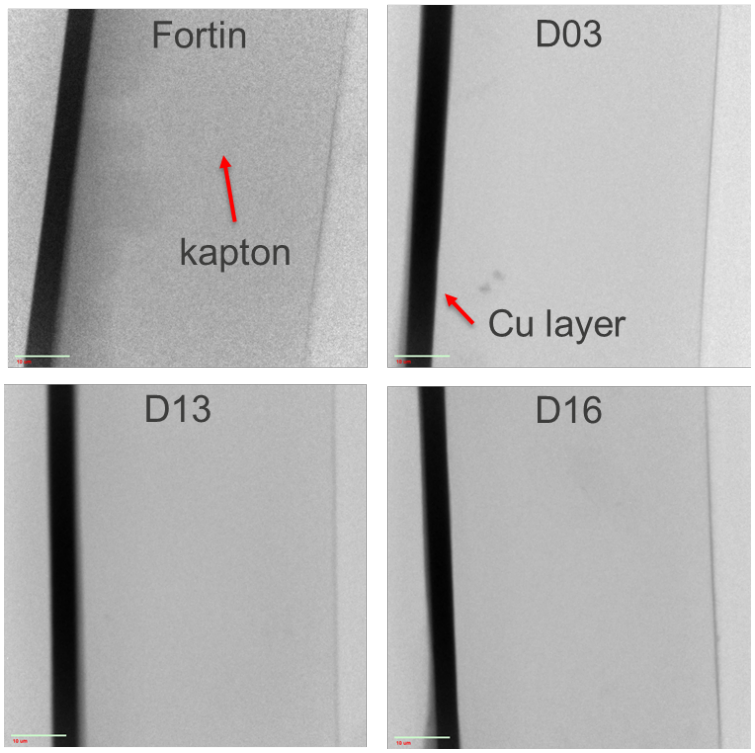

Figure 3: Representative radiographs of the cross section of the four sample types. The Cu layer is the dark line on the left. The back of the kapton is seen on the right of the radiograph. The scale bar is 10 micrometers. There is a medium gray region seen below and above the Cu layer, this is due to very slight miss alignment of the sample within the instrument and the medium gray region in the Fortin sample is due to the cutting of the specimen from the strip and can be ignored.

Figure 4: Measured thicknesses of the samples and sample types taken from line-outs from the cross sectional nano-scale radiographs. The low end of the thickness as provided by the manufacturer is shown by the dashed line. The resolution of the image is approximately 150 nm. Error bars are the standard deviation of multiple line profiles in one image.

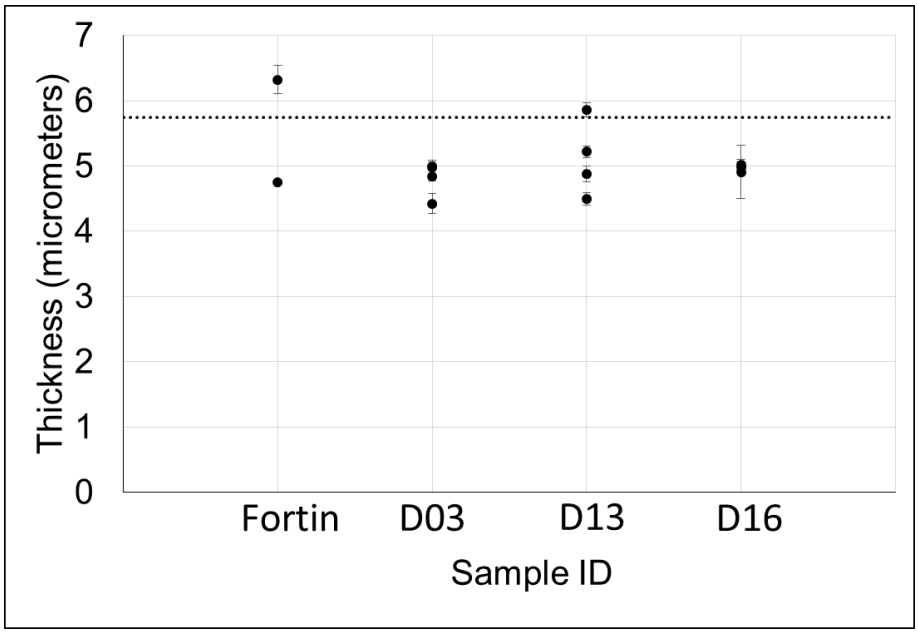

Monochromatic radiography is important in that the X-ray images can now be quantified. Measures can be taken of each of the sample over a large area of the equivalent thickness/density in two dimensions. Through the collection of these monochromatic

radiographs, it is possible to calculate the density of the material if several things are known about the sample and the experiment. From the elemental composition, (e.g., Cu, C, H, O) and their relative amounts, along with the X-ray energy, it is possible to calculate the opacity of the sample. Using equation 1:

$$\rho = \frac{-lnT(v_o)}{(K(v_o)z)} \qquad \text{eq. 1}$$

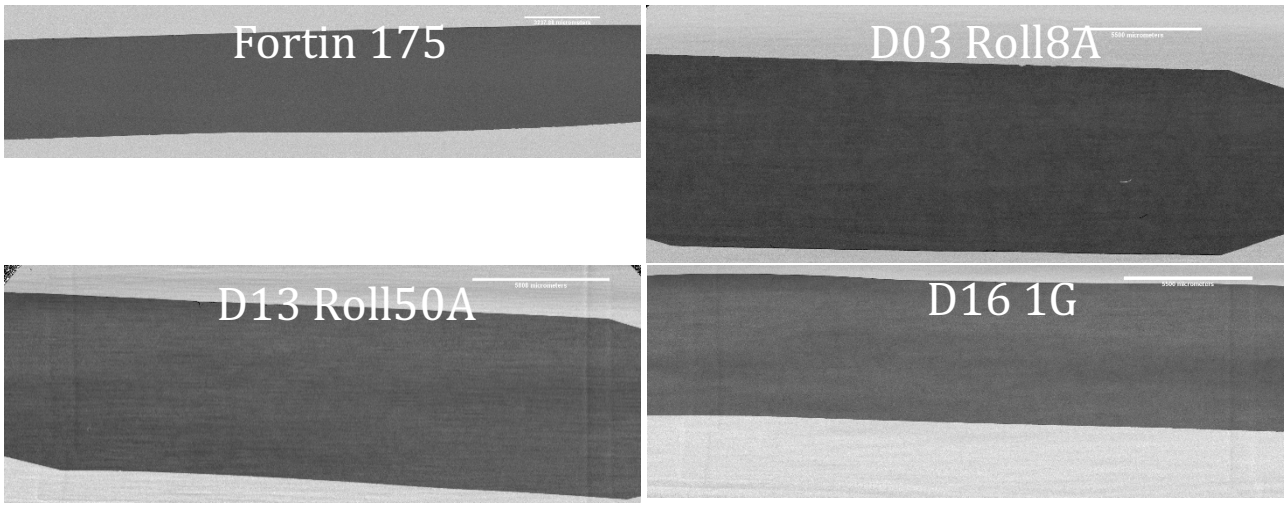

Figure 5: Monochromatic radiographs of the four sample types. The width of the roll is slightly larger than the field of view of the instrument. A region of interest was taken of the entire sample area.

Where T(v_o) is the transmittance at frequency T (v_o) = I/I$_o$, v_o is the frequency of the quasi-monochromatic X-ray source, K(v_o) is the opacity at frequency v_o in cm^2 g^{-1}, and z is the thickness of the sample in centimeters. From our calculations using the Helke tables, the opacity values of the Cu and the Kapton ($C_{22}H_{10}N_2O_5$) are 50.20267 and 5.884484 respectively. Radiographs were collected of all 14 samples (four representative radiographs are shown in Figure 5) as well as the Kapton.

Using ImageJ image analysis software (National Institute of Health), each of the radiographs were bound by a region of interest from which an average transmittance for each sample was collected. Across the width of the sample (left to right in the image, nearly the width of the roll), a transmittance profile was collected and is shown in Figure 6.

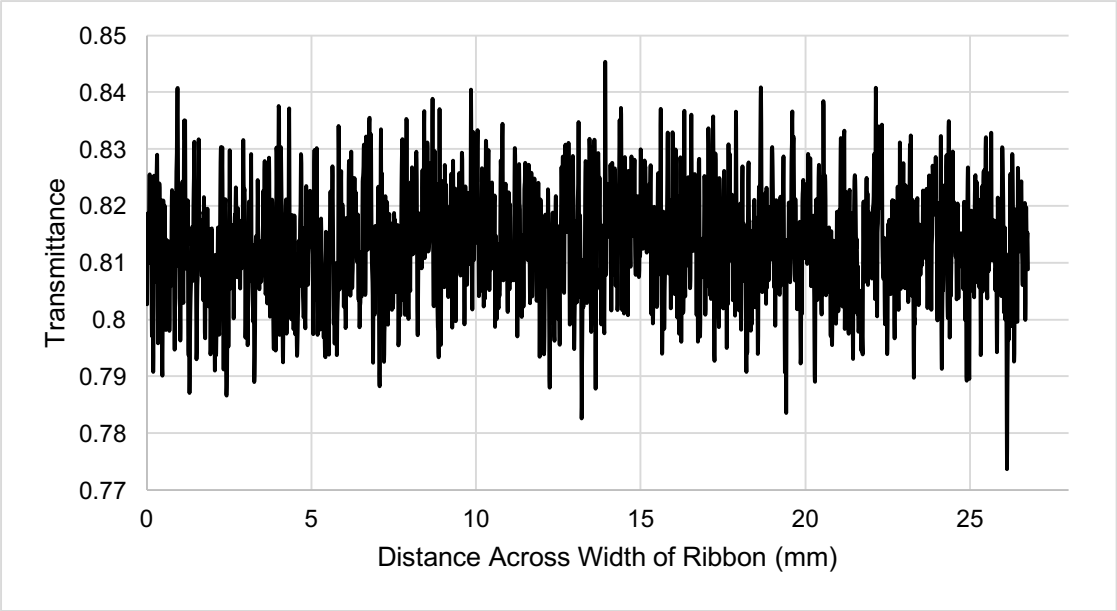

Figure 6: Plot of the transmittance across the width of Sample D13 Roll 70A indicating that the sample is uniform across the width of the roll.

This transmittance profile indicates that the samples are uniform for X-ray transmission. There are no changes in the thickness/density of the material across the width of the roll. Using the transmittance values and the thickness of the samples, a density of the layer for each sample is presented in Figure 7. The indicated densities are a little lower than the theoretical maximum density of Cu of 8.97 g/cm^3. However it is well know that these types of coatings do not produce films at the full density, and the measurements of the thickness of the Cu layer taken from the nano-scale radiographs is a little low.

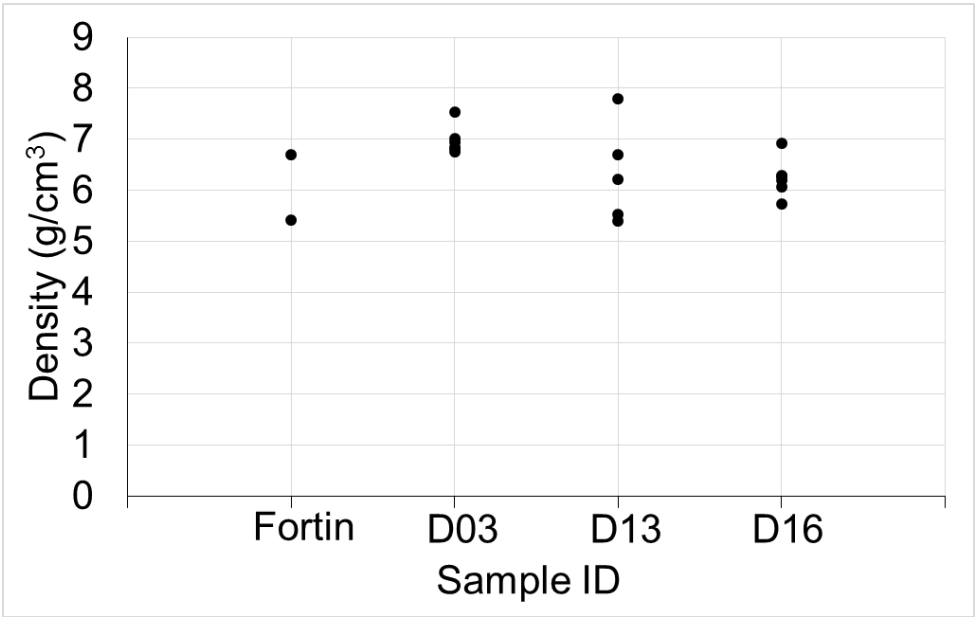

Figure 7: Plot of the density of the Cu coating on the Kapton measured using the thickness of the Cu from the nano-radiography, the calculated opacity, and the measured transmittance from the samples.

Conclusions

Using X-ray analysis, the four microclad samples were found:

1. To be identical in elemental composition (Copper)
2. To have a Cu thickness of 4.4 to 6.3 micrometers (thin according to the manufacturers' specification)
3. A copper density between 5.4 to 7.9 g/cm^3 about 60-88 % full density.
4. The copper layer is uniform.

The error in the measurements of the four samples and the error between them are overlapping and to the best of our abilities, the samples are found to be identical.

References

1. Lanier, N. E.; Hamilton, C.; Taccetti, J. M., A monochromatic x-ray imaging system for characterizing low-density foams. *Review of Scientific Instruments* **2012,** *83* (10), 10E521.

Microclad Characterization: Atomic Force Microscopy

Justin Tokash (Sigma-DO) and Samantha K. Lawrence (Sigma-DO)

Technique Overview

Atomic force microscopy (AFM) is a type of scanning probe microscopy where information is gathered by "scanning" the surface of a sample with a mechanical probe. The Z-height deflection of the tip is measured with sub-nanometer scale resolution via piezoelectric elements. The measurement of the probe reaction to the forces imposed on it by the sample facilitate the generation of a three-dimensional image of the shape of the surface (topography). Simultaneously, the forces imposed on the probe by the samples are recorded; recently a technique has been developed to assess these interactions to quantitatively measure the mechanical properties of the material surface. PeakForce Quantitative Nanomechanical Mapping (QNM) provides the ability to acquire and analyze the force curves from each tap that occurs during the imaging process [1]. Contributions from different material properties such as elastic modulus, dissipation, adhesion, and deformation can be separated by measuring the instantaneous force on the tip rather than the time-average of the force.

PeakForce QNM is applied in this study to quantitatively compare the topography/surface roughness and select mechanical properties among four lots of Microclad material. Surface roughness is an important parameter to quantify as it can affect two properties that are vital to Microclad performance: electrical conductivity and corrosion susceptibility. Similarly, variation in surface mechanical properties can impact material performance and must be quantified.

Experimental

Material Preparation

Samples for AFM analysis were prepared from four lots of Microclad material: Fortin, Datex 2003 (D03), Datex 2013 (D13), and Datex 2016 (D16). Square samples (10 mm x 10 mm) were cut from 35-mm wide Microclad strips; one sample was removed from the edge of a strip and one sample was removed from the middle of the strip (see Fig. 1). Samples were then ultrasonically cleaned in a methanol bath and rinsed with DI water. Prior to insertion in the AFM each sample was cut in half; the two halves were mounted on a magnetic AFM puck—one half was mounted with the Cu plating exposed, while the second half was mounted with the Kapton substrate exposed.

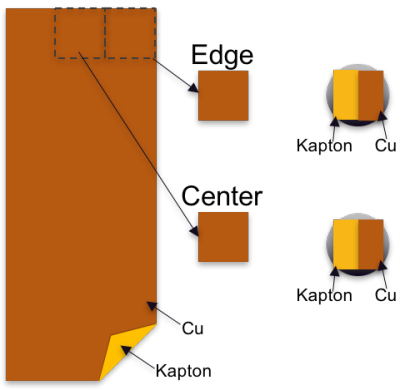

Figure 1: Schematic of AFM samples extraction from Microclad strips.

PeakForce QNM Imaging

Surface topography and surface material properties were obtained with nanometer-scale resolution using either a Dimension Icon Atomic Force Microscope (Bruker, Santa Barbara, CA) or a Multimode Nanoscope 8 (Bruker, Santa Barbara, CA) operating in PeakForce QNM mode. Doped silicon tips, TAP525A, were used for all measurements. The cantilevers were coated on the reverse side with a reflective aluminum coating and have an n-type, antimony doped tip with a nominal radius of 10 nm. The nominal spring constant and resonance frequency of the cantilevers were 375 N/m and 525 kHz, respectively. Using the Dimension Icon, images were acquired at a scan rate of 0.1Hz with a scan size of 50 µm x 50 µm, and a resolution of 1024 x 1024 pixels. Subsequently, during experiments using the Multimode, images were acquired at a scan rate of 0.2 Hz with a scan size of 3 µm x 15 µm, and a resolution of 1024 x 1024 pixels. The Multimode is located within a glovebox, greatly complicating both movement of the tip between sample locations and samples changes, hence the scan dimensions were reduced to expedite testing after determining that commensurate information could be acquired with a smaller scan. All AFM data analysis was performed using the NanoScope Analysis software, version 1.5.

Results

Surface Topography and Roughness Measurements

Surface topography is tracked directly through sample-tip interactions thereby generating a 'height' image, such as those shown for Cu in Fig. 2a and 2b, where variation in the color represents changes in the surface profiles. A root-mean-squared (RMS) surface roughness, representing the line average profile height deviations from the mean line, can be calculated from the topography data via:

$$RMS = Rq = \left[\left(\frac{1}{L}\right)\int_0^L Z(x)^2 dx\right]^{1/2}$$

where L is the evaluation length and $Z(x)$ is the profile height function. RMS roughness data collected for the Cu coatings are presented in a box-and-whisker plot in Fig. 3. Note that data collected from both center and edge samples are represented in Fig. 3 as the values were determined to be position independent. D16 displays both the highest mean value and largest variability in measured values.

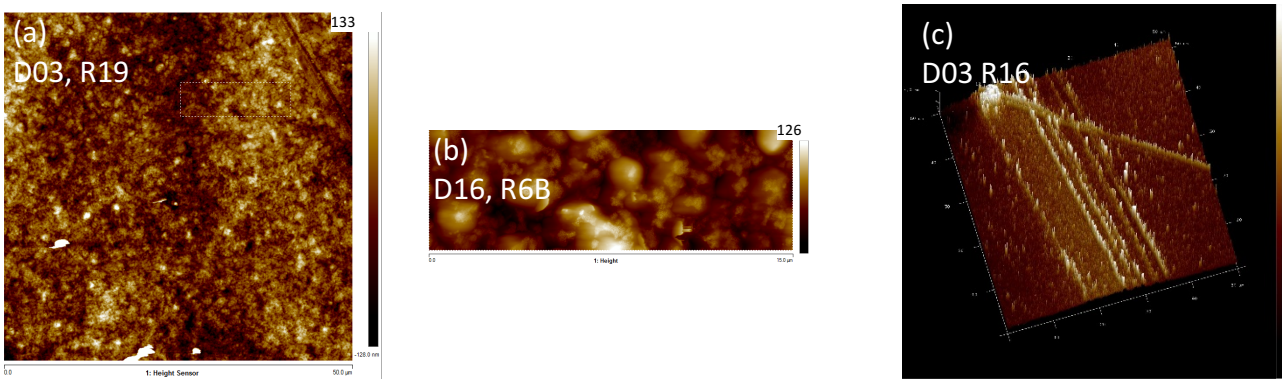

Figure 2: Representative 2D height images of Cu films (a and b) and 3D image of Kapton substrate (c).

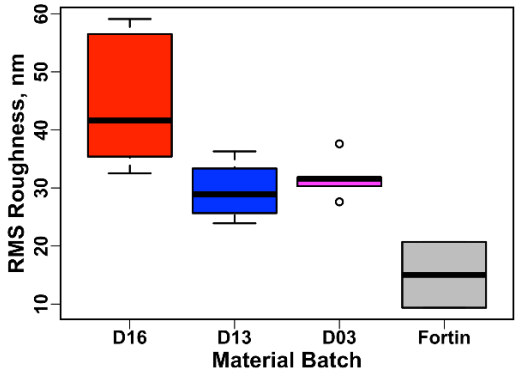

Figure 3. Box-and-whisker plot of RMS roughness values for Cu films from four material lots. D16 displays both the highest mean value and largest variability in measured values.

Similar height images were collected for the Kapton substrates from each material lot. It is often advantageous to view the height data in 3D, as is done in Fig. 2c, to determine the magnitude of specific defects. Three-dimensional height images reveal that the Kapton substrates contain deep scratches with material piled-up on either side of the gouge, as evident in Fig. 2c. Notably, these "tall" defects have a pronounced effect on the RMS roughness values, as shown in Fig. 4a and 4b. D13 material has the greatest variability in Kapton surface roughness (Fig. 4a), due to the presence of "tall" defects; when the D13 data is removed from the plot (Fig. 4b) the roughness values calculated for the other three material lots fall within an approximately 2 nm range.

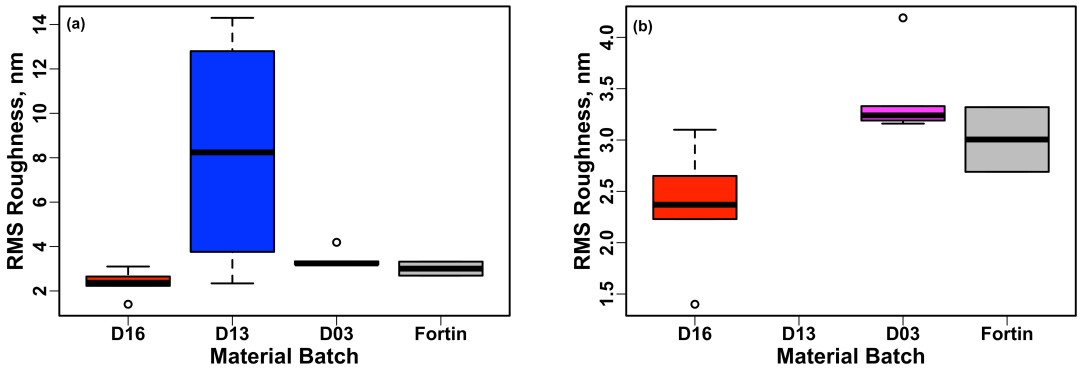

Figure 4. Box-and-whisker plot of RMS roughness values for Kapton from four material lots (a); D13 values are removed from (b) to highlight the similarity between D16, D03, and Fortin lots.

Surface mechanical property measurements

One advantage to the PeakForce QNM imaging mode is the ability to capture topography and surface mechanical properties, such as elastic modulus, adhesion, deformation, and dissipation during a single surface scan. QNM imaging of Kapton revealed uniform surface properties, so no further analysis of these properties will be presented here. Conversely, QNM imaging of Cu films revealed apparent microscale "features," or variations across the surface, in elastic modulus and deformation.

Elastic modulus is determined for each tip-surface interaction by fitting the force curve obtained during the interaction using the Derjaguin-Muller-Toporov (DMT) model [1]:

$$F - F_{adh} = \frac{4}{3} E^* \sqrt{R(d - d_0)^3}$$

where F-F_{adh} is the force on the cantilever relative to the adhesion force, R is the tip radius, and d-d_0 is the deformation of the sample. The fitting procedure determines the reduced modulus E^*, which can be converted to the elastic (Young's) modulus of the sample, E_s if Poisson's ratio of the sample, υ_s, and of the tip, υ_{tip}, are known:

$$E^* = \left[\frac{1-\upsilon_s^2}{E_s} + \frac{1-\upsilon_{tip}^2}{E_{tip}}\right]^{-1}.$$

Following this online analysis, modulus maps of the Cu surface are generated; a representative example is shown in Fig. 5a. A histogram of the moduli is shown below the map. Note the "ridge-and-valley" pattern that develops across the width of the map. The exact origin of this pattern is still unknown, but it is possible that it relates to the manufacturing process used to produce the Cu coating. This type of patterning was not observed in the Kapton substrate.

In addition to the elastic modulus, the maximum deformation of the surface is also measured during QNM imaging. The maximum deformation is defined as the penetration of the tip into the surface at the peak applied force, after subtracting cantilever compliance [1]. Sample deformation increases with increasing applied load under the tip. Measured deformation may include both elastic and plastic contributions, which can be deconvoluted with additional post-processing—this was not done for the present measurements. In cases where the deformation is mostly plastic, the deformation data can be converted into a harness value via contact mechanics relationships. Some error in the deformation data is expected due to an offset between the initial jump-to contact point and the measurement point, but at such low applied loads the error is expected to be minimal. A representative example of the deformation maps obtained for Cu during this study is shown in Figure 5b. Again, note the "ridge-and-valley" pattern evident in the deformation data, the origin of which is as yet unknown.

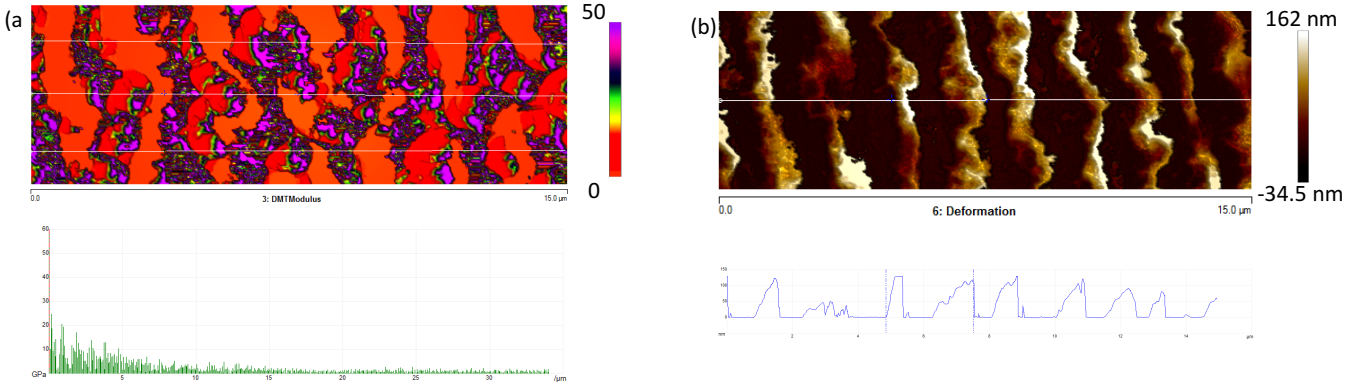

Figure 5. Representative DMT Modulus map (a) and deformation map (b) obtained from Cu films. A histogram of measured moduli is shown below the map in (a), while a line profile of deformation is shown below the map in (b).

Perhaps the most powerful application of the QNM data in this study is the ability to assess the variation in modulus as a function of surface deformation, which is in turn, 'topographical' data. As shown in Fig. 6 it is possible to overlay a color map of elastic modulus, measured in GPa, onto a 3D projection of the surface deformation, measured in nm. These maps, in effect, represent a four-dimensional picture of the surface material properties of the Cu films. In the 4D projection it is obvious that the elastic modulus and surface deformation are correlated—regions of the sample with limited deformation (low height values) display the highest modulus values (purple regions). This relationship is reasonable given that modulus is a measure of the material stiffness

and stiffer regions should be expected to deform less. Additionally, the least deformable regions of the surface have moduli on the order of 50 GPa, a value that is reasonable given the Cu film (E=70 GPa) is deposited on a more compliant Kapton substrate (E=3 GPa).

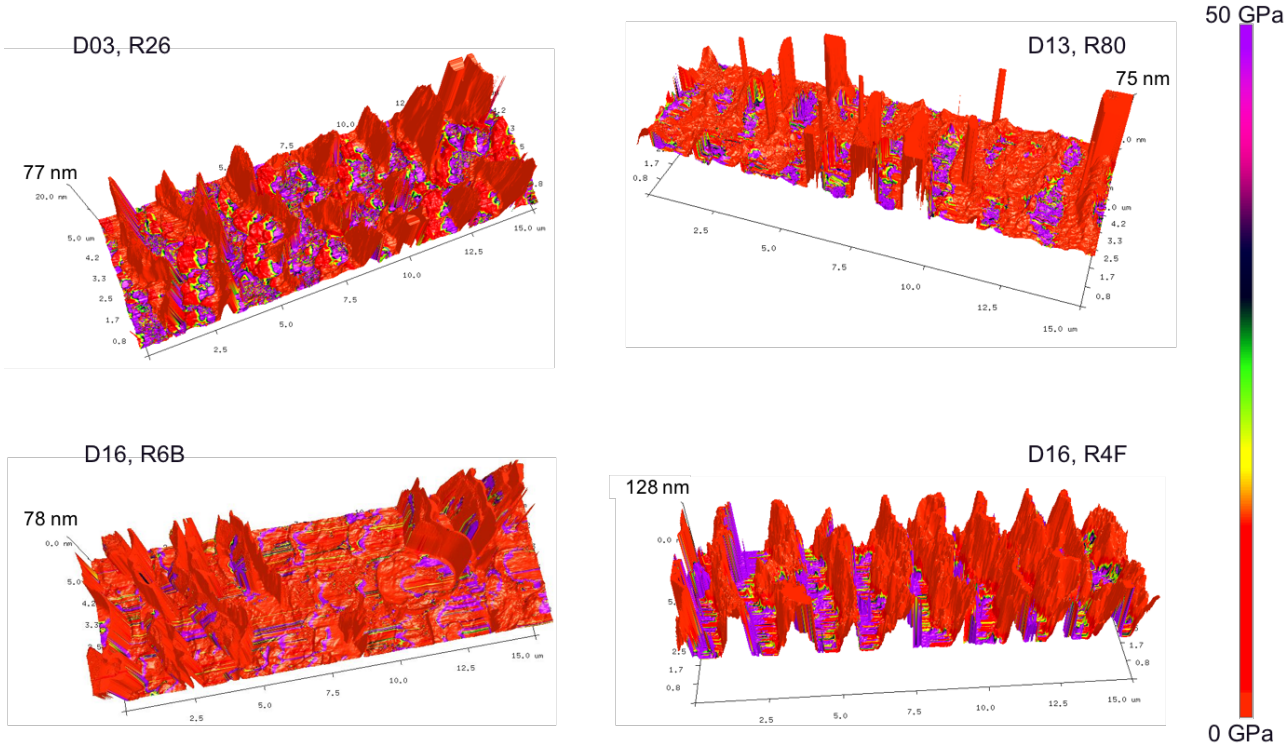

Figure 6. Color maps of elastic modulus overlain on 3D deformation topography maps. Resulting maps are effectively 4D projections of the correlation between modulus and deformation. Regions with highest modulus deform the least.

Assessment of Similitude

In general, there is strong similarity among all four tested lots of Microclad material. Both the Kapton substrate and Cu coating are smooth and flat (Kapton RMS: ~3 nm; Cu RMS: 20-50 nm) regardless of the material lot. However, it should be noted that the Cu films from the D16 lot have the highest RMS roughness and largest variation in measured values, as compared with the other Datex and Fortin materials. Mechanical properties are also uniform within the measured areas, both for the Cu films and the Kapton substrates.

Based on these data, D16 material should be subjected to performance testing and its response compared with that of qualified materials. Furthermore, given that surface roughness has been shown to impact the electrical conductivity and corrosion susceptibility of metal thin films, it may be important to identify an experimental matrix for "accelerated aging" of D16 materials to make a truly quantitative performance comparison with qualified and stockpiled materials.

Acknowledgements

The authors would like to thank Miles Beaux and Miguel Santiago Cordova of MST-7 for assistance with using the Multimode AFM while the Dimension Icon was out of service. The Multimode is part of the Plutonium Surface Science Laboratory. The Plutonium Surface Science

Laboratory is operated as a collaboration between the Engineered Materials Group (MST-7) and the Nuclear Materials Science Group (MST-16) at Los Alamos National Laboratory..

References

1. B. Pittenger, N. Erina, C. Su: “Quantitative Mechanical Property Mapping at the Nanoscale with PeakForce QNM”, Bruker Application Note #128 (2012)

Thermal Analysis of Microclad: TGA and DSC of Polyimide film

Matthew Dirmyer

Chemistry Division, C-CDE

The polyimide component of the microclad system was characterized via Thermogravimetric Analysis (TGA) and Differential Scanning Calorimetry (DSC). These thermal analyses show a great deal of inter- and intra- similitude with the exception of some D-16 samples.

Introduction

Thermal analysis methods such as Thermogravimetric Analysis (TGA) and Differential Scanning Calorimetry (DSC) can be very informative for characterizing polymeric composite materials. TGA provides weigh loss as a function of temperature. Features such as weight loss at low temperatures indicate loss of low molecular weight species (entrapped solvents, unreacted monomer, etc.). The onset of decomposition temperatures (T_d) can be used to compare the thermal stability of the material. DSC measures heat flow as a function of temperature and is used to determine phase change information (melt, crystallization, etc.).

Experimental

The microclad samples were obtained from the Microclad Characterization Team. The samples that were analyzed are shown in Table 1. Sample were etched in ~25% HNO_3 for 5 minutes to remove the copper. The remaining polyimide Kapton film was removed from the acid and dried.

TGA thermograms were collected using a Thermal Analysis TA-Q-5000-IR. Sample mass was approximately 2-4 mg. Samples were ramped at 10 °C/min to 800 °C under a nitrogen atmosphere. Thermogram analysis was accomplished using TA-Universal Analysis software.

DSC thermograms were collected using a Thermal Analysis TA-Q-20-a. Sample mass was approximately 5-7 mg. The heating program for conventional DSC measurements was carried out as follows: 1) Samples were equilibrated at 35 °C, 2) Ramped to 425 °C at 10 °C/min, 3) Ramped to 35 °C at 10 °C/min, and 4) Ramped to 425 °C at 10 °C/min. Thermogram analysis was accomplished using TA-Universal Analysis software.

Datex 2003 Lot	Datex 2013 Lot	Datex 2016 Lot	Fortin Lot
D03-8B	D13-68A	D16-10-I	FORTIN 160
D03-9B	D13-75A	D16-4-G	FORTIN 175
D03-24B	D13-83A	D16-5-G	
D03-19A	D13-56A	D16-7-D	
D03-6A	D13-57A	D16-5-D	
	D13-79B	D16-4-D	
	D13-62A	D16-9-F	
	D13-71B		

Table 1. List of samples analyzed using TGA and DSC.

Results and Discussion

TGA

Overall, TGA shows good similitude between the lots and within each lot with one exception. Figure 1 shows TGA thermograms for each lot; each solid trace is an average of replicates with the dashed lines representing +/- one standard deviation. The average plots all agree well with one another in a gross sense. The onset of decomposition temperatures all agree well with each showing an equivalency in thermal stability (Table 2).

Lot D-16 shows greater variability than all other lots, specifically at lower temperatures. Three out of the seven of the samples show a substantial weight loss at low temperature. The inset in figure 1, highlights this low temperature loss. The D-16 lot is represented by black traces in the inset figure. The weight loss onset occurred around 130°C and represents 1.62 +/- 0.54 weight %. The low temperature loss was also observed in one case in D-13. The potential origins of this weight loss will be discussed in the conclusions.

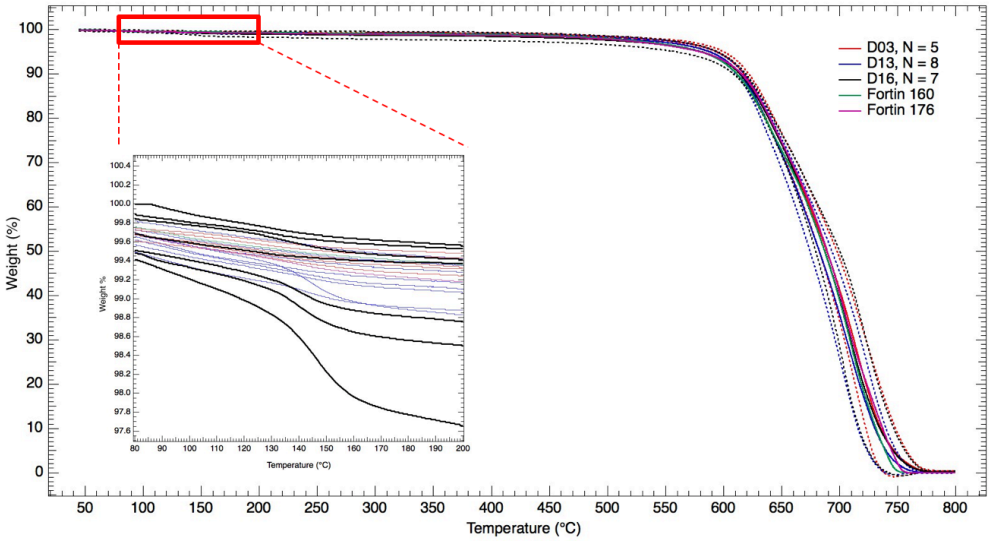

Figure 1. TGA thermograms showing weight loss as a function of temperature for all lots. Solid lines represent an average of N replicates with dashed lines representing +/- one standard deviation. Inset: TGA thermograms showing 80-200 °C highlighting the low temperature weight loss observed in show D-16 samples (black traces).

Lot	N	Weight % at 180°C		Onset of Decomposition (°C)	
		average	σ	average	σ
D-16	4	99.45	0.1	617.3	4.65
D-16 Low T weight loss	3	98.38	0.54	621.83	3.87
D-13	8	99.17	0.2	615.11	5.59
D-03	5	99.38	0.088	616.62	6.02
Fortin 160	1	99.4	--	619.44	--
Fortin 175	1	99.22	--	605.73	--

Table 2: Weight % at 180 °C and Onset of Decomposition temperature for all lots.

DSC

Similarly, DSC data shows a great degree of similitude between the lots of material. A representative DSC thermogram is shown in Figure 2. During the first heat cycle (solid red), an exothermic peak is centered around 130°C, with an enthalpy of formation ~6-9 J/g. An exothermic peak is characteristic of some sort of chemical reaction, and typically in polymer systems could be some sort of further cure in the material. Furthermore, this exotherm is not observed in the second heating cycle (dashed red), implying a complete reaction after the first cycle. Nothing is observed the cooling cycle. A glass transition temperature (T_g) wasn't observed over the temperature range probed. While literature reports show a second order transition in the range between 360-410°C that can be assumed to be the T_g often different measurement techniques produce differing results therefore a glass transition temperature wouldn't be a very reliable property for similitude comparisons.

The T_{max} and enthalpy (ΔH) of the exotherm compare well with each other. The enthalpy of the D-16 samples which showed the low temperature weight loss is slightly higher than other observed enthalpies.

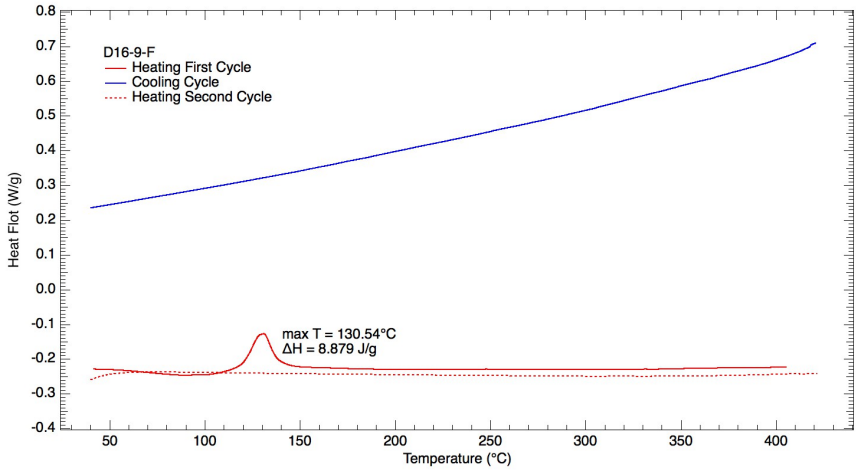

Figure 2. A representative DSC thermogram for the samples analyzed.

Lot	N	T_{max} of Exotherm		ΔH of Exotherm	
		average	σ	average	σ
D-16	4	129.01	1.49	5.15	1.54
D-16 Low T weight loss	3	129.95	0.52	7.68	1.6
D-13	8	134.41	0.53	5.49	2.64
D-03	5	127.96	1.94	5.45	2.25
Fortin 160	1	128.94	--	3.45	--
Fortin 175	1	129.89	--	7.94	--

Table 3. DSC data presenting T_{max} and ΔH for all of the lots analyzed.

Conclusion

The TGA and DSC results on the thermal properties of the polyimide Kapton film suggest the lots show a great deal of inter- and intra- similitude. D-03, D-13, and Fortin materials exhibit very similar thermal behavior, whereas some D-16 samples behave similar to D-03, D-13, and Fortin others do not. D-16 exhibits more widely varied thermal behavior. All the materials exhibit an exotherm observed via DSC the is centered around 130°C. This is also the temperature at which some D-16 samples show a significant weight loss (~1.5 %). The exotherm seems to be more prevalent in the D-16 samples that show this weight loss. It is hypothesized that these D-16 samples have slightly elevated levels of poly(amic acid) intermediate that has yet to be fully thermally converted to polyimide (Figure 3). The heat of the reaction is what is observed as the exotherm in the DSC and the weight loss observed in TGA would be explained by the release of water as a byproduct.

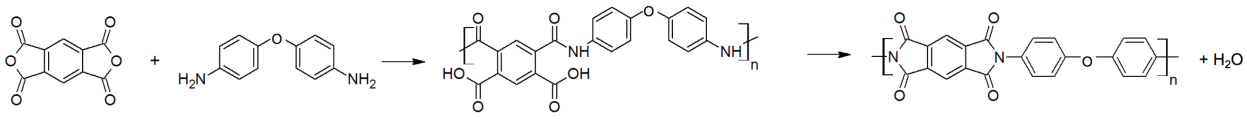

Figure 3: Conversion of poly(amic acid) to polyimide; potential hypothesis to explain thermal properties anomalies observed in some D-16 samples analyzed.

Microclad DMA Testing

Jennie Keller & Trevor Shear

MATERIALS AND METHODS

Dynamic Mechanical Analysis (DMA) tensile testing was performed to determine the Young's Modulus of microclad samples at elevated temperatures. Detonator function significantly depends on the modulus and yield strength of the microclad material; therefore, mechanical properties and the similitude among different lots of microclad provide crucial information. All testing was performed on a TA Instruments Q800 DMA with tension film clamp geometry. Samples were cut width-wise from 15.75 ± 1.31 mm strips of microclad to widths of 9.23 ± 0.99 mm using a razor blade. Thicknesses were measured by caliper and were on average 0.06 ± 0.02 mm. The procedure involved equilibrating the samples at 50°C, holding isothermally for 5 min, then applying an amplitude sweep from 15-150 μm. This method was repeated at multiple temperatures in increments of 50°C up to 300°C. Microclad from four different years was tested: Fortin (1985), D03 (Datex 2003), D13 (Datex 2013), and D16 (Datex 2016). Pure Kapton® was also tested to help determine if the Kapton® or the copper coating had a larger influence on mechanical properties.

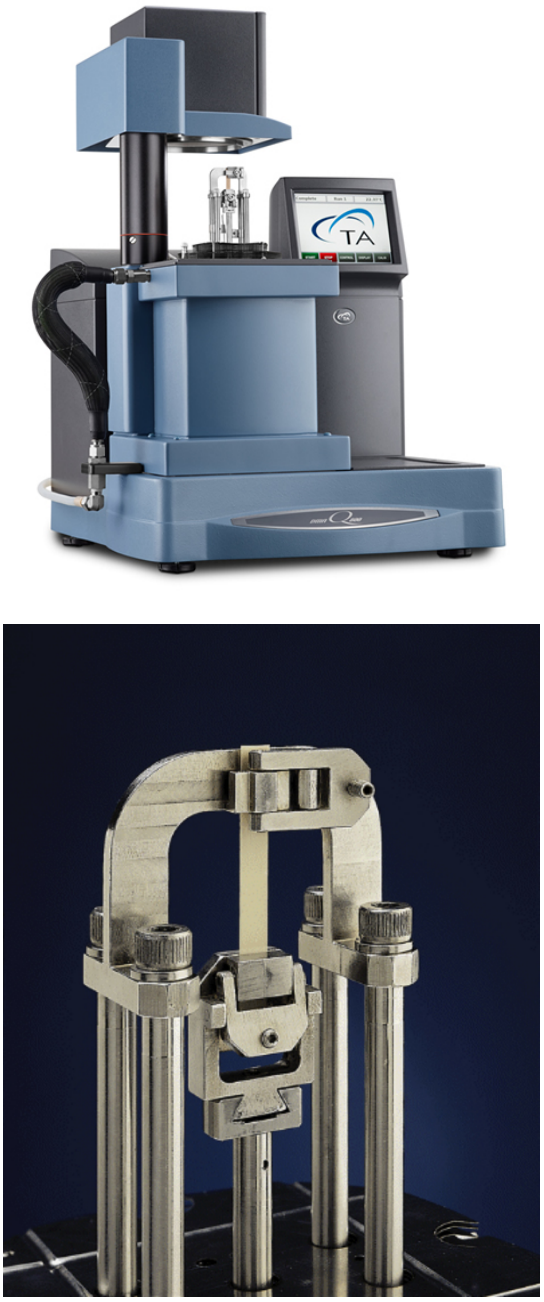

Figure 1. TA Instruments Q800 DMA (left) and the film tension clamp (right).

RESULTS

There was significant variation in DMA results, both within sample sets (same year, different lots) and across samples sets (different years, different lots). Stress/strain curves were created of replicate data through each temperature range (Figure 2). The number of replicate tests varied from sample to sample.

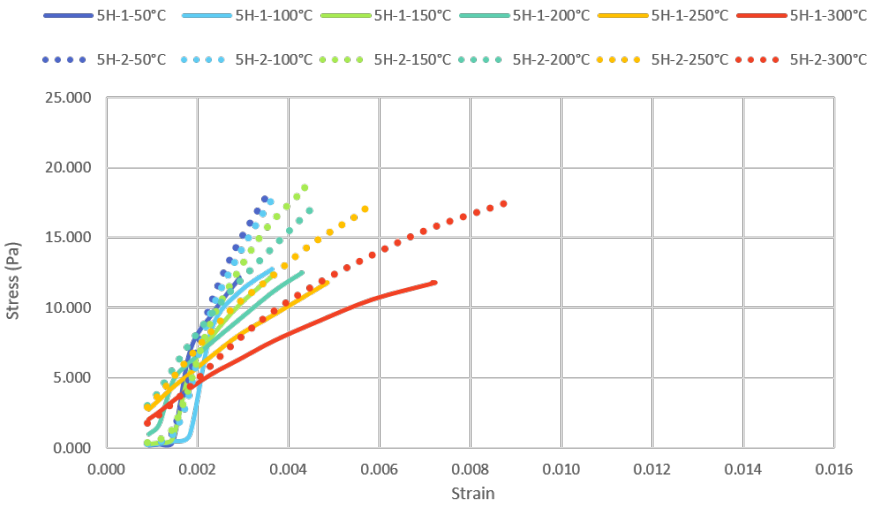

D16-5H

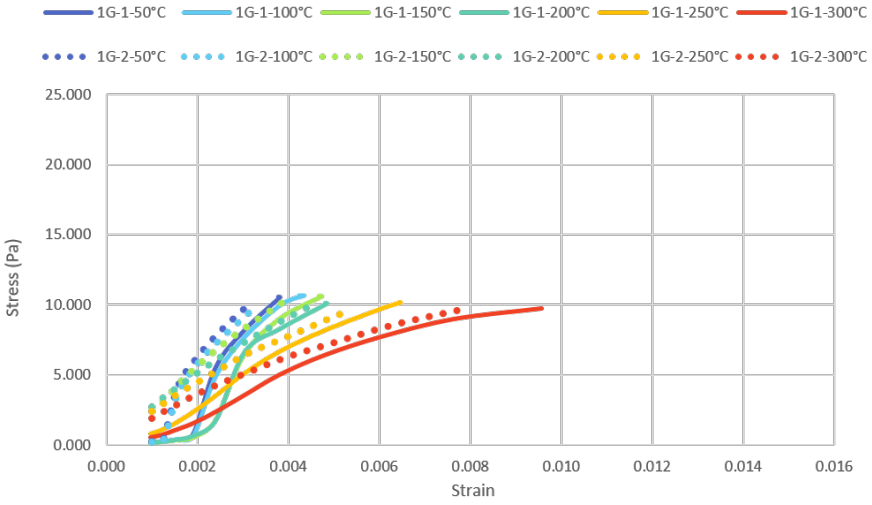

D16-1G

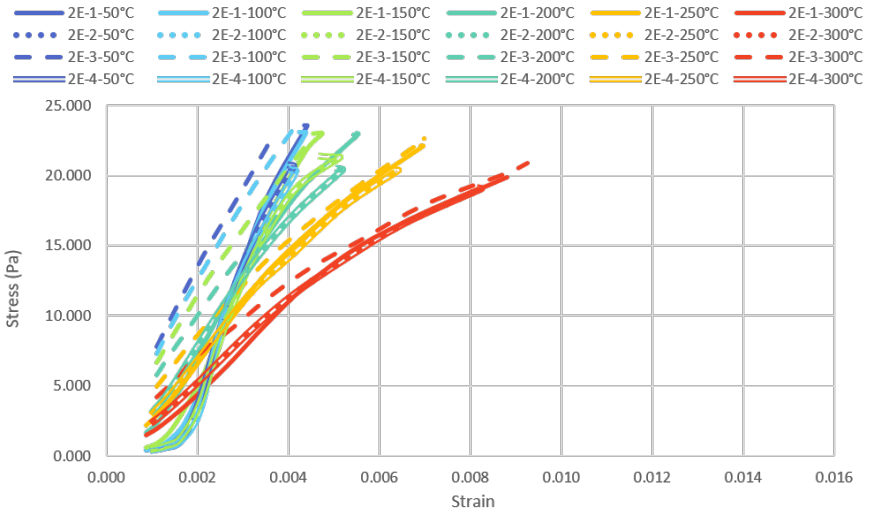

D16-2E

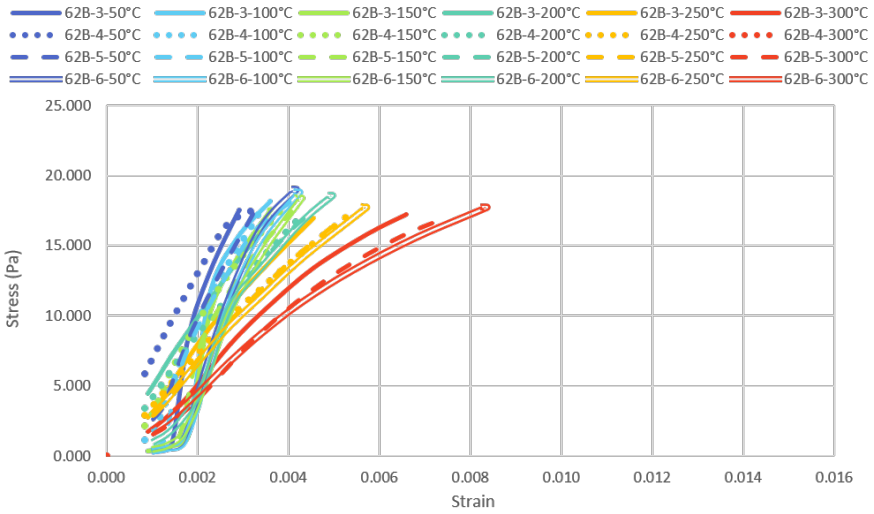

D13-62B

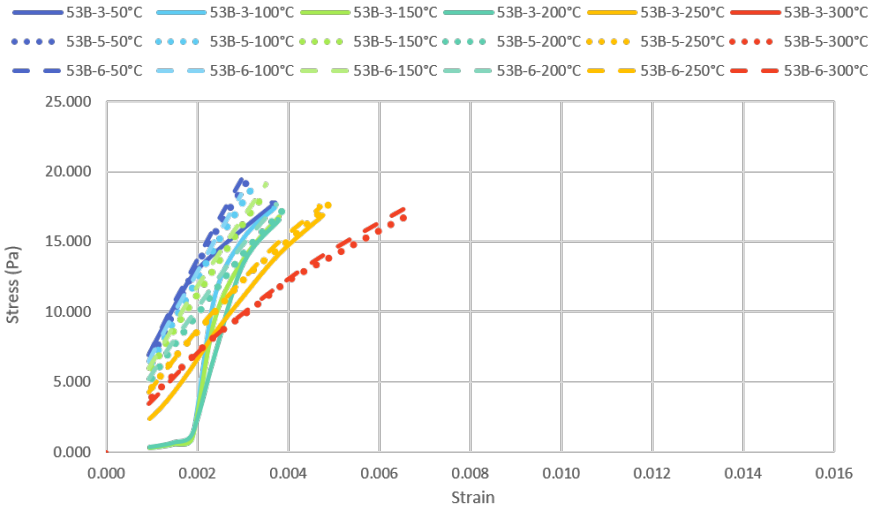

D13-53B

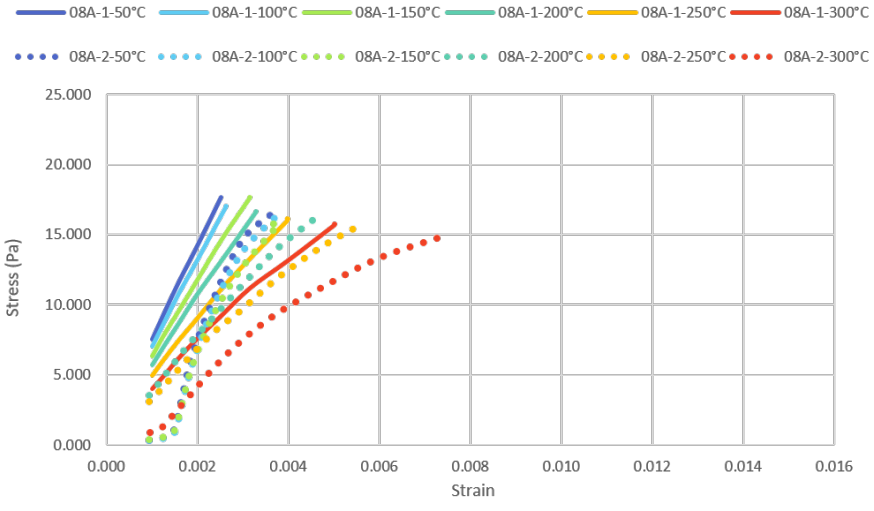

D03-08A

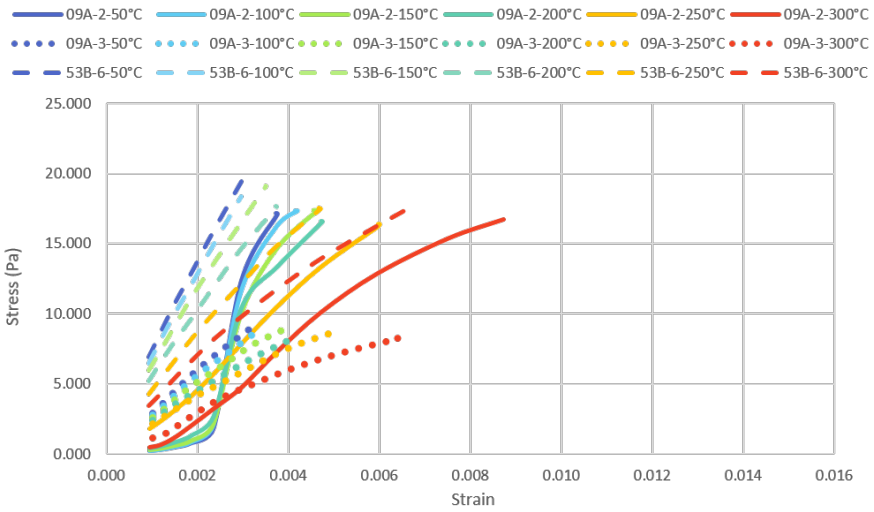

D03-09A

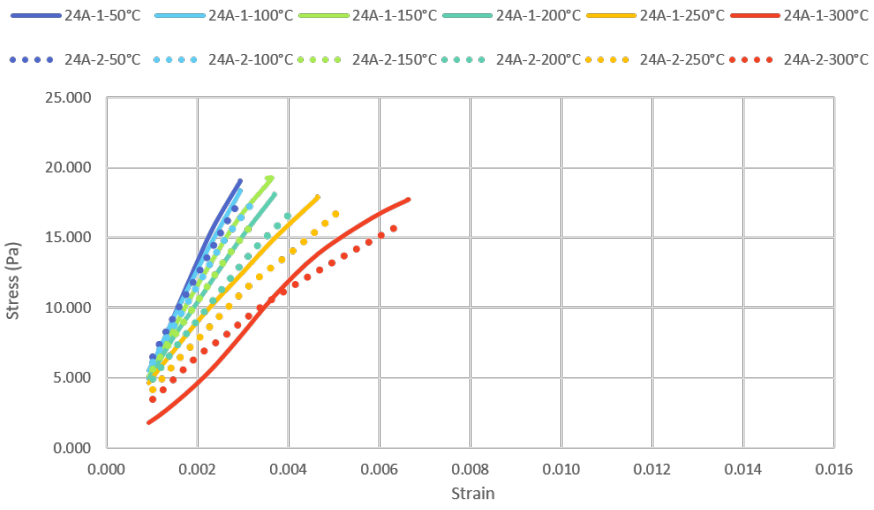

D03-24A

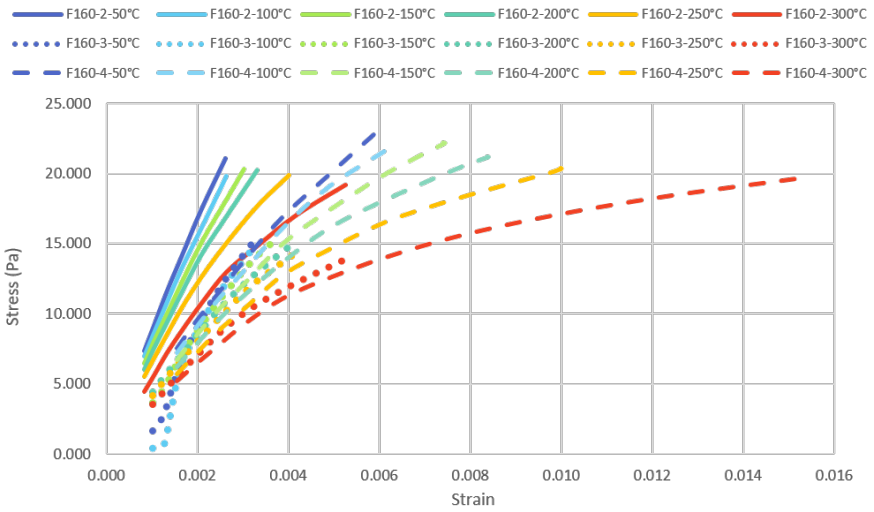

FORTIN-160

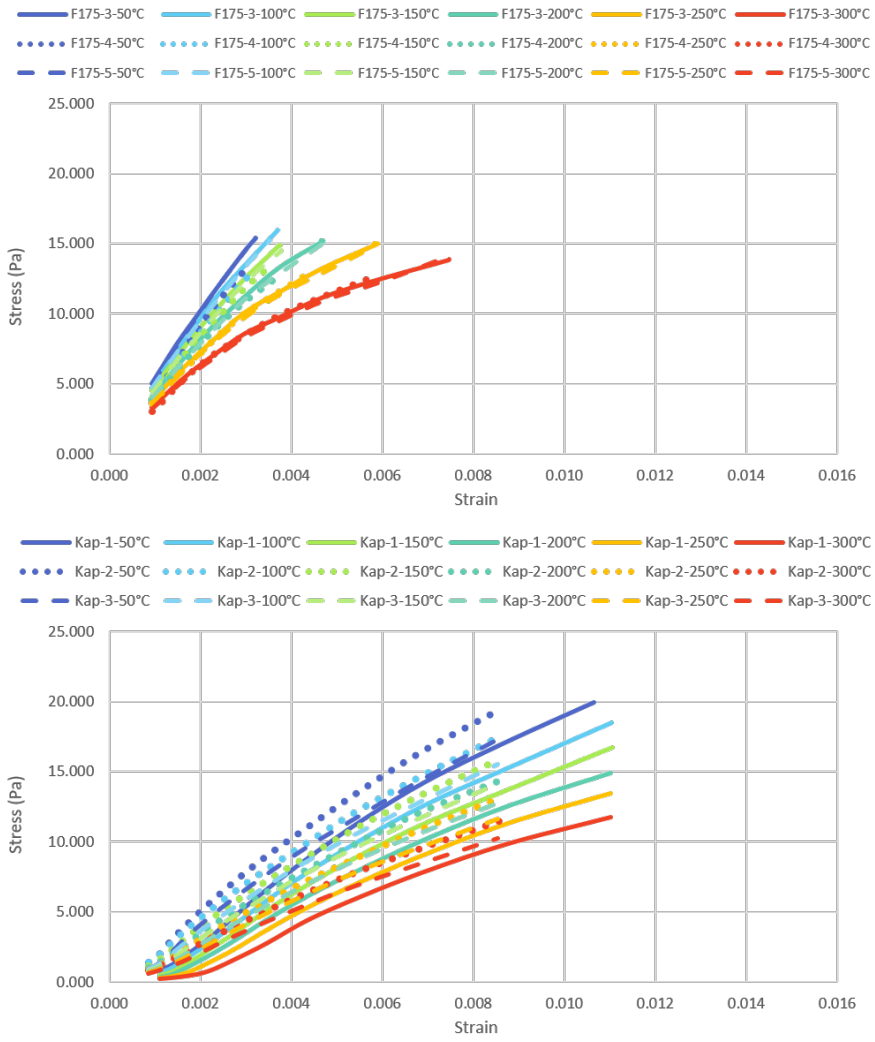

Figure 2. Stress/Strain curves for microclad and Kapton® samples.

From stress/strain curves, Young's Modulus values were calculated by taking the slope in the linear region of the stress/strain curves (Figure 3). Some replicate tests show non-linear behavior at strains less than 0.002. In this region, a sigmoidal curve can be identified. This shape is seen primarily at temperatures below 200°C. Although these curvatures are seen in all sample replicates, the modulus values were taken above 0.002 strain in an effort to exclude this abnormality. Standard deviations of replicate tests are given by error bars in Figure 3. Additionally, the DuPont™ data sheet value for Kapton® Type 100 HN Film (1 mil) can be seen in Figure 3 as the black bar at 200°C. This value closely resembles the modulus calculated for the pure Kapton® samples tested by DMA at the same temperature.

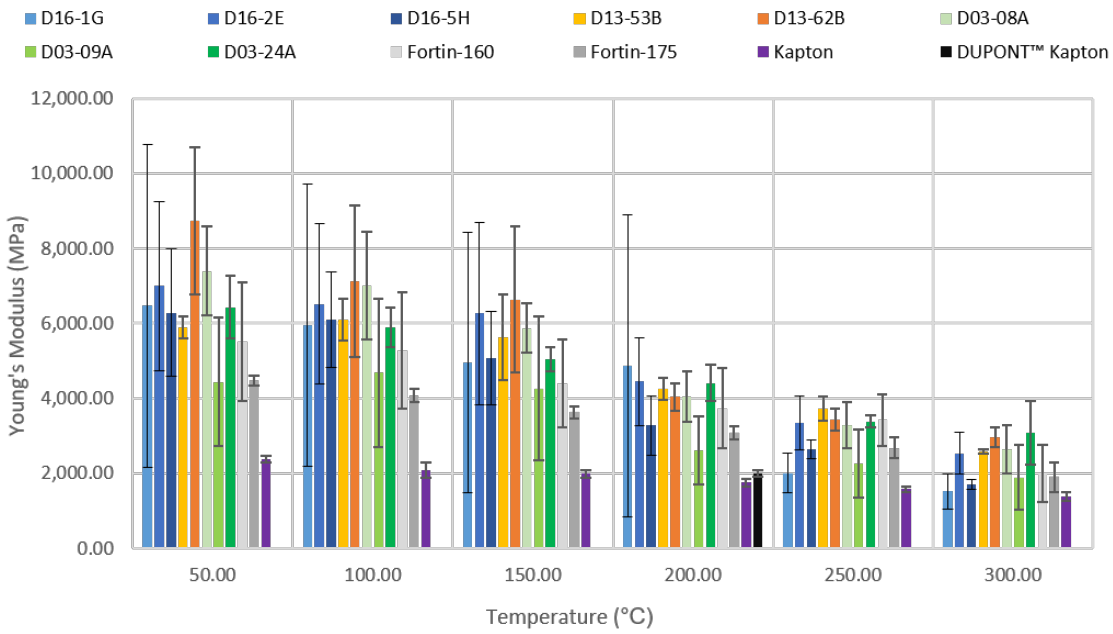

Figure 3. Young's Modulus values of microclad and Kapton® samples.

As temperature increases, the modulus of each material decreases. Because Young's Modulus is a measure of stiffness, this trend indicates that the material becomes more elastic with increasing temperature. Interestingly, as temperature increases, the magnitude of error also decreases. Based on this, it appears that the similitude of microclad materials improves with higher temperatures. A combined average of the modulus values for each sample year was calculated as an additional comparison of similitude (Figure 4).

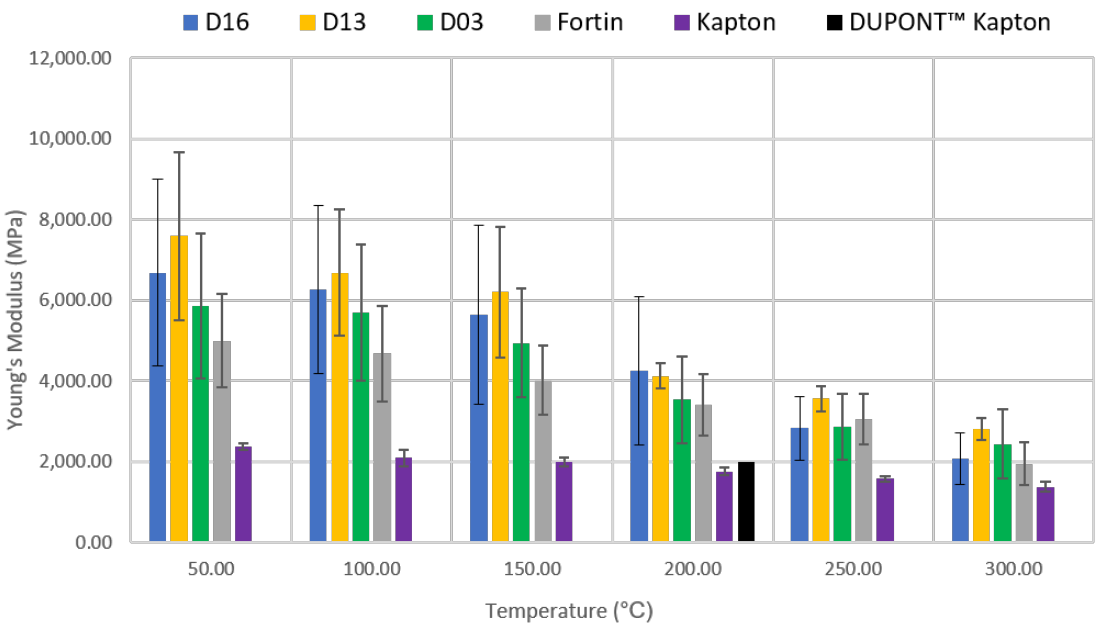

Figure 4. Combined average of Young's Modulus values by sample year.

Based on visual comparison, the combined averages show that each sample set is reasonably similar to one another. To verify this, JMP statistical analysis software by SAS® was utilized to statisically determine if there are differences in modulus data.

The first objective in the statisitcal analysis was to determine if the three lots of D16 (1G, 2E and 5H) were statisically different from one another. As mentioned above, the number of replicates tested for each sample was not consistent. To obtain reliable statistical results, each sample had to have the same number of data points. For example, to compare 50°C data of D16 1G (which had two replicates) to D16 2E (which had four replicates), two data points from D16 2E had to be eliminated. This was accomplished by using a random number genertor in Excel to select two random replicates of D16 2E for exclusion, thereby removing any human bias. Next, the F-ratio p-value was determined at a 0.10 significance level, with the null hypothesis that there was no difference between the D16 lots. In this test, if the p-value returned is greater than 0.1, the null hypothesis is validated; if the p-value is below 0.1, there are statistical differerences between lots. Results showed that for temperatures from 50°C to 200°C there were no differences in moduli data. However, it was revealed that at least one difference between lots existed at 250°C and 300°C (see Table 1).

Table 1. F-ratio p-values for D16 Lot Comparison at a Significance Level of 0.1

Temp (°C)	F-ratio p-value	Result
50	0.5761	No Difference
100	0.5098	No Difference
150	0.8545	No Difference
200	0.7626	No Difference
250	**0.0556**	**At least one difference**
300	**0.0795**	**At least one difference**

In order to find which lots were significantly different at 250°C and 300°C, the Student's t-test was employed. This analysis revealed that at 250°C, D16-2E was statstically different from both D16-1G (p-value of 0.026) and D16-5H (p-value of 0.072). The same lots were also found to be different at 300°C with p-values of 0.044 and 0.062, respectively (see Table 2).

Table 2. Student's t-test for D16 Lot Comparison at a Significance Level of 0.1

Temp (°C)	Sample 1	Sample 2	p-value
250	D162E	D161G	**0.0259**
	D162E	D165H	**0.0718**
	D165H	D161G	0.2592
300	D162E	D161G	**0.0443**
	D162E	D165H	**0.0619**
	D165H	D161G	0.6954

The second objective in the statistical analysis was to compare D16 samples to D13, D03 and Fortin. For these samples, F-ratio p-values were calculated between D16 and each other sample, and then the Student's t-test was performed. Again, to obtain reliable results, the analysis required the same number of data points for D16 and the contrasting year. Results showed no differences at any temperature interval between D16 and D03 or D16 and Fortin. There was one difference found between D16 and D13 at 250°C (see Table 3).

Table 3. Student's t-test Comparison of D16 and Other Sample Years at a Significance Level of 0.1

	Temp (°C)	F-ratio p-value	Result
D16 vs. D13	50	0.4948	No Difference
	100	0.7259	No Difference
	150	0.7868	No Difference
	200	0.8097	No Difference
	250	**0.0732**	**Samples Differ**
	300	0.1827	No Difference
D16 vs. D03	50	0.4971	No Difference
	100	0.5157	No Difference
	150	0.537	No Difference
	200	0.4049	No Difference
	250	0.9422	No Difference
	300	0.4828	No Difference
D16 vs. Fortin	50	0.1466	No Difference
	100	0.1211	No Difference
	150	0.1522	No Difference
	200	0.3151	No Difference
	250	0.6470	No Difference
	300	0.8562	No Difference

CONCLUSIONS

Variations were observed in stress/strain data among microclad samples, especially at combinations of low temperature and low strain rates. There are many possible causes for these disparities including sample processing, sample handling, as well as surface defects and/or imperfections in the materials. Young's Modulus values were calculated from linear regions above 0.002 strain in stress/strain data using TA Instruments Universal Analysis software. Comparison of average modulus values by year suggest little differences among samples. To confirm this theory, statistical analysis methods were used to determine if modulus values from each sample year were statistically different. Results did indicate that at high temperatures, D16-2E was statistically different from both D16-1G and D16-5H. However, further analysis indicated that D16 materials are statistically similar to D13, D03 and Fortin materials. The analysis only found one exception to this similitude; the Student's t-test revealed significant differences between moduli data of D16 and D13 at 250°C. Nevertheless, based on overall statistical results we can say with 90% confidence that D16 samples are statistically similar to D13, D03 and Fortin samples.

APPENDIX

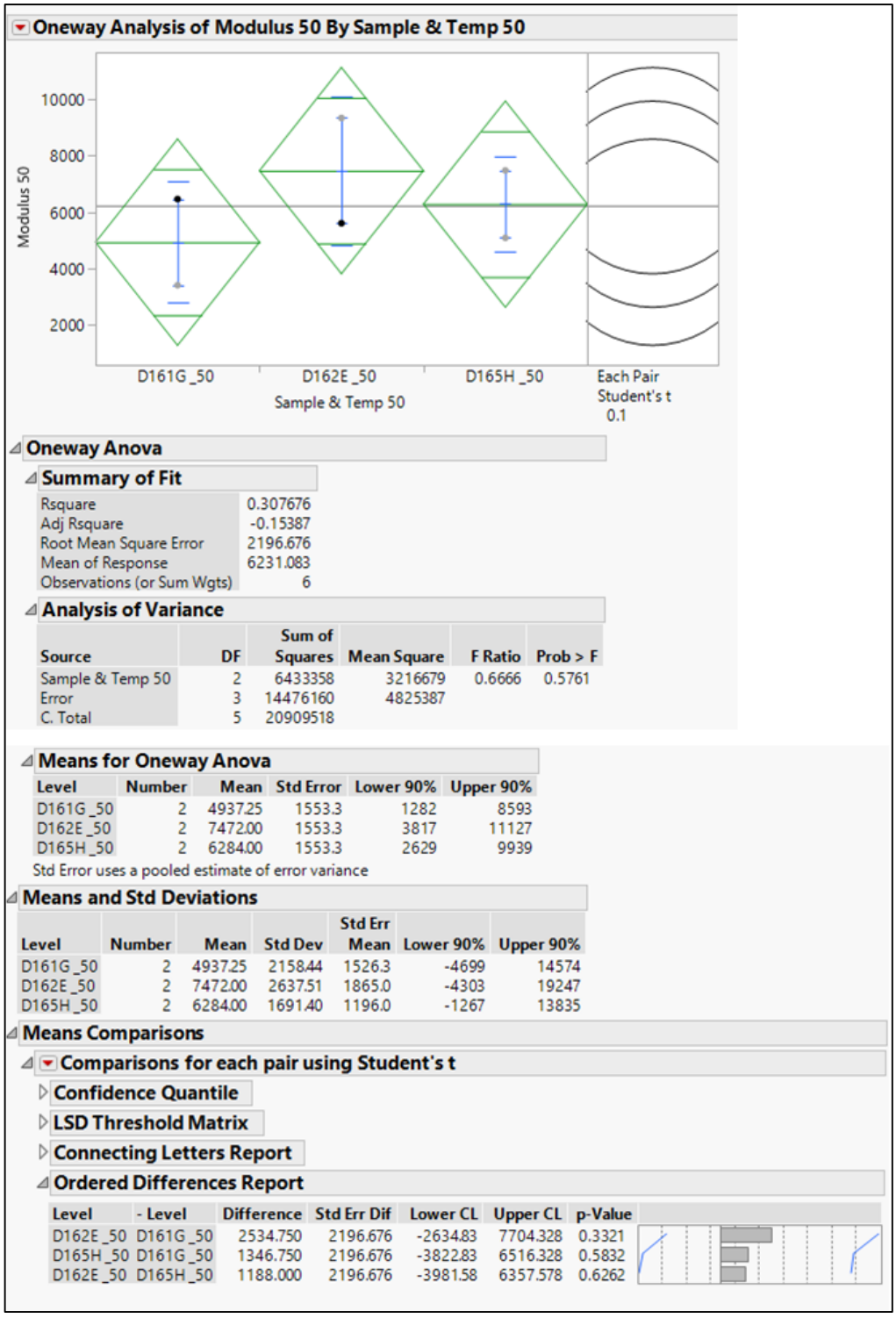

Figure 5. JMP Software Statistical Data for moduli comparison of D16 lots @ 50°C.

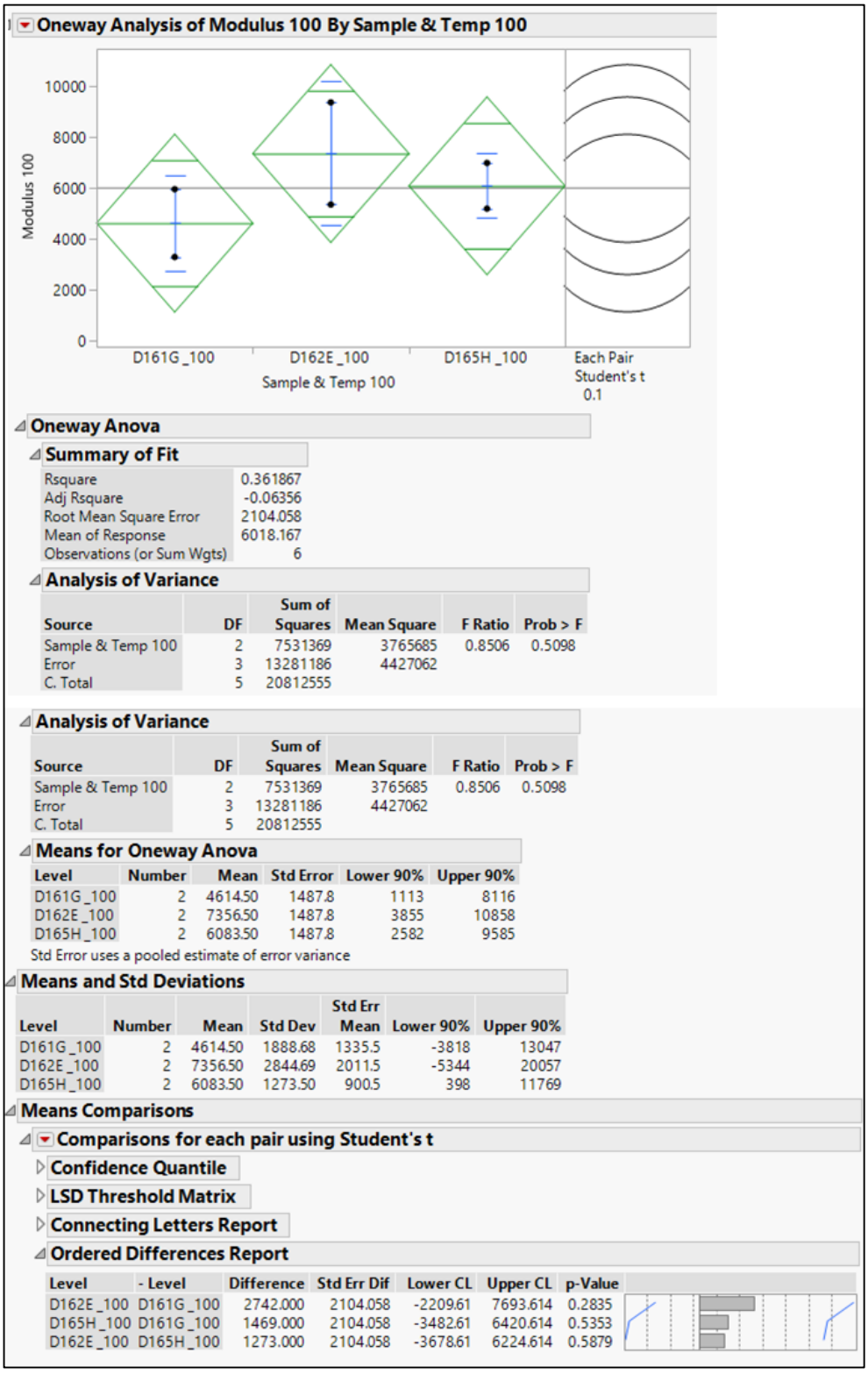

Figure 6. JMP Software Statistical Data for moduli comparison of D16 lots @ 100°C.

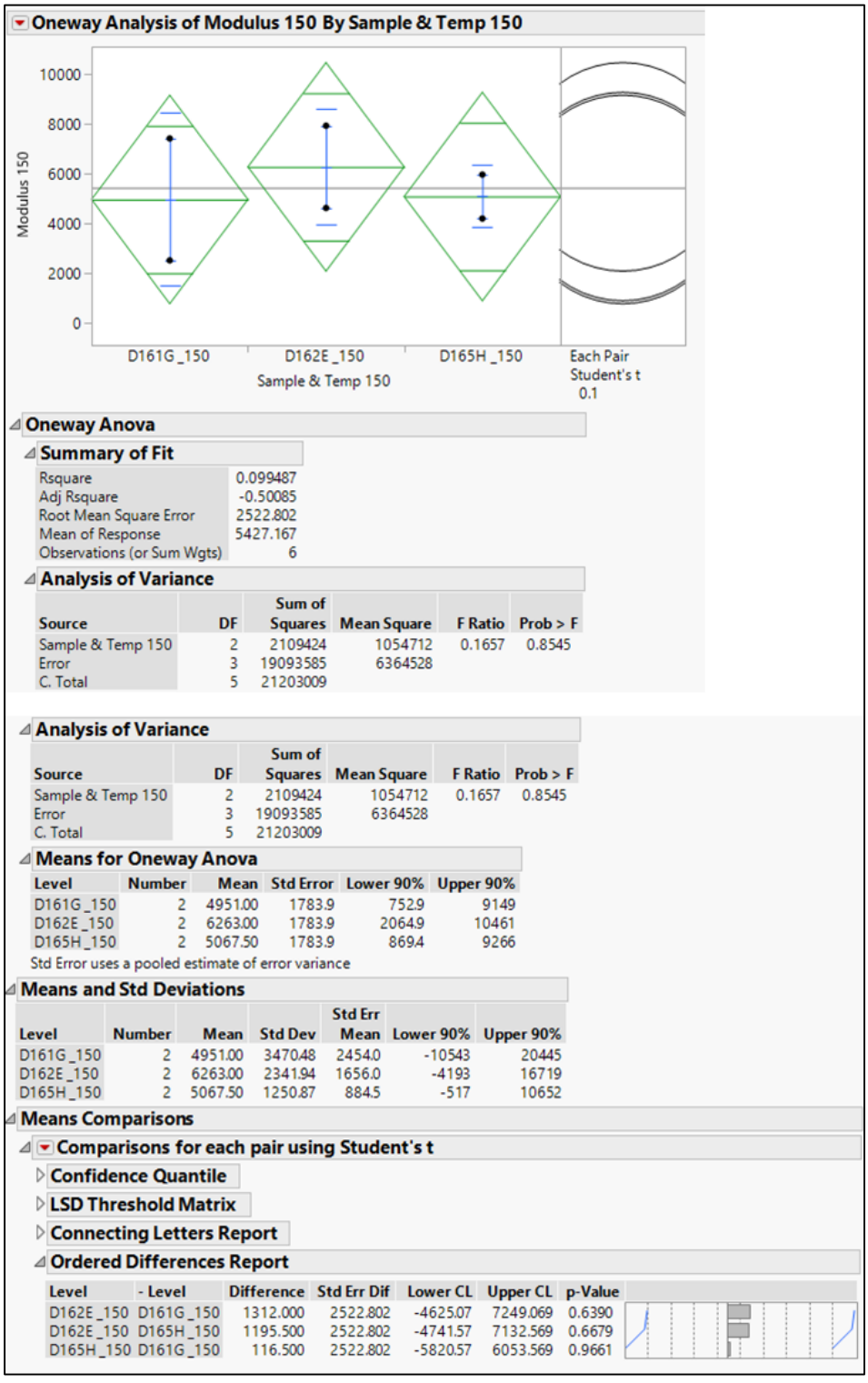

Figure 7. JMP Software Statistical Data for moduli comparison of D16 lots @ 150°C.

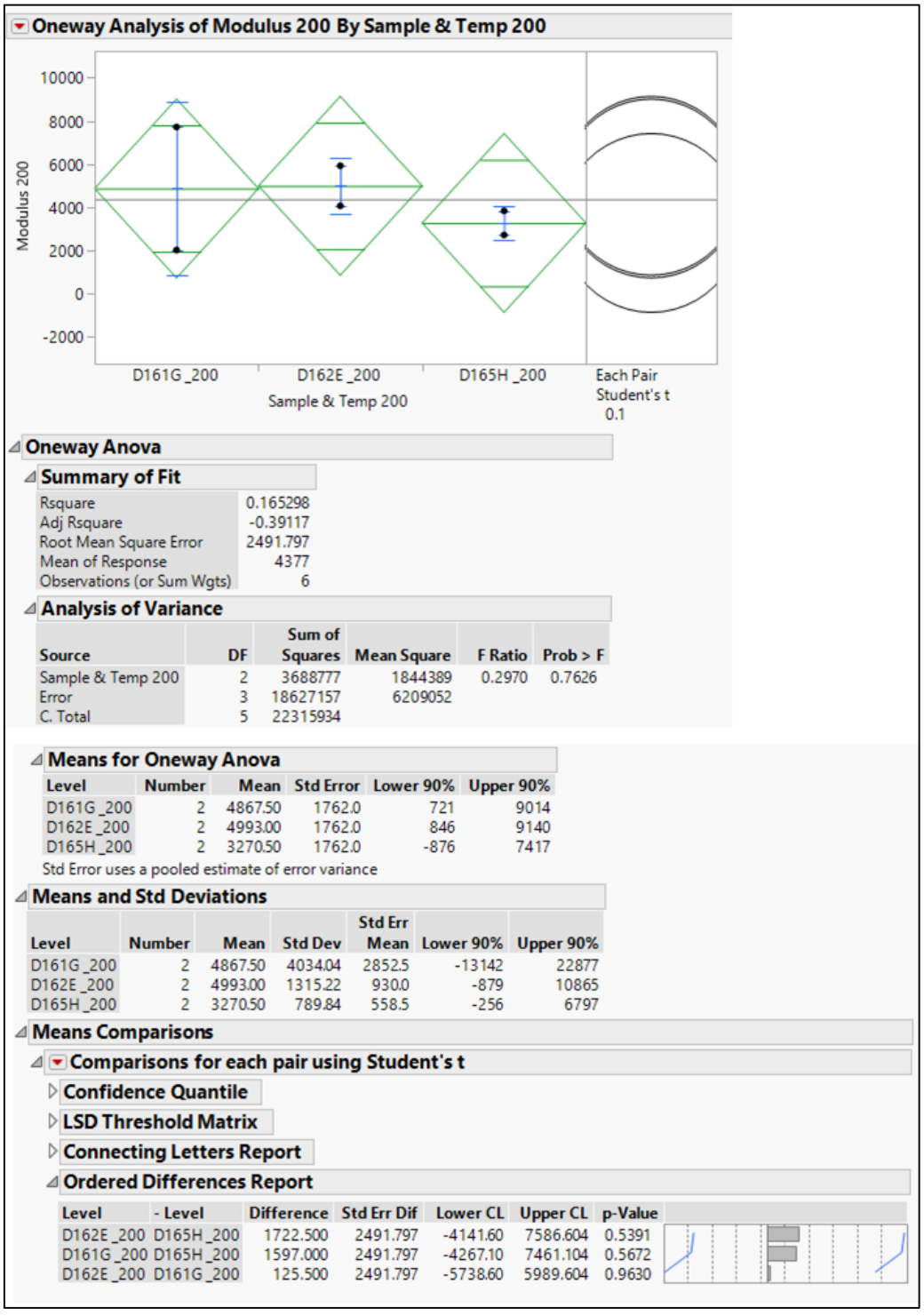

Figure 8. JMP Software Statistical Data for moduli comparison of D16 lots @ 200°C.

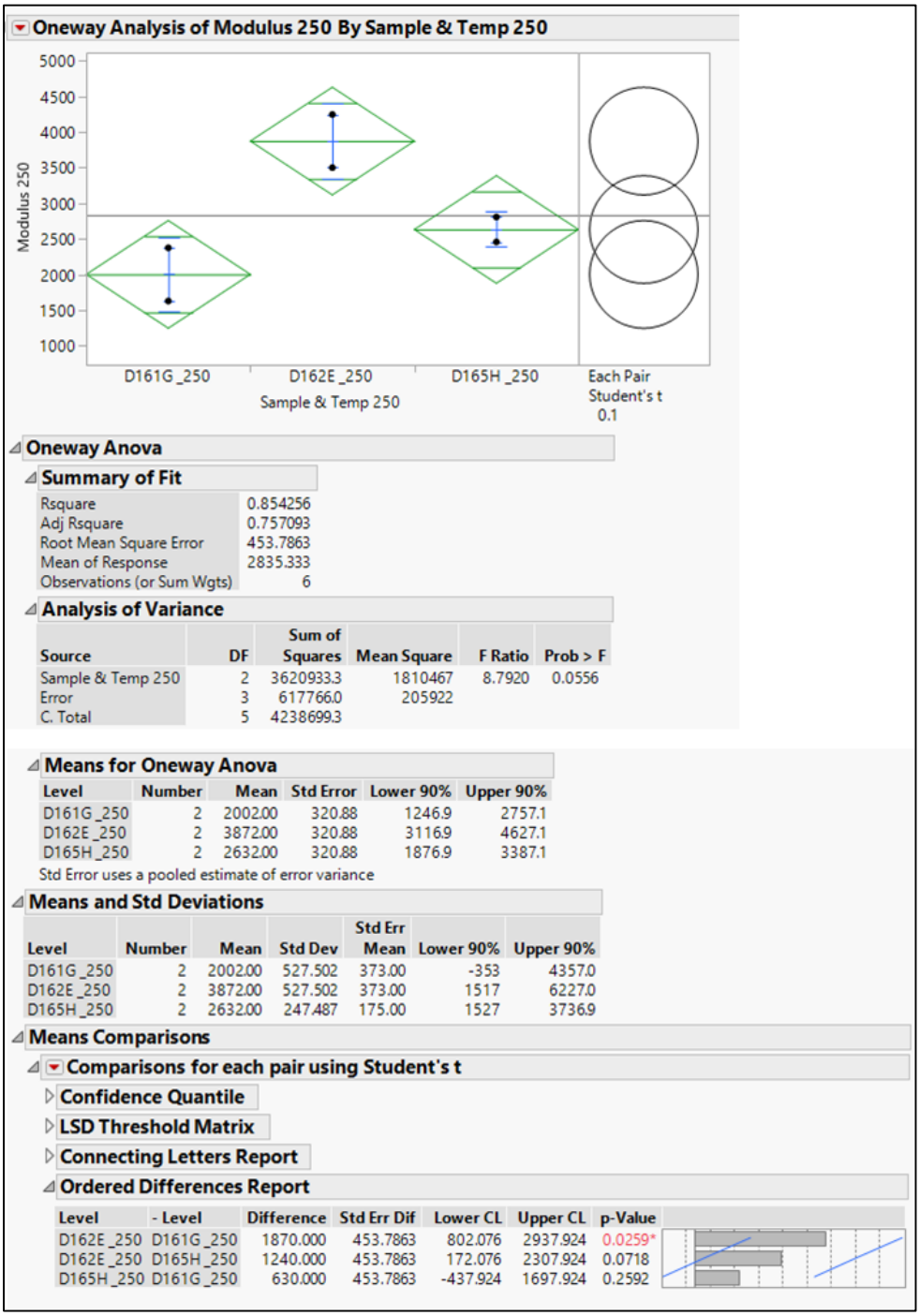

Figure 9. JMP Software Statistical Data for moduli comparison of D16 lots @ 250°C.

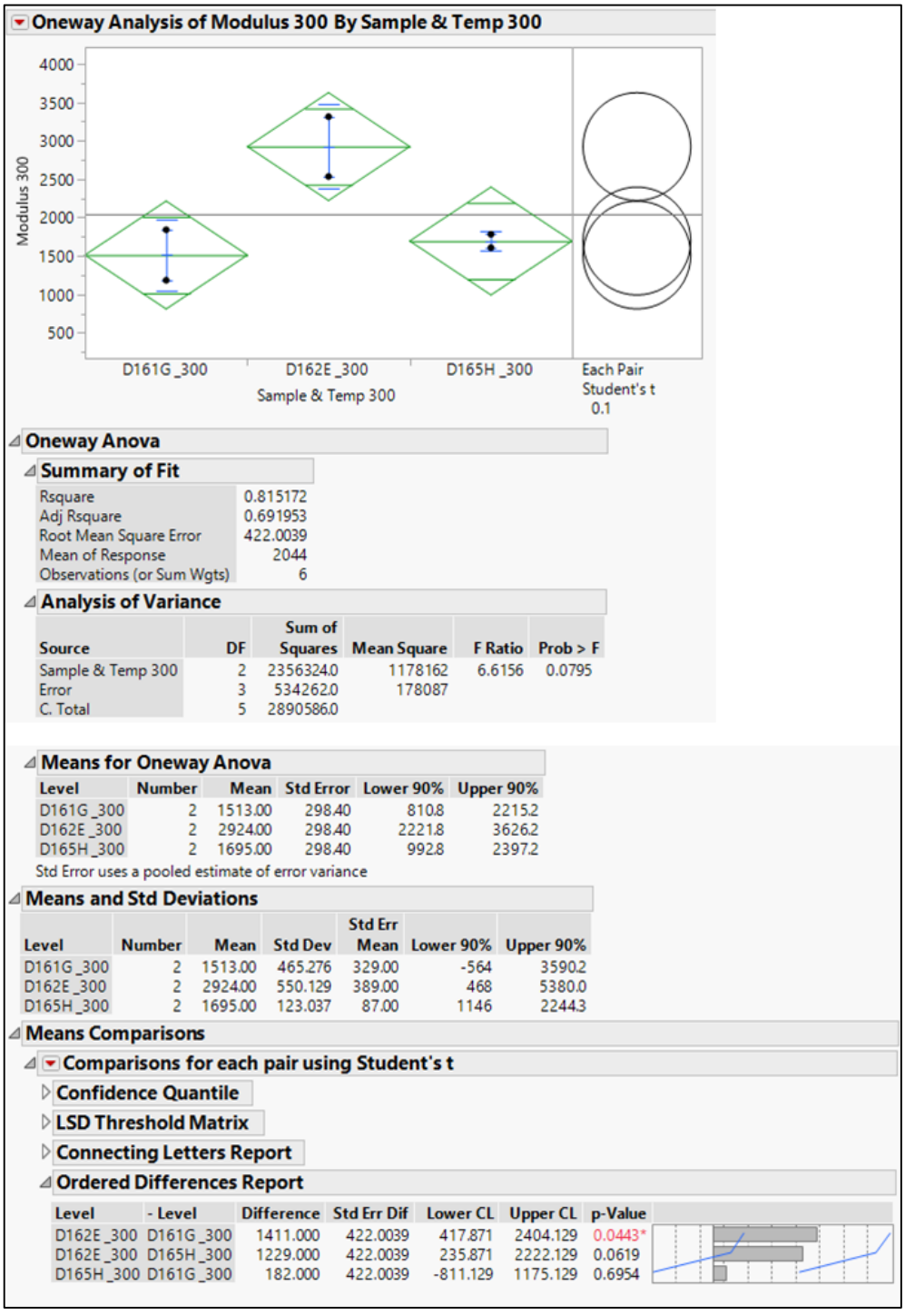

Figure 10. JMP Software Statistical Data for moduli comparison of D16 lots @ 300°C.

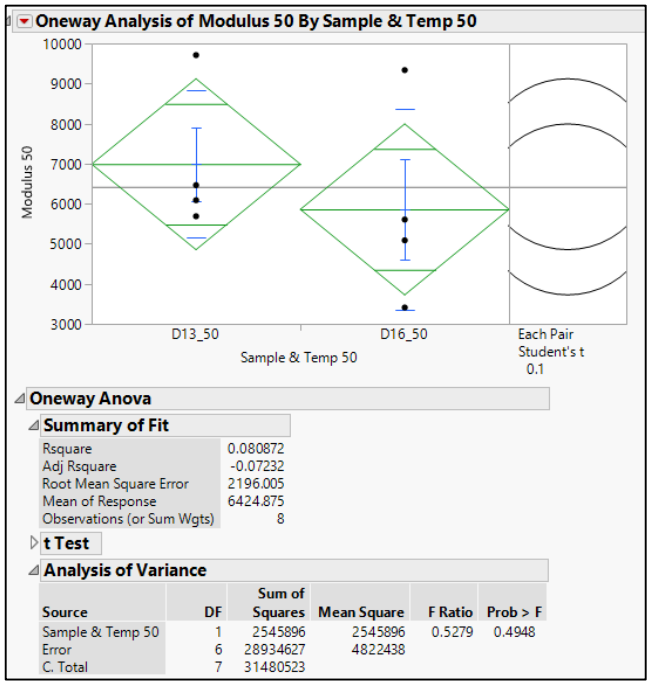

Figure 11. JMP Software Statistical Data for D16 vs. D13 moduli comparison @ 50°C.

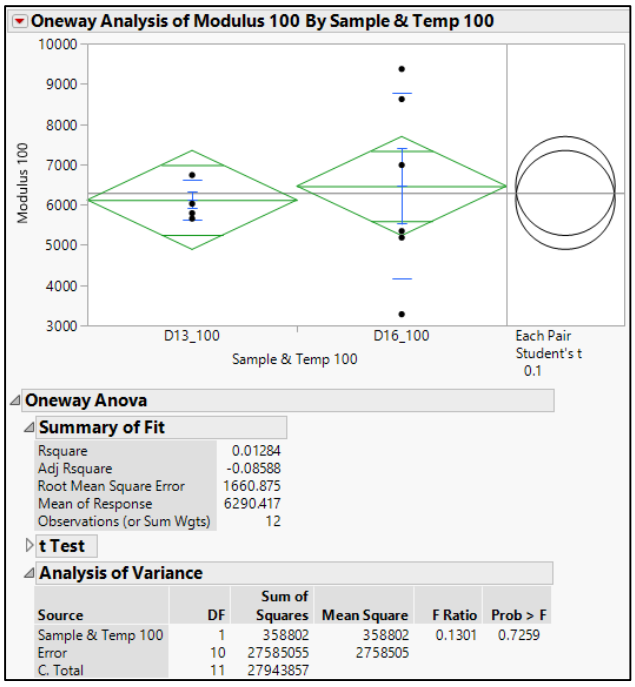

Figure 12. JMP Software Statistical Data for D16 vs. D13 moduli comparison @ 100°C.

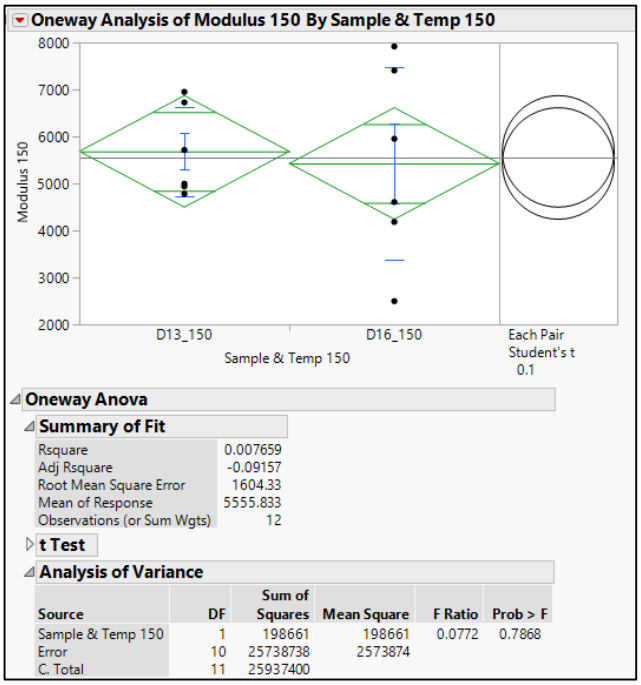

Figure 13. JMP Software Statistical Data for D16 vs. D13 moduli comparison @ 150°C.

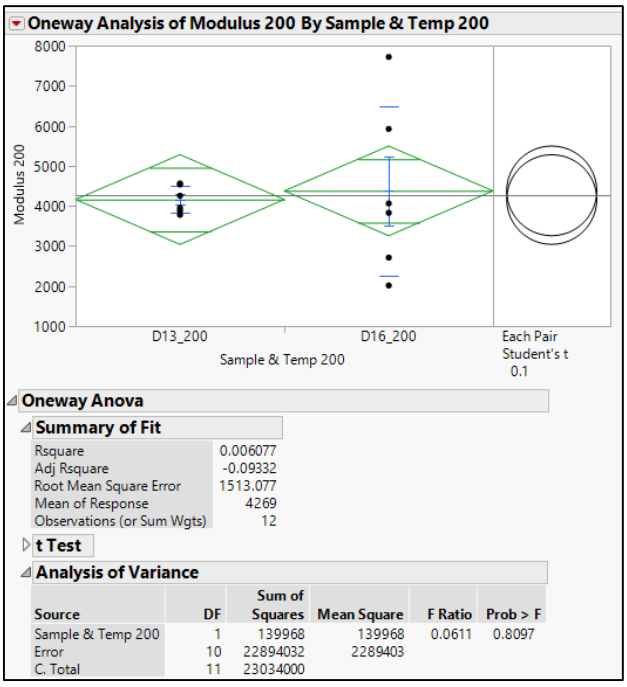

Figure 14. JMP Software Statistical Data for D16 vs. D13 moduli comparison @ 200°C.

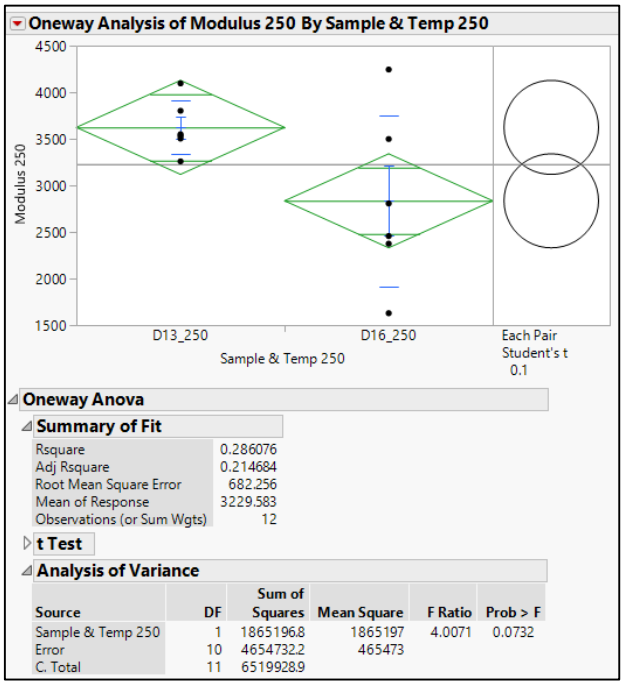

Figure 15. JMP Software Statistical Data for D16 vs. D13 moduli comparison @ 250°C.

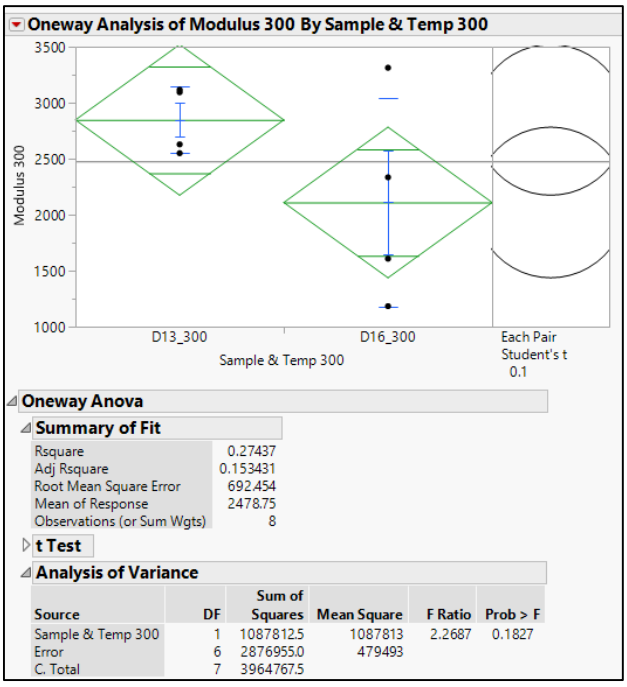

Figure 16. JMP Software Statistical Data for D16 vs. D13 moduli comparison @ 300°C.

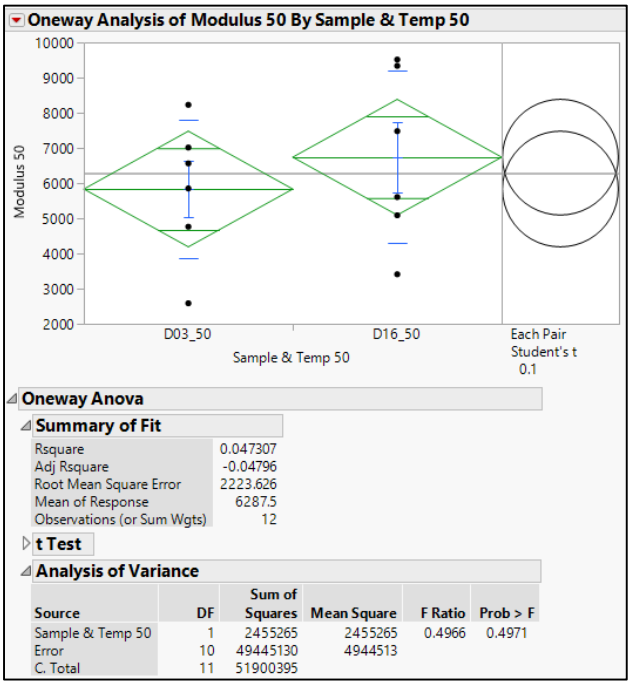

Figure 17. JMP Software Statistical Data for D16 vs. D03 moduli comparison @ 50°C.

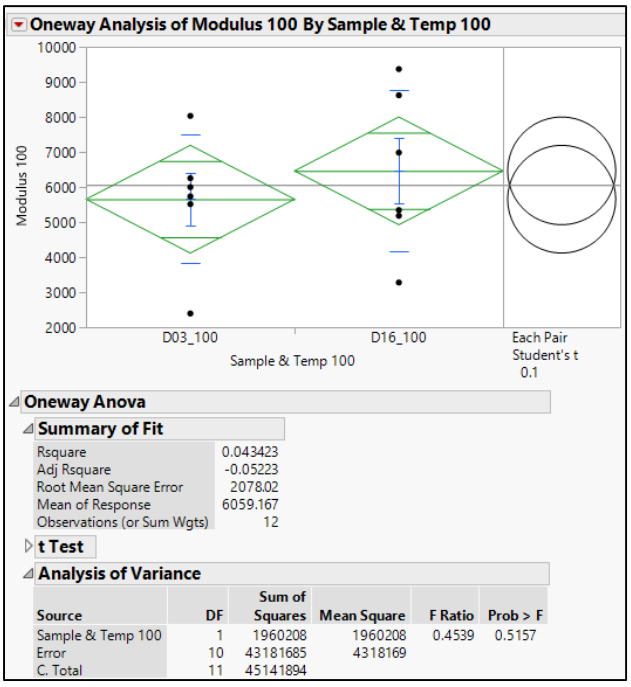

Figure 18. JMP Software Statistical Data for D16 vs. D03 moduli comparison @ 100°C.

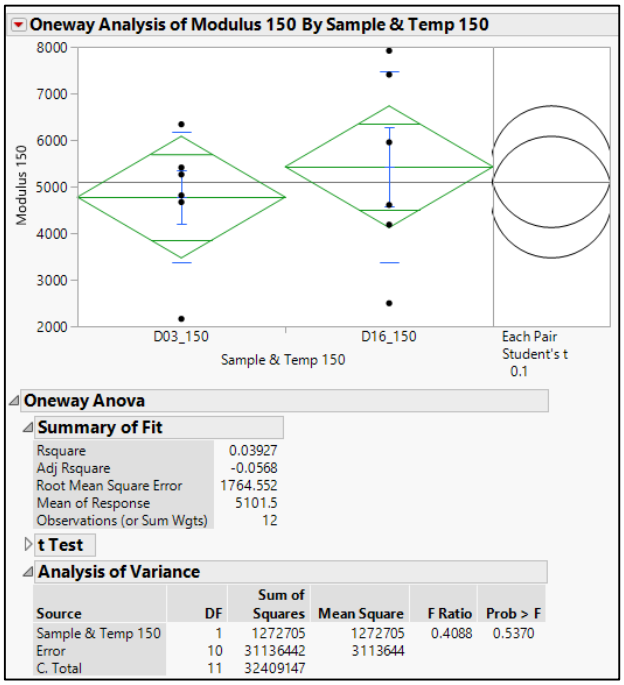

Figure 19. JMP Software Statistical Data for D16 vs. D03 moduli comparison @ 150°C.

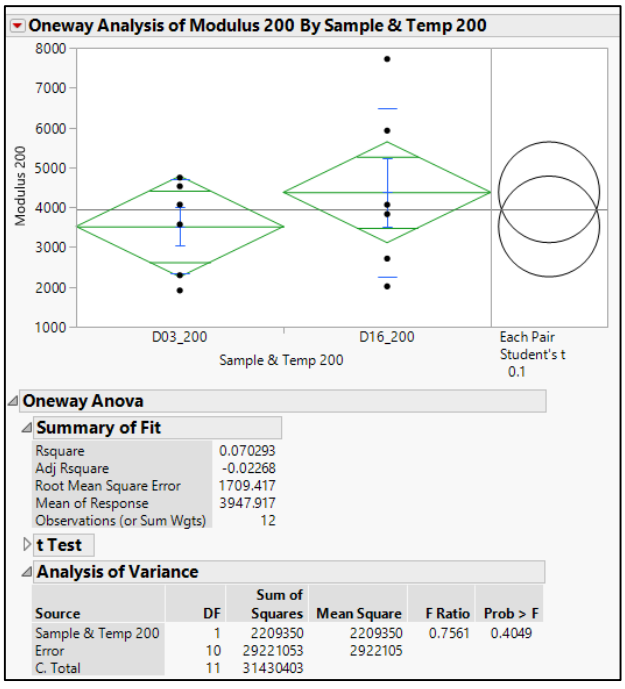

Figure 20. JMP Software Statistical Data for D16 vs. D03 moduli comparison @ 200°C.

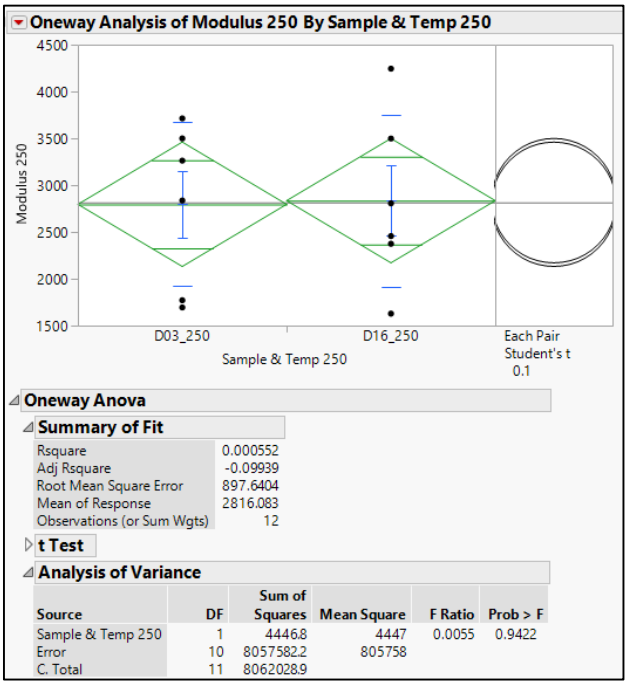

Figure 21. JMP Software Statistical Data for D16 vs. D03 moduli comparison @ 250°C.

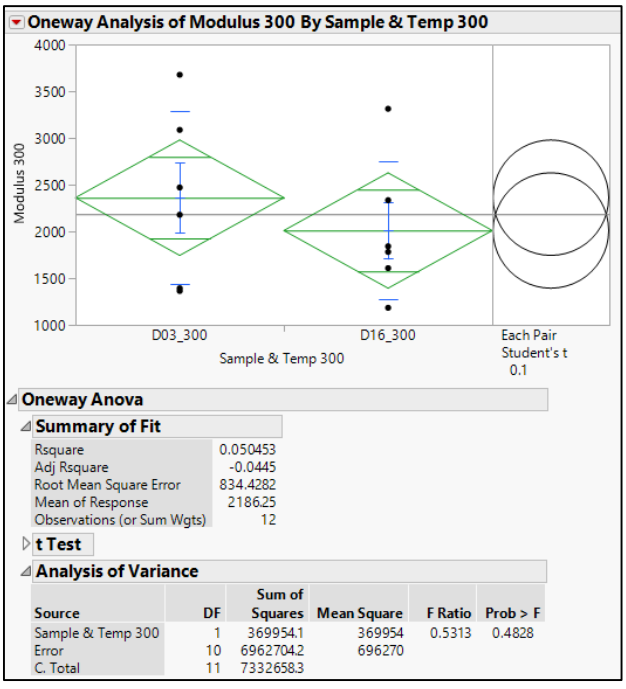

Figure 22. JMP Software Statistical Data for D16 vs. D03 moduli comparison @ 300°C.

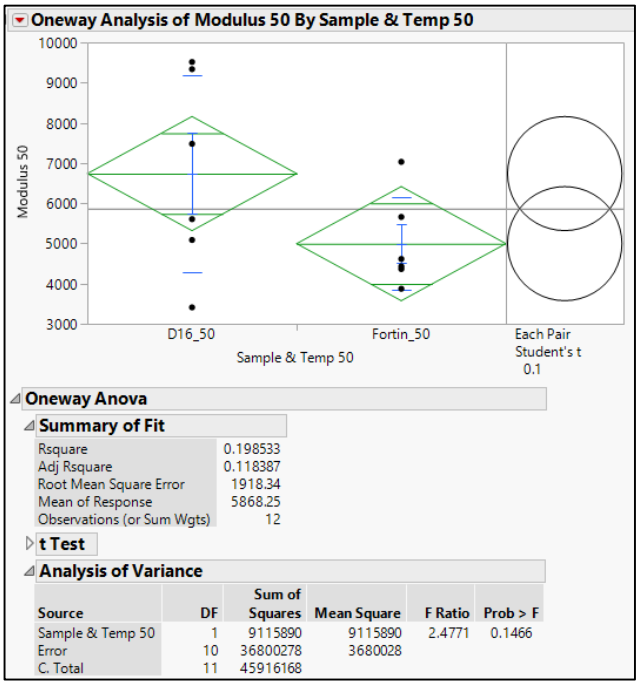

Figure 23. JMP Software Statistical Data for D16 vs. Fortin moduli comparison @ 50°C.

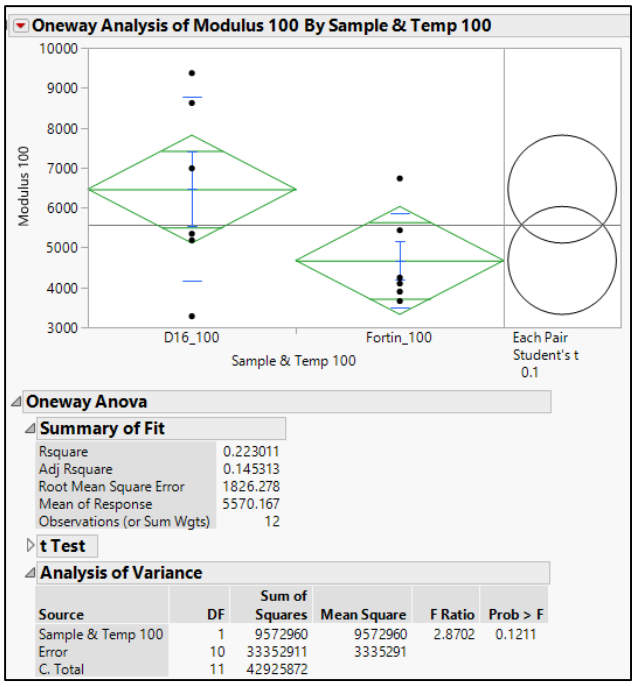

Figure 24. JMP Software Statistical Data for D16 vs. Fortin moduli comparison @ 100°C.

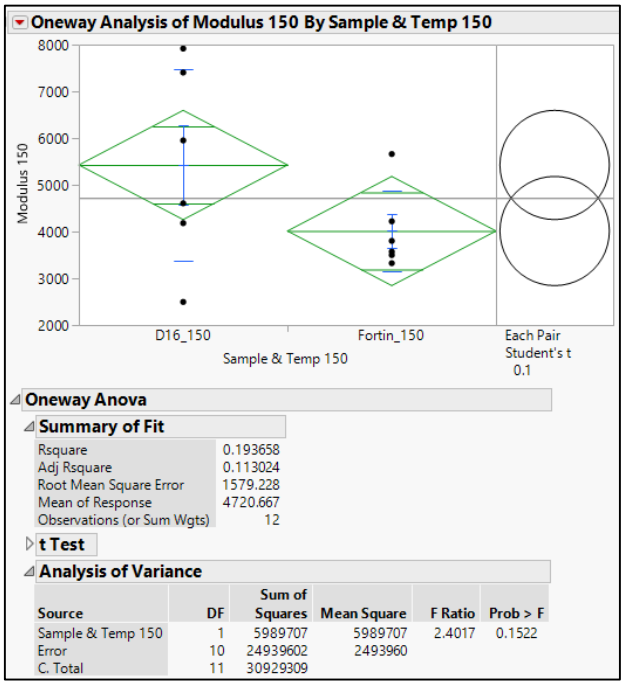

Figure 25. JMP Software Statistical Data for D16 vs. Fortin moduli comparison @ 150°C.

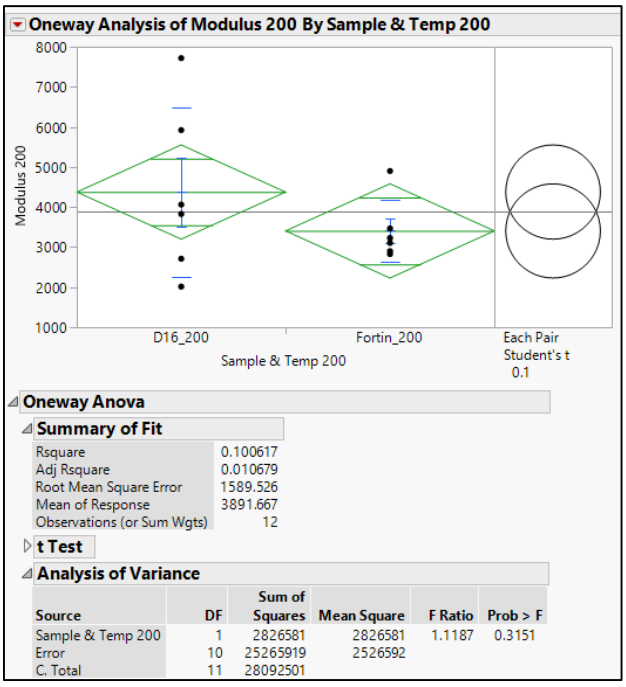

Figure 26. JMP Software Statistical Data for D16 vs. Fortin moduli comparison @ 200°C.

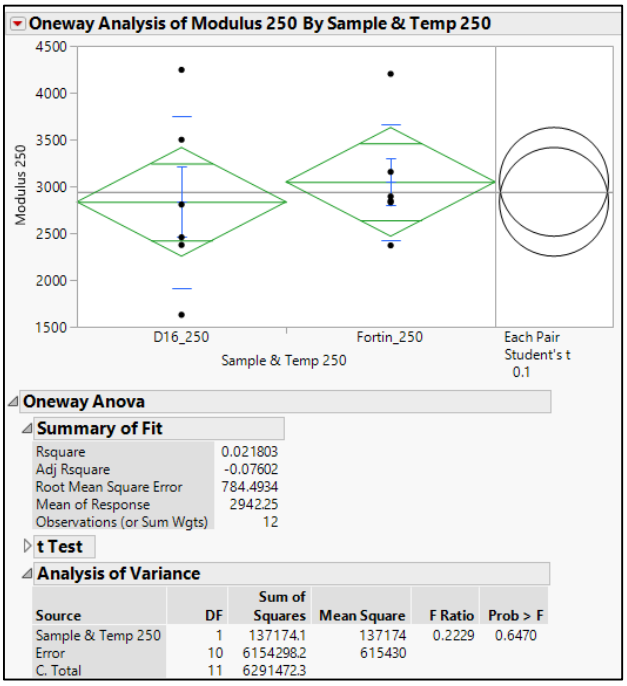

Figure 27. JMP Software Statistical Data for D16 vs. Fortin moduli comparison @ 250°C.

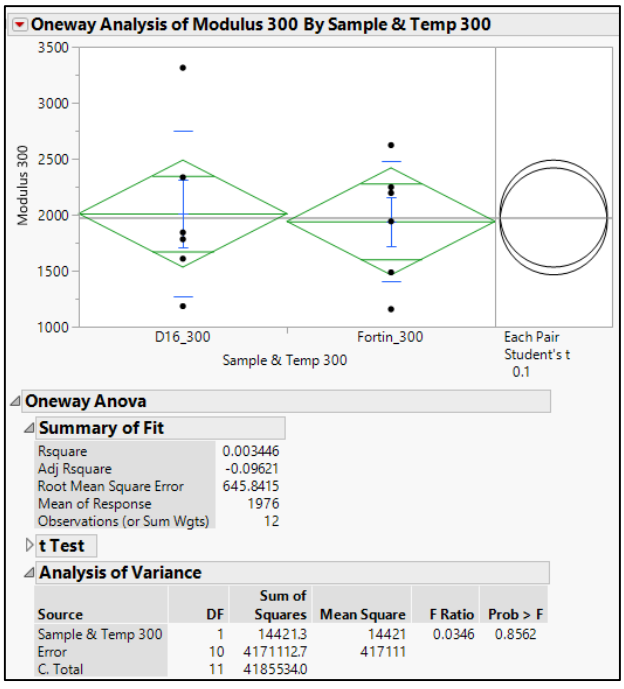

Figure 28. JMP Software Statistical Data for D16 vs. Fortin moduli comparison @ 300°C.

Microclad Tensile Testing

Stephanie Edwards & Anthony Sanchez

MATERIALS AND METHODS

Tensile testing was performed to determine the Young's modulus and ultimate tensile strength of a variety of microclad materials. Because of the use of the microclad in the flyer, it is crucial to know these mechanical properties and the similitude between the different lots of microclad. All tensile testing was performed on a MTS Insight 30 load frame and with screw grips (Figure 1). ASTM D882 was followed. The sample size was 4in x 0.65in (L x W). Samples were cut from a larger section of microclad to the sample size with a razor blade. Materials were tested at a rate of 1in/min. Microclad from four different years was tested: Fortin (1985), D03 (Datex 2003), D13 (Datex 2013), and D16 (Datex 2016). Pure Kapton was tested as well to help determine if the Kapton or the copper coating had a larger influence on the mechanical properties. The Kapton that was tested was the same Kapton that was used in the D03, D13, and D16 samples. In order to keep the samples from slipping out of the grips, transfer adhesive was used on the 1 inch grip sections (Figure 2). All samples were tested a room temperature in TA35-0213-H2.

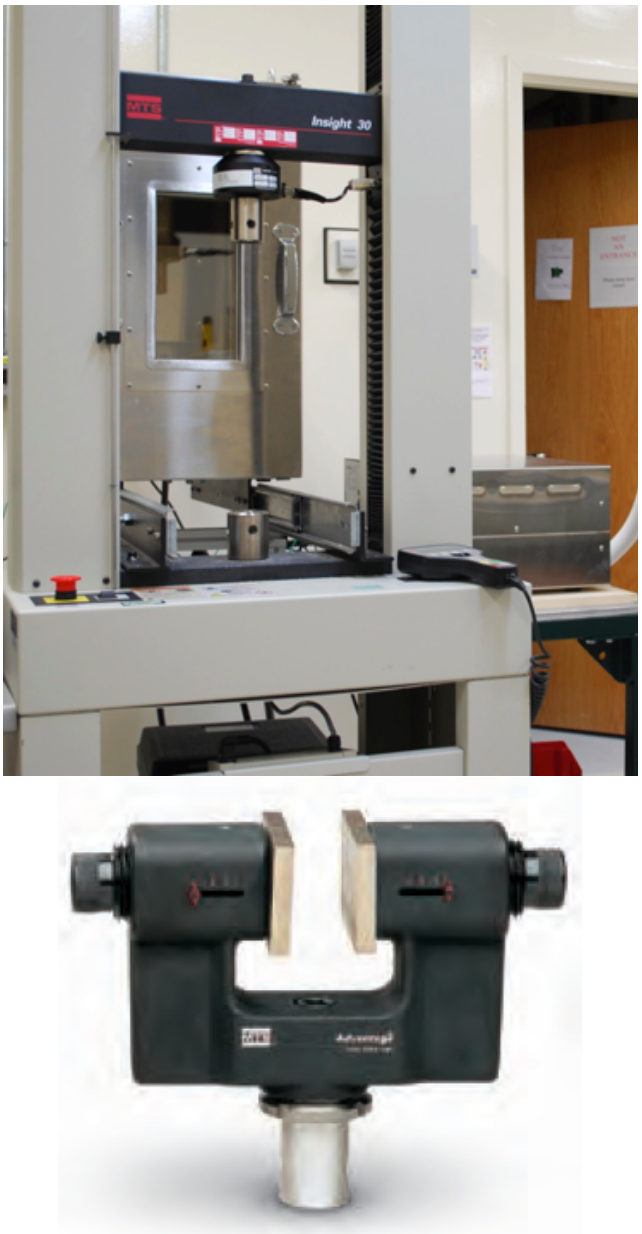

Figure 1. MTS Insight 30 (left) and the screw advantage grips (right).

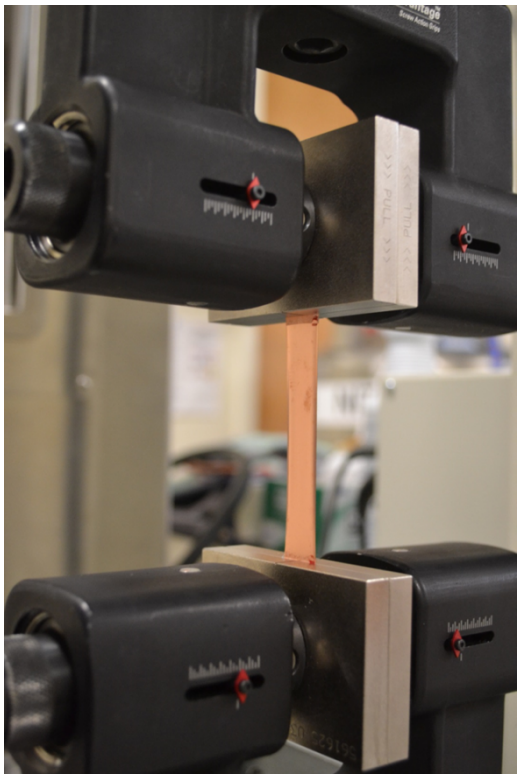

Figure 2. A Microclad sample in the tension grips during a test

RESULTS

There was a great deal of variation among samples (within the same year) and from year to year. Certain microclad samples had a greater elongation before break than others (Figure 3). While all of the tests were performed to failure, the samples did not all fracture in the same location. This could be the cause of the elongation variation.

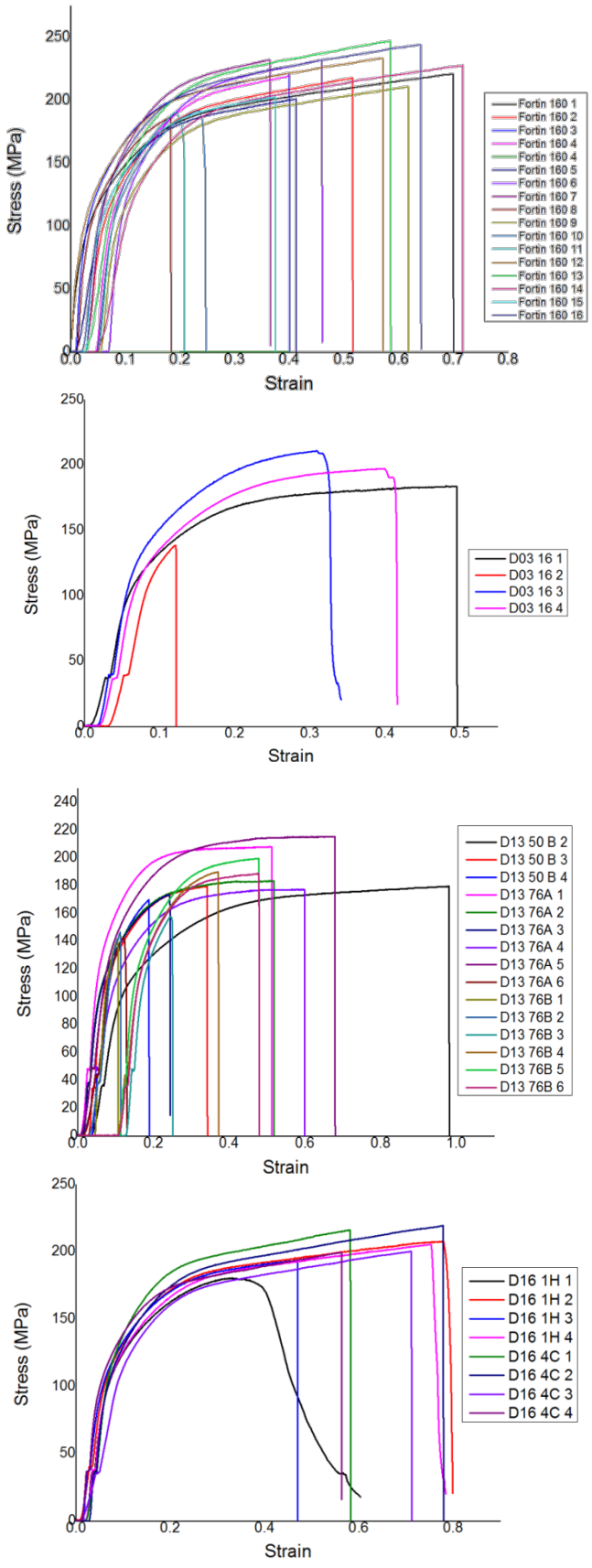
Stress (MPa)
Strain
Fortin 160 1
Fortin 160 2
Fortin 160 3
Fortin 160 4
Fortin 160 4
Fortin 160 5
Fortin 160 6
Fortin 160 7
Fortin 160 8
Fortin 160 9
Fortin 160 10
Fortin 160 11
Fortin 160 12
Fortin 160 13
Fortin 160 14
Fortin 160 15
Fortin 160 16
D03 16 1
D03 16 2
D03 16 3
D03 16 4
D13 50 B 2
D13 50 B 3
D13 50 B 4
D13 76A 1
D13 76A 2
D13 76A 3
D13 76A 4
D13 76A 5
D13 76A 6
D13 76B 1
D13 76B 2
D13 76B 3
D13 76B 4
D13 76B 5
D13 76B 6
D16 1H 1
D16 1H 2
D16 1H 3
D16 1H 4
D16 4C 1
D16 4C 2
D16 4C 3
D16 4C 4

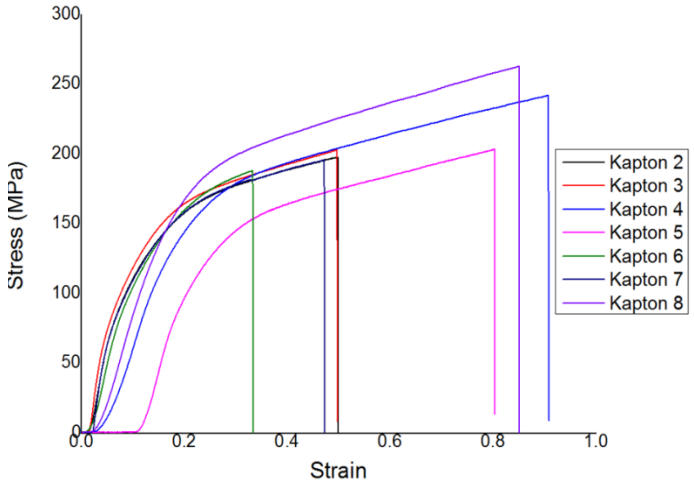

Figure 3. Stress/Strain curves for the different microclad and Kapton samples

There was also variation in the ultimate tensile strength and the Young's modulus (Table 1). The modulus values were calculated by taking the slope in the linear region of the stress/strain curves. Strain was calculated from crosshead displacement which is calibrated yearly by an MTS Technician and then calibrated again by the instrument user before each test. D03, D13, and D16 all have a plateaued ledge region in the data around 40MPa. This ledge is not seen in the Kapton or the Fortin 160 samples. At first, it would appear to be instrument compliance, but since it was only seen in select samples, it seems sample dependent.

Sample Name	Average Ultimate Tensile Strength (MPa)	Modulus (MPa)
Fortin 160	218.62 ± 19.28	3789.42 ± 979.76
D03	182.79 ± 31.41	3301.49 ± 405.57
D13	177.04 ± 22.60	3041.54 ± 813.87
D16	202.98 ± 12.42	2840.32 ± 487.84
Kapton (Tested at MST-7)	213.40 ± 27.89	1772.34 ± 543.04
Kapton (DuPont)	231	2500-3000
Copper	220	70000

Table 1. Overview of the tensile results

CONCLUSIONS

Overall, there is variation in the data. While the original Fortin 160 has the strongest average tensile strength on average, the other samples were within a standard deviation (Figure 4). The variations within the samples could be due to processing, sample handling, and/or sample preparation. Any surface defects or dents in the samples could have a significant effect on the mechanical properties. We do not know all of the previous sample history. Samples were cut for tensile testing using a razor blade; this could have also introduced some variations in the measurements. The tensile tests themselves also caused some variation since the samples did not all break in the same location. While all samples broke in the testing region (not in the grips), some samples broke closer to the middle, while other samples broke closer to the grips.

Introducing a different sample configuration, i.e. tapered samples instead of rectangular, could help reduce the elongation variation.

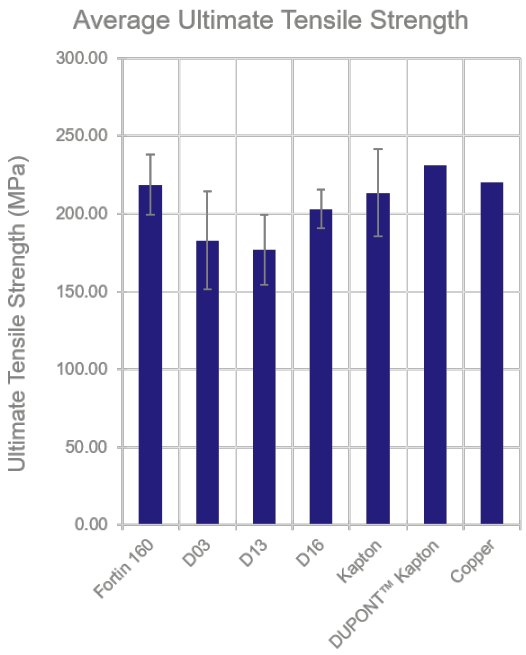

Figure 4. Average ultimate tensile strength

The modulus values for the microclad were higher than the Kapton, which is expected since copper has a much higher modulus than Kapton (Figure 5). The modulus for the pure Kapton that was tested was less than the published value from DuPont, but this could be due to additives present in the DuPont samples that were not present in ours as well as the test method and sample preparation.

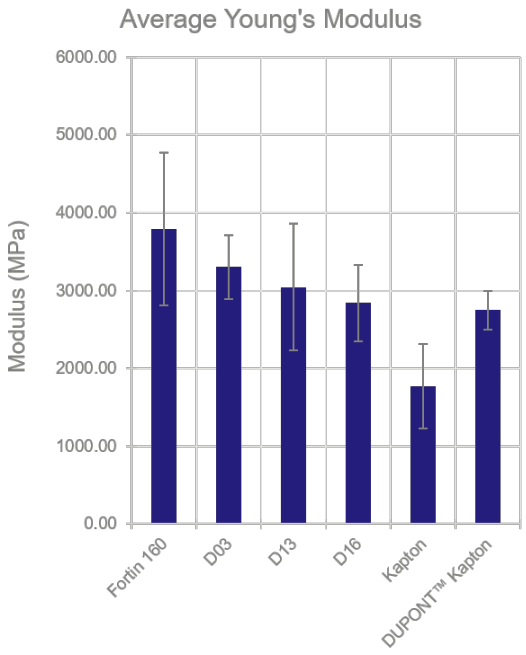

Figure 5. Average Young's modulus

Even though there are many variations between the data, the ultimate tensile strengths and the modulus values are within a standard deviation of each other. This implies that there is a degree of similitude among all samples when it comes to mechanical properties.

Analysis of microclad materials using Thermomechanical Analysis

Joseph Torres, Olivia Trautschold, Jillian Adams

MST-7, Engineered Materials, Los Alamos National Laboratory

Background

Thermomechanical Analysis (TMA) measures sample dimensional changes under the conditions of controlled temperature, time, force, or atmosphere.[1] Microclad samples from different years were obtained to look at dimensional change as a function of temperature. Using a linear heating rate, standard determines the coefficient of thermal expansion. In addition to standard TMA, modulated TMA (MTMA) was used to separate reversing and non-reversing signals in order to investigate overlapping events. In modulated thermal analysis, a sinusoidal temperature program is applied to a linearly changing temperature program. The information collected during MTMA can be represented by the equation below[1].

$$\frac{dL}{dt} = A\,\frac{dT}{dt} + f(t,T)$$

Where L is length, T is temperature, t is time, A is expansivity. This equation can be simplified to separate reversing and nonreversing signals with the equation below:

$$L_{total} = L_{reversing} + L_{nonrevesing}$$

Separating reversing and nonreversing signals allow heat shrinkage and CTE to be investigated.

Experimental

Microclad samples tested were from different years, rolls, and positions on the rolls. Table 1. presents a summary of samples measured for this report. All samples were handled with nitrile gloves. Tests were performed on microclad samples (kapton + copper) as well as one kapton-only sample.

Samples Tested:

Kapton	Fortin	D03	D13	D16
1	160	08A	53B	1G
	175	09A	62B	2E
		24A		5H

Table 1.

All TMA experiments were performed on a TA Q400EM instrument using a 2.54 mm expansion probe. Experiments were conducted in nitrogen atmosphere. For standard TMA, the samples were heated from -40°C to 160°C with a heating rate of 3°C/min. For MTMA, the samples experienced the combined effects of a linear ramp and a sinusoidal temperature regime of specified amplitude

and period.[1] For these experiments, the temperature was modulated ± 3°C every 100s with a linear ramp of 5°C/min. The temperature range was from 0°C to 150°C.

Results

1. *Standard TMA*

Table 2. lists sample percent shrinkage upon heating, along with the initial thickness of the Kapton and microclad.

Sample	L initial (mm)	% Shrinkage
D03-08A	0.0618	0.97
D03-24A	0.0579	4.77
D13-62B	0.0607	4.27
D13-53B	0.0505	3.71
D16-1G	0.0912	1.44
D16-5H	0.0542	1.92
Fortin-160	0.0598	13.41
Fortin-175	0.0728	19.62
Kapton	0.0495	3.39

Table 2.

Figure 1. shows a summary of the TMA measurements. All samples shrunk as they were heated. D03, D13, and D16 samples all have similar shrinkage values: 1-5%. The Fortin samples have larger shrinkage values: 10-20%.

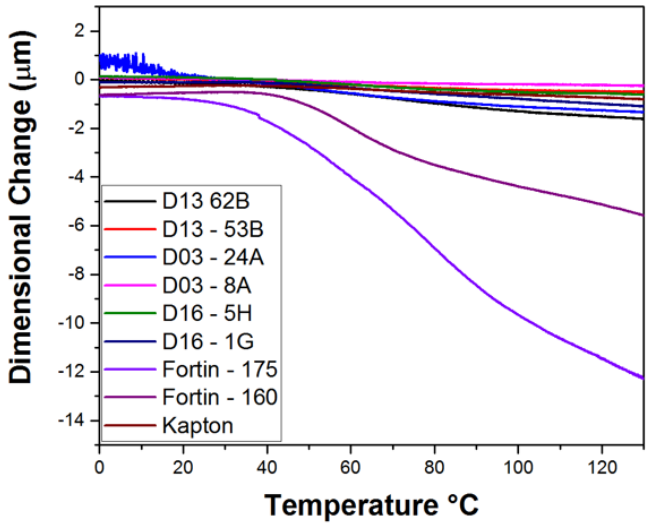

Figure 1.

Modulated TMA

MTMA was used to investigate overlapping dimensional changes by separating reversing and non-reversing signals. Using the non-reversing signal, heat shrinkage, stress relaxations, and softening are determined. Heat shrinkage is the dominant event seen in standard TMA data. Using the reversing signal, the CTE is revealed. Figure 2. presents the results for a D13 sample.

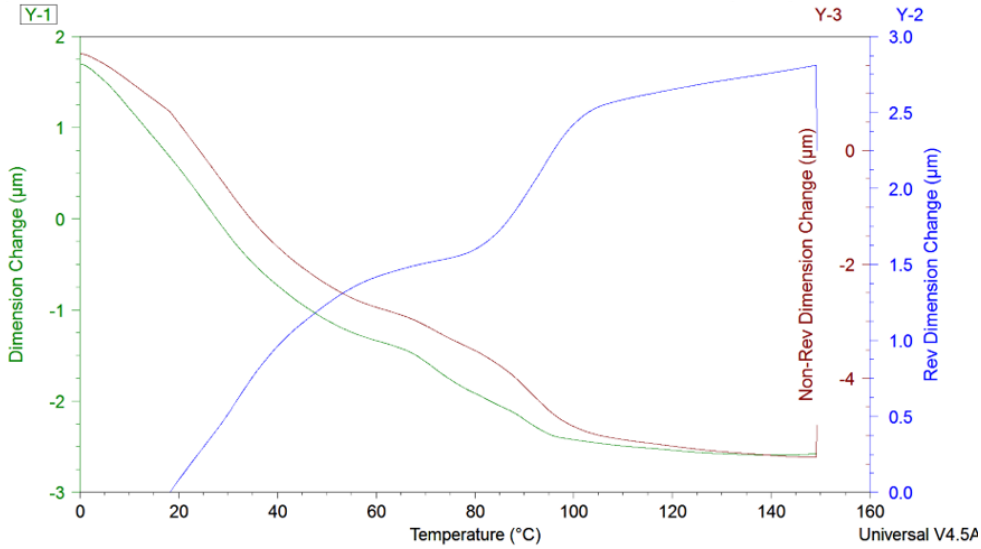

Figure 2. MTMA Measurement: D13

The non-reversing signal shows heat shrinkage, whereas the reversing signal shows the sample expansion. Total dimensional change is the sum of the reversing and non-reversing signals, which is the only signal seen in standard TMA. Focusing on the reversing signal, there is slope change around 100°C. Figure 3. presents the reversible signal slope changes for all samples measured with MTMA.

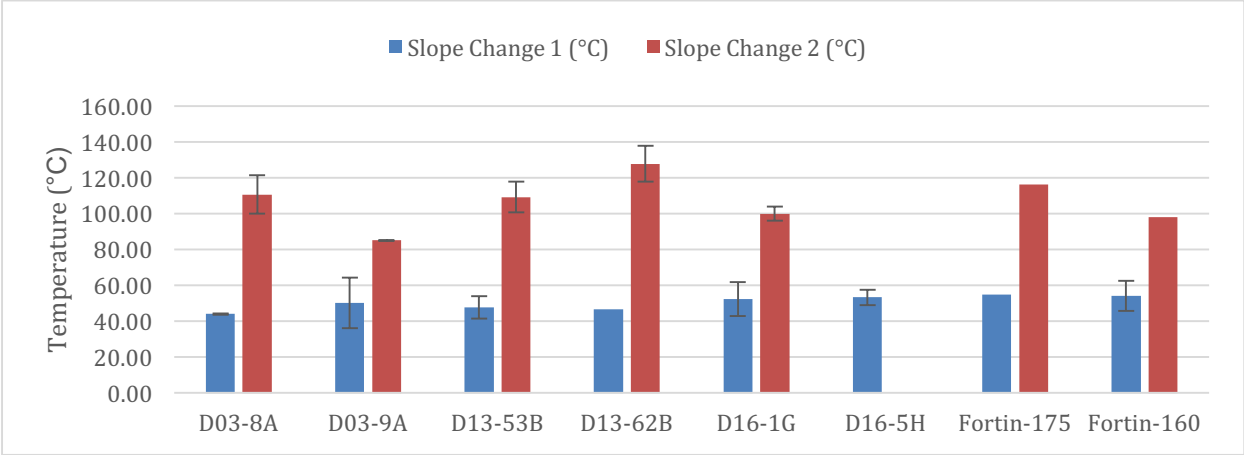

Figure 3.

This slope change could be water leaving the sample upon heating. Water acts as a plasticizer and changes the CTE of the material. Additional studies need to be conducted along with TMA to confirm the presence of water. MTMA was also performed on pure Kapton and the reversible signal showed a linear expansion with no slope changes. This may imply that the slope changes present in the microclad MTMA are due to the copper-Kapton interface.

Conclusions

Standard and Modulated TMA was performed on D03, D13, D16, and Fortin microclad samples to determine their similitude. All samples displayed shrinkage when exposed to heat. The D03, D13, and D16 samples were the most similar, as they all shrank 1-5% upon heating to 160°C. Whereas the Fortin samples shrank 10-20% upon heating to 160°C. MTMA was conducted to separate the reversing and non-reversing signals. Focusing on the reversible signal, microclad samples exhibit slope changes in the thermal expansion signal at around 100°C. This could be due to water coming off of the samples. Overall, the microclad samples all behave similarly both inter and intra lot with MTMA.

Reference

Blaine, L.R., Modulated Thermomechanical Analysis – Measuring Expansion and Contraction Simultaneously. *TA Instruments Series*

Adhesion between Cu and Kapton in Microclad Materials

Douglas Vodnik, MST-7

Summary

The maximum adhesion strength between the copper and Kapton layers of microclad samples from various rolls and lots was quantified using the Romulus Adhesion Tester. The delamination of the copper from the Kapton was observed to involve multiple sequential failure mechanisms. A large variation in the maximum adhesion strengths was measured across all lots, and even within a given roll. However, there was found to be no clear difference between the adhesive performance of samples from the Fortin, D03, D13, and D16 lots.

Introduction

The strength of adhesion of one film to another is the measure of how much the two films adhere, or stick, to each other. The maximum adhesion strength of two films is often determined by measuring how much tension can be applied to one of the two films over a given area in the direction perpendicular to the film surface before it separates from the second film at the interface. Hence, maximum adhesion strength is measured in units of force per area. Adhesion strength is an important measure of manufacturing quality, and it can also inform understanding of sample aging behavior. In this study, the strength of adhesion between the copper and Kapton layers of microclad samples from various rolls and lots was investigated.

Figure 1: Romulus Adhesion Tester by Quad Group Inc.

Method

Lot	Fortin	Datex 2003 (D03)	Datex 2013 (D13)	Datex 2016 (D16)
Rolls	160, 175	24A, 8A, 9A	50A, 53B, 62B, 65A, 70A	1G, 2E, 5H

Table 2: List of lots and rolls from which tested microclad samples originated.

Table 1 contains the list of lots and rolls from which the tested microclad samples originated. One sample, roughly three square inches in size, was obtained for each Datex roll; this was enough material on which to conduct four measurements. For each Fortin roll, only enough material for one measurement was obtained.

All Datex samples passed the pass/fail tape test specification IPC-TM-650 2.4.10; the Fortin samples were not tested due to insufficient material. However, as a pass/fail test, this specification conveys limited information. Additionally, this test method is intended for use on patterned thin films, and may have limited applicability for solid films such as those on the samples in this study. However, the Romulus Adhesion Tester, manufactured by Quad Group Inc., is able to quantify the maximum adhesion strength of films and so was used in this study (Figure 1).

Figure 2: Microclad samples after being bonded to mounting studs with cured epoxy.

Samples are placed in tension by the Romulus with the aid of small mounting studs, also provided by QuadGroup Inc. Each stud has an epoxy on its face which bonds the stud to any surface it is in good contact with after a one hour, 150°C cure. The copper films of all microclad samples were simultaneously bonded to their respective studs in this manner (Figure 2).

Once the stud is attached to the sample, the sample can be loaded into the Romulus. The Romulus pulls on the stud with a known force through a small hole while the sample rests over the hole (Figure 3). Since the diameter of the stud face is also known, the maximum adhesion strength for a given run can then be calculated. As the Romulus is not designed to test standalone flexible samples, all microclad samples were glued to silicon backing plates with AngstromBond AB9110LV prior to testing.

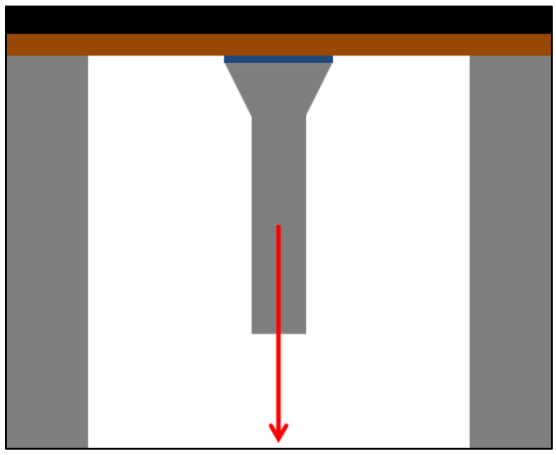

Figure 3: Illustration of the stud pull adhesion test method. The stud is attached to the copper (brown) by an epoxy (blue), and is pulled perpendicularly away from the sample through a hole while the sample rests over the hole.

Observations

During these runs, three general failure modes were observed to occur during the delamination process (Figure 4). The first failure occurred when the copper attached to the stud delaminated from the Kapton but maintained its

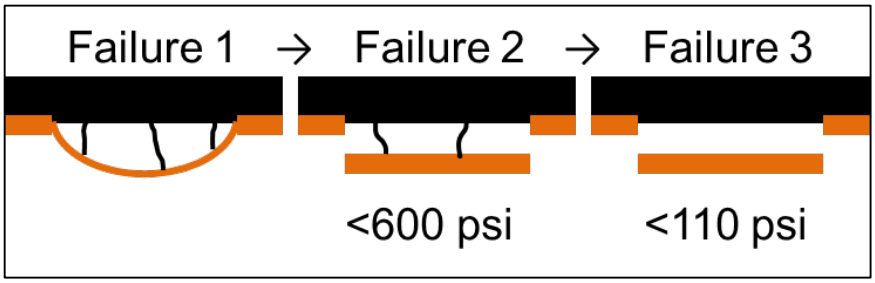

Figure 4: The three sequential failure modes observed during testing. Failure 1 occurred when the copper (orange) attached to the stud (not shown) delaminated from the Kapton (black) but maintained its connection to the surrounding copper, forming a "blister." Failure 2 occurred when the copper attached to the stud ripped off of the surrounding copper. If there were any residual pieces of Kapton still holding the copper to the sample, they were broken and complete separation was achieved.

connection to the surrounding copper, forming a "blister." This first failure corresponded to a wide range of maximum adhesion strength values. Next, the copper attached to the stud ripped away from the surrounding copper. This second type of failure was never observed to occur at adhesion strengths greater than 600psi. Often, the stud and attached copper were separated from the sample at this point. However, infrequently there were residual pieces of Kapton still holding the copper to the sample (Figure 5). In this case, the third and final failure resulted in these Kapton pieces breaking and complete separation being achieved. This third type of failure never occurred at adhesion strengths greater than 110psi.

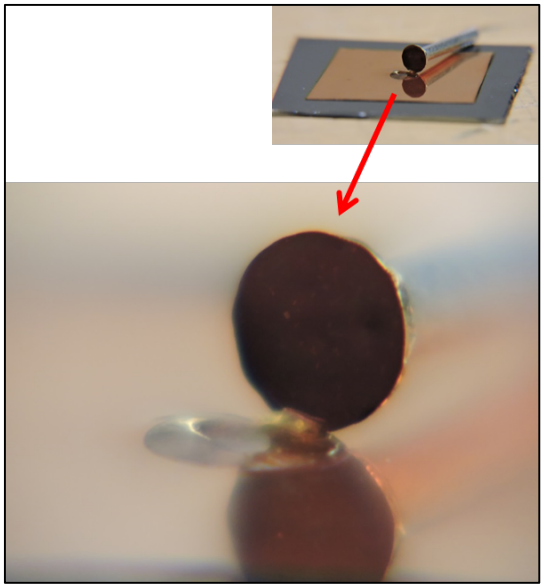

Figure 5: A small piece of Kapton keeping the stud from being completely separated from the sample.

Results and Discussion

The collected data are shown in Table 2 and Figure 6. A great deal of variation in all the measured values is obvious, even within most any given roll. This could possibly be an inherent variability within the samples, or perhaps the epoxy cure or another part of the sample preparation affected the adhesion strength. However, if the former is true, this may not be much of a concern if the test specification IPC-TM-650 2.4.10 was passed. It might also be noteworthy that roll D16 produced samples with the two greatest measured maximum adhesion strengths, which could be due to a function of sample aging. But overall, no clear difference in adhesive performance between the microclad samples was observed.

Roll	Maximum Adhesion Strength (psi), Sample 1	Maximum Adhesion Strength (psi), Sample 2	Maximum Adhesion Strength (psi), Sample 3	Maximum Adhesion Strength (psi), Sample 4
160	2003	-	-	-
175	258	-	-	-
D03#24A	1805	1484	1213	1979
D03#8A	414	319	417	351
D03#9A	1977	1191	1780	61
D13#50A	505	356	542	364
D13#53B	218	1057	568	412
D13#62B	755	449	1853	495
D13#65A	961	1031	703	725
D13#70A	1110	723	266	334
D16#1G	1219	1189	2244	841
D16#2E	513	1118	435	730
D16#5H	290	1158	2417	-

Table 3: Maximum adhesion strength data. The Fortin samples (rolls 160 and 175) only had enough material for one test. D16#5H sample 4 was damaged before testing could be performed.

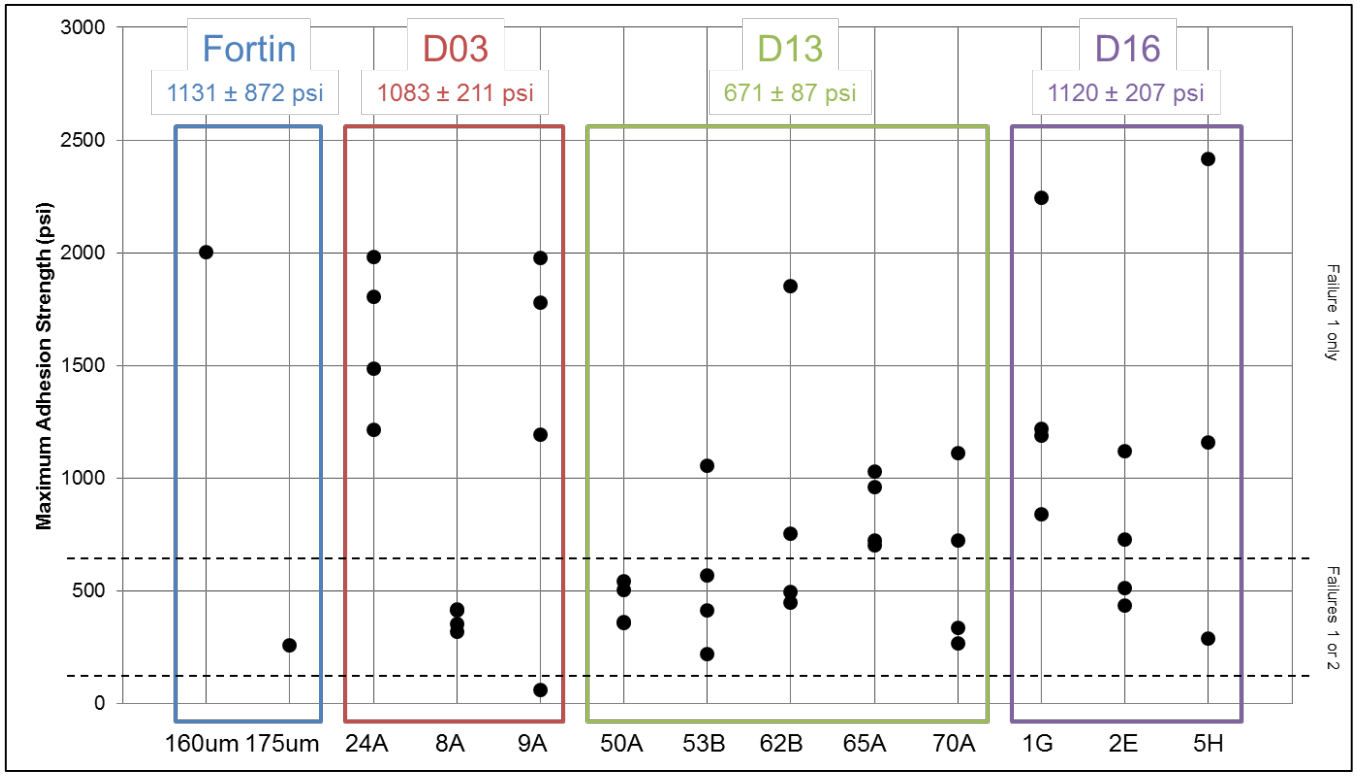

Figure 6: Maximum adhesion strength data. Each point corresponds to one run while each column of points corresponds to one roll. Most rolls yielded four samples, which were each run once. The dashed lines correspond to the failure modes: for any points above the top dashed line the maximum adhesion strength measured for that sample corresponded to the first failure mode. For any points between the two dashed lines, the maximum adhesion strength measured for that sample may correspond to either the first or second failure mode. The numbers below the lot names are the average maximum adhesion strength for that lot ± standard error.